Deep Level Characterization of GaAs and AlGaAs by Capacitance Spectroscopy

Tadashi HASHIZUME

Deep Level Characterization of GaAs and AlGaAs by Chapacitance Spectroscopy

Tamotsu Hashizume

September 1990

DEDICATION

to my wife

ACKNOWLEDGMENTS

I would like to express my sincere appreciation to Professor Hideki Hasegawa of Hokkaido University for his constant guidance, suggestion and encouragement; without his support this work could not have been achieved.

I would also like to thank Associate Professor Hideo Ohno of Hokkaido University. I have benefited significantly from his suggestions and discussions throughout this work.

I am further indebted to Associate Professor Mitsuo Shimozuma of Hokkaido University for the growth of insulator films and his encouragement, and to Associate Professor Takayuki Sawada, The University of Electro-communications, for his helpful discussions and encouragements during the early stage of this work.

Special thanks are to Kouichi Iizuka and Masamichi Akazawa, Research Associate of Hokkaido University, for their useful discussions.

I would like to thank Dr. Akihiro Wakahara, Kyoto University, for the gamma-irradiation of GaAs and valuable discussions, and Hiroto Nagabuchi, Sumitomo Metal and Mining Ltd., for the supply of LEC GaAs and useful discussions. Thanks are also due to Professor Isamu Tohdoh and Professor Hiroshi Itoh, Kushiro National College of Technology, for their encouragements.

I would like to express my gratitude to Dr. Eiji Ikeda, Dr. Yuji Akatsu and Dr. Ryuuichi Katsumi for the MOVPE and MBE growth and their helpful discussions. I would also like to thank Dr. Shouhei Seki and Dr. Ji-Kui Luo for their fruitful discussions. Thanks are also due to Hirotatsu Ishii for his usuful comments on XPS measurement, and Shunsuke Ohtsuka and Yoshinori Matsubara for the MOVPE growth of AlGaAs. Thanks are also conveyed to the graduate students at the Material Reaserch Laboratory in Hokkaido University for their technical assistance.

I am also grateful to Yoshihito Nakane and Motokazu Nishino, Hokkaido Polytechnic College, for the deposition of insulator films and their technical assistance in AES and XPS measurements. Thanks are to Shinji Hiramatsu, Yasuyuki Masuyama, Masayuki Saitoh and Akira Nakahara for their technical assistance. Thanks are also due to Dr. Yoshiyuki Ohmori, Toshihiko Tanaka, Satoshi Nakamura and Kunihiko Mori, Hokkaido Polytechnic College, for their encouragements.

I would like to express my sincere thanks to Professor Hiroaki Tagashira, Professor Toshihisa Honma and Professor Kouichi Mukasa, Hokkaido University, for helpful suggestions and encouragements.

Finally, I wish to thank my brother and sisters for their constant support and my wife Yohko for her assistance in many ways.

CONTENTS

CHAPTER 1

INTRODUCTION

1.1 Historical Backgrounds

As compared with silicon (Si), compound semiconductors possess several attractive material properties such as direct band gaps, high electron mobilities and large saturation velocities, availability of semi-insulating (SI) property, and resistance against cosmic ray irradiation. Another important and unique features of compound semiconductors are the availability of wide varieties of mixed alloys semiconductor and capability to form heterojunction structures. These attractive features have given rise to large interests in both fundamental and applied research in these materials. Major devices based on compound semiconductors include metal semiconductor field effect transistors (MESFET), high electron mobility transistors (HEMT), heterojunction bipolar transitors (HBT), laser diodes (LD) and other optical devices. Encouraging progresses have recently been made on their integration to form their integrated circuits (ICs).

In order to obtain devices with high performance, it is

necessary to prepare high quality bulk and epitaxial semiconductor materials. For instance, fabrication of GaAs integrated circuits relies on the direct implantation into high-quality and highly uniform semi-isulating substrate to form device active layers. Thus, recent strong demands for well behaved integrated circuits have accelerated the study of SI GaAs bulk materials for quality improvements. On the other hands, novel devices using hetrostructures and superlattice structures have become possible through the availability of high-quality epitaxial materials by the molecular beam epitaxy (MBE), the metalorganic vapor phase epitaxy (MOVPE) and the atomic layer epitaxy (ALE) growth techniques.

The quality of the bulk substrates and epitaxial layers is greatly affected by the nature of the native defects and the chemical impurities which are formed or incorporated in the crystal, depending on the thermodynamic conditions for crystal growth and the chemical composition of the starting materials. These defects and impurities, or their complexes, have a tendency to introduce localized levels in the band gap of the host material.

Among these, 'shallow' impurities, which normally substitute the host atom in the crystal, give rise to bound states in the fundamental band gap very close to the band edges and generally contribute to extra charged carriers, electrons or

holes. Their role, therefore, is primarily to control the type and magnitude of the conductivity. The overall behavior of such impurities can be understood quite adequately in terms of the simplest hydrogenic model.

There exist other types of impurities as well as a variety of lattice defects (vacancies,interstitials, antisite defects, etc.) that cause more severe local perturbations. They give rise to bound states that are considerably more localized, and have energies deeper in the band gap. The energy levels by such impurities, lattice defects and impurity-defect complexes, which cannot be described by the hydrogenic model, are referred to as 'deep levels'. Unlike shallow levels, deep levels act primarily as carrier traps or recombination centers.

Deep levels are therefore undesirable in devices where carrier must have long lifetimes. They are also responsible for long-term instability of devices. On the other hand, they are useful when the carrier concentration needs to be reduced, to obtain so called semi-insulating materials. In addition, in case that the recombination energy is released as light of a suitable wavelength, deep levels can be used in making light-emitting diodes (LED). Thus, by carefully controlling the various types of defects, one can manipulate the properties of semiconductors which form the active part of most electronic devices today.

Progress in the field of deep levels has been driven primarily by technological needs. For example, oxygen-related levels and recombination centers in GaP have been studied in order to improve the efficiency of LEDs.[1,2] The compound semiconductor integrated circuit technology requires the production of adequately controlled and uniform semi-insulating substrates.

It has been shown that the electrical resistivity of bulk-grown undoped GaAs is dominated by the presence of a native deep level called EL2 which compensates the shallow impurities present in the material. This level presents some strange properties such as metastable behavior. In addition, EL2 exists in III-V ternary alloys and may act as a recombination center. Thus, considerable effort has been devoted to the understanding of its properties and microscopic structure,[3] but its origin is not completely understood yet except for a consensus that the EL2 is associated with excess arsenic. The transition metal impurities, namely Cr and Fe, in compound semiconductors are also of great scientific and technological importance as they are main compensators in semi-insulating materials.[4-6]

Deep donor levels, which are often called DX centers, have been observed in many III-V alloy semiconductors. In $Al_xGa_{1-x}As$, for example, the DX center controls the conductivity of the material when $x>0.2$ and persistent photoconductivity (PPC),

attributed to a large lattice relaxation of the DX center, is also observed in this composition range.[7] These properties produce detrimental effects on HEMT device characteristics, e.g., the persistent threshold shifts at low temperature, transient in the source-drain current with time constants of the order of 10 μs at room temperature and the collapse of the I-V curves.[8] Thus, the microscopic nature of the DX center and the mechanism for capture and emission of electrons have been studied as well as the EL2 level.[7,8] On the other hand, near-midgap deep levels behave as recombination centers and affect the operating characteristics of minority carrier devices such as HBTs, LDs, LEDs, and solar cells.[9] However, properties of deep levels except for the DX center are not clarified in III-V alloy semiconductors

A new class of defects that are attracting attention are process-induced defects. The very large scale integration (VLSI) technology requires for device sizes to be smaller and the number of processing steps to be larger. These trends and new processing technologies can induce new defects or enhance the activity of the kinds of impurities that have always been present but so far largely electrically inactive. One such examples are the so-called oxygen thermal donors in Si, namely a number of closely related oxygen centers that appear after a wafer has been processed at temperatures of 300-400 C.[10]

Doping by ion implantation remains as the key processing step in the fabrication of GaAs MESFETs. After implantation, the damages introduced by implantation must be removed by annealing process. These elements form large families of defects due to the implantation damage, the redistribution of impurities and the stress induced by post-annealing. For example, the EL2 properties are severely affected by implantation[11] and the creation and the annihilation of defects are observed by various annealing processes.[12-14] However, the behavior of the implantaion- or irradiation related defects in bulk and epitaxial materials is not completely clarified, and annealing processing still suffers from various problems. Another key technology for the development of VLSI and novel devices in compound semiconductors is the epitaxial growth technology. During epitaxy, impurities trend to segregate at the surface and have a significant effects on the growth rate and the formation of the complex-defects. The understanding of deep level properties at surface or interface of epitaxial layers is important for high quality homo- or heterostructures.

1.2 Objective of The Thesis

In the present thesis, deep levels in epitaxial GaAs and AlGaAs, as well as bulk GaAs, are investigated. As the epitaxial layers, MOVPE AlGaAs layers are studied since they allow us to

make nearly ideal abrupt heterostructures owing to recent advances in the epitaxial growth technology. Because of their unique matching properties to the GaAs lattice over the whole composition range, AlGaAs layers are the most useful ternary alloy for many advanced devices. As bulk material, liquid encapsulated Czochralski (LEC) GaAs is studied since it is a key material for improving the performance of high speed and optoelectronic integrated circuits. The properties of irradiation induced defects and the effect of an annealing process on the deep levels are also studied in detail, since they are closely associated with the process-induced defects.

Thus, the objective of this thesis can be summarized as follows.

(1) to investigate the role of the deep levels in compensation mechanism in bulk grown GaAs.

(2) to clarify the relationship between deep levels and growth conditions in the epitaxial GaAs layers.

(3) to investigate the electrical and optical properties of midgap levels in the epitaxial AlGaAs layers.

(4) to investigate the effect of γ-irradiation and various annealing processes on the deep levels in bulk GaAs.

1.2 Synopsis of Chapters

Chapter 2 describes electrical behavior of deep levels and capacitance spectroscopy methods for characterization of deep levels. In these methods, the changes in the electron occupancies of deep levels in the depletion region of junction barriers are used to measure absolute values of thermal and optical emission rates, capture cross sections and concentrations. The occupation function of deep levels can be given by the rate equation and is controlled by temperature, bias voltage and illumination of monochromatic light. Based on the bias and time dependence of junction capacitance, deep level transient spectroscopy (DLTS) is summarized. DLTS is a straightforward technique to analyze, thereby being widely used to investigate deep levels. Photocapacitance (PHCAP) methods is employed to investigate the optical properties of deep levels. Steady-state and transient PHCAP techniques are described.

Chapter 3 investigates deep electron levels in undoped n-type GaAs grown by the liquid encapsulated Czochralski (LEC) method. Deep level properties are characterized by DLTS and temperature-dependent Hall measurements. DLTS spectrum shows that six electron traps exist in as-grown materials. Analysis of temperature-dependent carrier concentration indicates that electron traps shallower than the EL2 level, e.g., EL6, can play

a significant role in the compensation mechanism in LEC GaAs which has a low concentration of acceptor impurities. The effect of face-to-face annealing on the electron traps is investigated. EL2 in bulk region remains stable at around 800 ℃. The drastic reduction of EL6 concentration by 800 ℃ treatment indicates that EL6 seems to cause large resistivity change of the LEC materials in annealing process.

In chapter 4, deep levels in epitaxial GaAs grown by MOVPE and MBE are investigated. The effect of the purity of source materials on deep levels in MOVPE GaAs is clarified using different trimethylgallium (TMG) sources. DLTS study confirms that the dominant electron trap in undoped MOVPE layers is the EL2 level. It is shown that another traps are detected only in the layers grown with particular TMG source, indicating that these traps are related to impurities introduced with the TMG source. Properties of the electron traps in undoped MBE layers are investigated by changing growth conditions, especially focusing on the effect of coincident Pb flux on deep level concentration in order to probe into the surface process of the growing layer. It is shown that the application of Pb flux modifies the growing surface process of GaAs, thereby reducing the concentration of the electron traps.

Chapter 5 deals with near-midgap levels in $Al_xGa_{1-x}As$ layers grown by MOVPE. The composition dependence of the energy level of

the midgap levels shows that one of them is closely related to the EL2 in GaAs. Optical properties of the midgap levels are clarified by a new PHCAP measurement procedure by which the effect of the photoionization of the DX center is separated from the photoquenching of the midgap levels. PHCAP measurement confirms that one of the midgap levels exhibits an remarkable photoquenching for $x<0.3$ and that the optical cross sections of the level almost the same with those of the EL2 in GaAs and $GaAs_xP_{1-x}$. It is shown that the excited state of the midgap level seems to change its character as the alloy composition is varied, resulting in the disappearance of photoquenching for $x>0.3$.

Chapter 6 describes the variation of deep levels in GaAs by γ-irradiation. The effect of the irradiation on deep levels in LEC GaAs is compared to that in epitaxial GaAs. Annealing behavior and the concentration profile of the levels observed indicate that the complex defects are created in LEC GaAs by an interaction between the grown-in defects and the irradiation-induced defects. It is shown that the defects introduced by γ-irradiation in epitaxial GaAs are the same with those by electron irradiation and that the electrical and optical properties of the EL2 level is not affected by irradiation.

Chapter 7 investigates the effect of annealing process on near-surface deep levels in Al_2O_3-capped GaAs. Al_2O_3 film as an improved encapsulant for GaAs prepared by the dynamic mixing

method are analyzed by Auger electron spectroscopy (AES) and X-ray photoelectron spectroscopy (XPS). Results of AES and XPS analysis indicate that there is no evidence of As or Ga outdiffusion into Al_2O_3 film during furnace annealing and rapid thermal annealing (RTA). It is shown that the different structural change at the Al_2O_3/GaAs interface are observed with the different annealing processes. In addition, the EL2 concentration is increased and non-exponential photoquenching behavior is observed near the surface only after RTA.

Chapter 8 summarizes the present work and gives the conclusions.

References

1) P.J.Dean, *Deep centers in semiconductors*, edited by S.T.Pantelides (Gordon and Breach Science Publishers, New York, U.S.A.,1986), p.185

2) A.Peaker and B.Hamilton, *Deep centers in semiconductors*, edited by S.T.Pantelides (Gordon and Breach Science Publishers, New York, U.S.A., 1986), p.349

3) For recent reviews, see for example, "Recent developments in the study of the EL2 defect in GaAs", Rev.Phys.Appl.,23,727-869 (1988), edited by H.J.von Bardeleben and B.Pajot; G.Martin and S.Makram-Ebeid, *Deep centers in semiconductors*, edited by S.T. Pantelides (Gordon and Breach Science Publishers, New York, U.S.A., 1986), p399

4) S.G.Bishop, *Deep centers in semiconductors*, edited by S.T.Pantelides (Gordon and Breach Science Publishers, New York, U.S.A., 1986), p.541

5) J.W.Allen, *Deep centers in semiconductors*, edited by S.T.Pantelides (Gordon and Breach Science Publishers, New York, U.S.A., 1986), p.627

6) H.Hasegawa, Solid State Commun., 58,157(1986)

7) D.V.Lang., *Deep centers in semiconductors*, edited by S.T. Pantelides (Gordon and Breach Science Publishers, New York, U.S.A., 1986), p489

8) P.M.Mooney, J.Appl.Phys.,67, R1(1990)

9) P.M.Mooney, *Semi-Insulating III-V Materials* (Hilger, Bristol,

UK, 1988), p.277

10) G.S.Oehrlein, J.Appl.Phys., 54,5453(1983)

11) G.Guillot, Rev.Phys.Appl., 23,833(1988)

12) D.C.look, *Semi-Insulating III-V Materials* (Hilger, Bristol, UK, 1988), p.1

13) M.Nishitsuji and F.Hasegawa, Jpn.J.Appl.Phys., 28,L895(1989)

14) M.Katayama,A.Usami,T.Wada and Y.Tokuda, J.Appl.Phys., 62, 528(1987)

CHAPTER 2

ELECTRICAL BEHAVIOR OF DEEP LEVELS AND CAPACITANCE SPECTROSCOPY

2.1 Introduction

A number of techniques of the experimental study of deep levels in semiconductors are presented. In these techniques, the capacitance spectroscopy techniques have become a powerful tool for the characterization of deep levels because they are sensitive, spectroscopic and convenient to analyze. The junction capacitance varies according to charging and discharging of deep levels in the depletion region. The charging and discharging can be controlled by temperature, illumination of monochromatic light and bias voltage.

Deep level transient spectroscopy (DLTS) developed by Lang,[1] that is a capacitance transient thermal scanning technique, has been widely used to detect deep levels, since it is a straightforward method to analyze and rapidly provides information about the concentration, energy level and thermal capture cross section of deep levels. In addition, if one wants to really understand the deep level properties, several

experimental approaches must be used. As is generally the case in atomic structure of defects, optical measurements such as photocapacitance (PHCAP) are very useful tool. They provide information not only about the optical ionization energies of the levels but also about the electron-phonon interaction and temperature dependence of the energy level. Furthermore, the samples and measurement system used for PHCAP are the same as those used for the thermal spectroscopy of deep levels such as DLTS. This will give the most reliable results and yield a clear identification of the investigated levels.

In this chapter, the electrical behavior of deep levels and the basic analysis of the capacitance spectroscopy are described, and the principles of DLTS and PHCAP are summarized.

2.2 Occupation Function of The Deep Level

Figure 1 shows the interaction between the deep level lying in the forbidden gap and the free electron and hole. It consists of four processes[2]:electron capture, electron emission, hole capture and hole emission. The rate equation of the electron occupancy function f_T of the level is

$$\frac{df_T}{dt} = -(e_n^t+e_n^o)f_T+(e_p^t+e_p^o)(1-f_T)+nC_n(1-f_T)-pC_pf_T \quad (2.1)$$

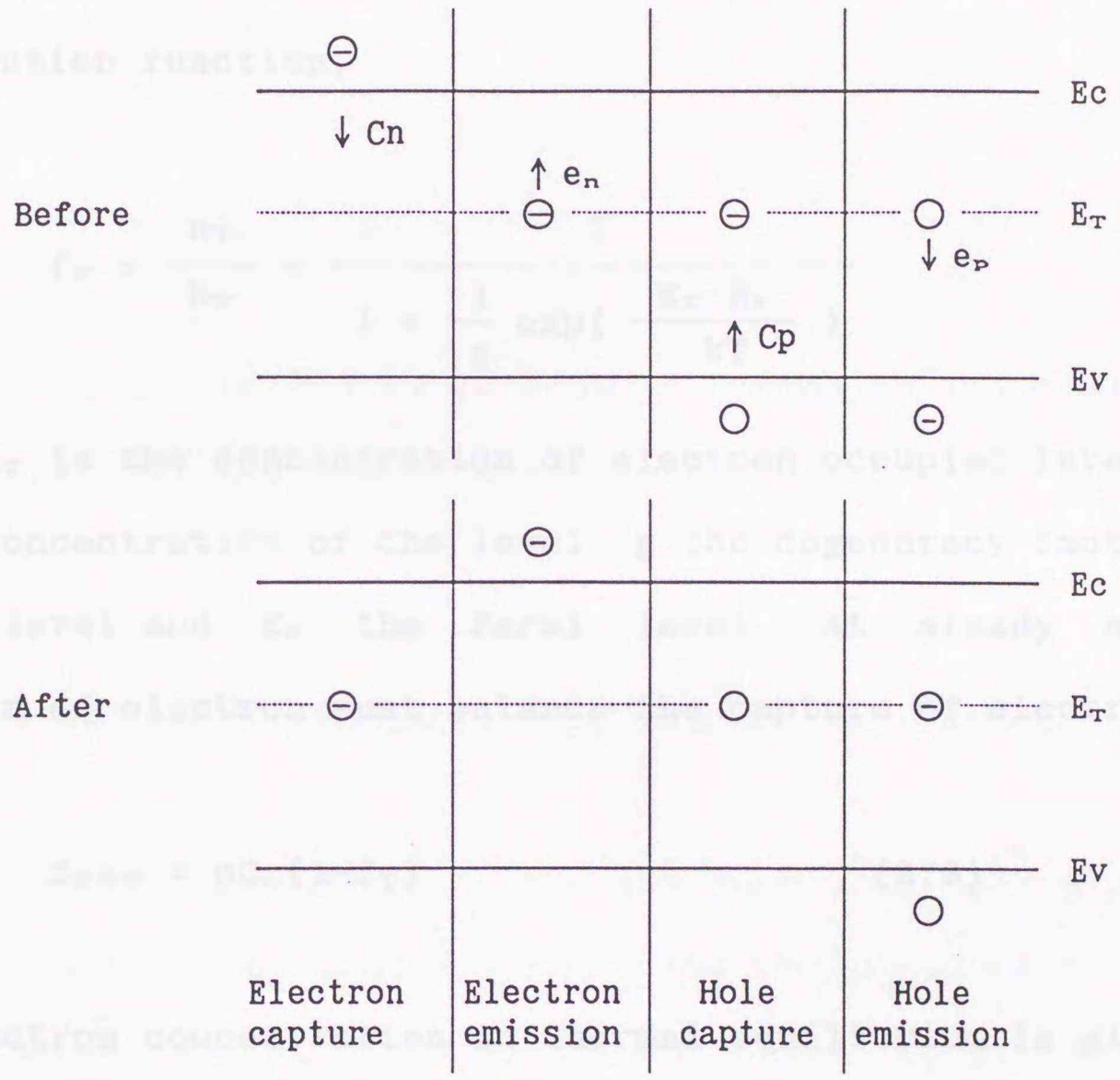

Figure 1. Schematic summary of the emission and capture process which describe a particular level in the bandgap.

where e_n^t and e_p^t are the thermal emission rates, e_n^o and e_p^o the optical emission rates, C_n and C_p the capture probabilities and n and p the concentrations for electrons and holes, respectively.

In thermal equilibrium, f_T is given by the Fermi-Dirac distribution function,

$$f_T = \frac{n_T}{N_T} = \frac{1}{1 + \frac{1}{g}\exp\left(\frac{E_T - E_F}{kT}\right)} \qquad (2.2)$$

where n_T is the concentration of electron-occupied level, N_T the total concentration of the level, g the degeneracy factor, E_T the energy level and E_F the Fermi level. At steady state, the emission of electron must balance the capture of electron.

$$f_T e_n = nC_n(1-f_T) \qquad (2.3)$$

The electron concentration in thermal equilibrium is given by

$$n = N_C \exp\left(\frac{E_C - E_F}{kT}\right) \qquad (2.4)$$

where N_C is the effective density of states in the conduction band and E_C the energy level of the conduction band. Equations (2.2), (2.3) and (2.4) reduce to

$$e_n = \frac{C_n N_C}{g} \exp\left(-\frac{E_C - E_T}{kT}\right). \qquad (2.5)$$

Similarly, the relationship between the emission rate e_p and the capture probability C_p for holes is expressed as

$$e_p = g C_p N_V \exp\left(-\frac{E_T - E_V}{kT}\right) \qquad (2.6)$$

where N_V is the effective density of states in the valence band and E_V the energy level of the valence band.

2.3 Bias and Time dependence of Junction Capacitance

A schottky barrier on n-type semiconductor or p^+n junction will be considered. Figure 2 shows the change of band bending and space charges during bias voltage switching. In steady state the charge state of the deep level above the Fermi level is positive as shown in Fig.2 (a). By a change of the bias applied to the junction (Fig.2 (b)), the depletion width w(t) as well as the crossover position ($x_\lambda(t)$) of Fermi level and the deep level will be shifted. Then, the electrons trapped at $x_A < x < x_\lambda(t)$ are emitted according to the change of the occupation function. Thus, both effects, variation of bias and ionization of the deep level, cause a change in junction capacitance.

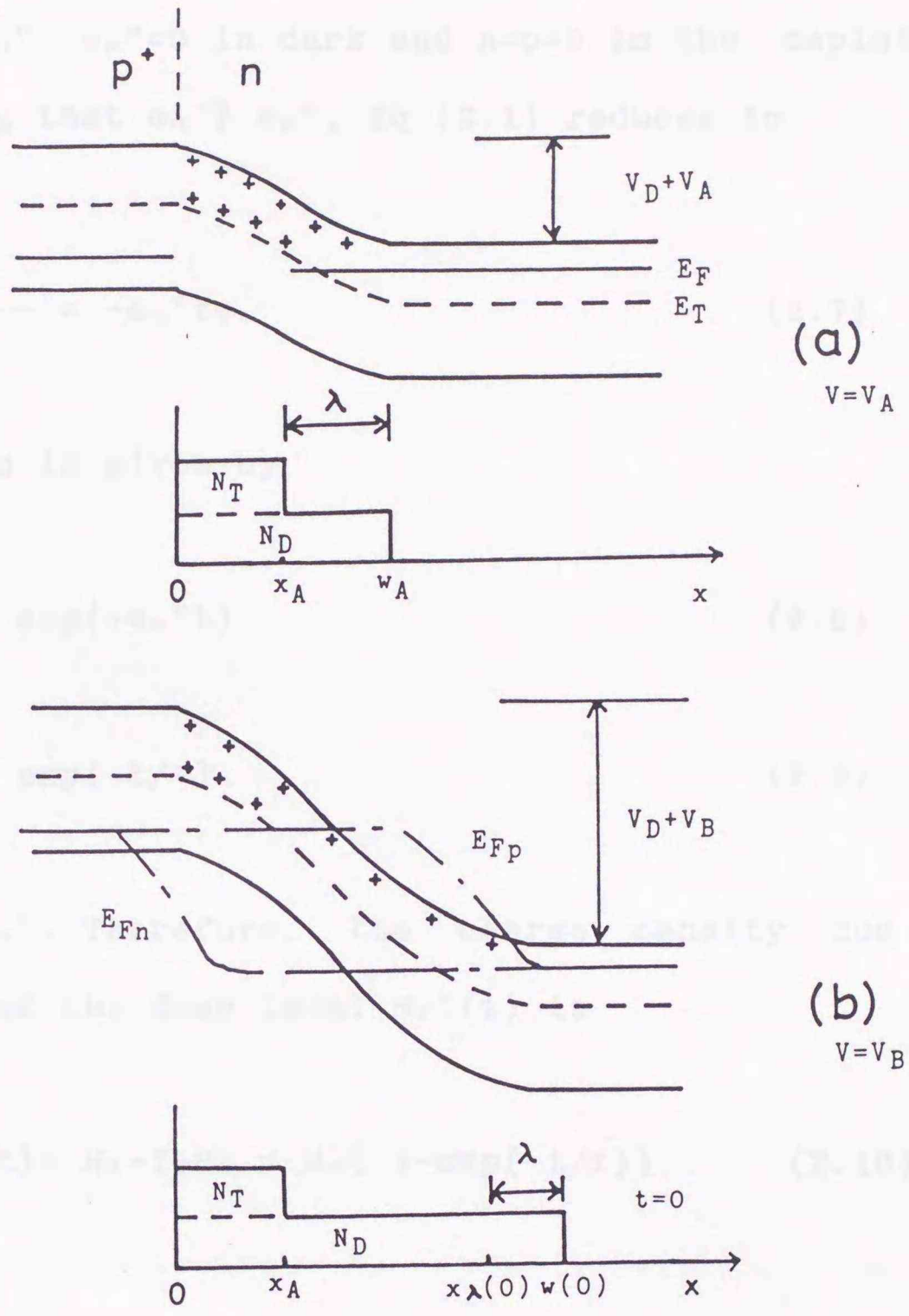

Figure 2. The change of band bending and space charge distribution during voltage switching.

Since e_n°, $e_p^{\circ}=0$ in dark and n=p=0 in the depletion region, and assuming that $e_n^{t} \gg e_p^{t}$, Eq.(2.1) reduces to

$$\frac{df_T}{dt} = -e_n^{t} f_T. \qquad (2.7)$$

The solution is given by

$$f_T = \exp(-e_n^{t} t) \qquad (2.8)$$

or

$$f_T = \exp(-t/\tau) \qquad (2.9)$$

where $\tau=1/e_n^{t}$. Therefore, the charge density due to thermal ionization of the deep level $N_T^{+}(t)$ is

$$N_T^{+}(t)= N_T-f_T N_T = N_T\{ 1-\exp(-t/\tau)\}. \qquad (2.10)$$

From a double integration of Poisson's equation over the depletion region

$$\frac{\varepsilon(V_D+V_B)}{q} = \int_0^{x_A} (N_D+N_T)x\,dx + \int_{x_A}^{x_\lambda(t)} (N_D+N_T^{+}(t))x\,dx + \int_{x_\lambda(t)}^{w(t)} N_D x\,dx \qquad (2.11)$$

where V_D is the diffusion potential, V_B the bias voltage and N_D the shallow donor concentration. Since $x_\lambda(t)=w(t)-\lambda$, the depletion width w(t) can be written as follows:

$$w(t) = \frac{\lambda N_T^+(t) + \sqrt{\{\lambda N_T^+(t)\}^2 - \{N_D+N_T^+(t)\}\{N_T X_A^2 + N_T^+(t)(\lambda^2 - X_A^2) - \frac{2\varepsilon(V_D+V_B)}{q}\}}}{N_D+N_T^+(t)} \qquad (2.12)$$

where

$$\lambda = \sqrt{2\varepsilon(E_F-E_T)/(qN_D)}. \qquad (2.13)$$

The junction capacitance, therefore, is given by

$$C(t) = \frac{\varepsilon S}{w(t)}. \qquad (2.14)$$

If the concentration of deep level, N_T, is very small compared with that of the shallow donor concentration, N_D, $x_\lambda(t)$ nearly equals $x_\lambda(t=\infty)$. In this case, the capacitance transient can be expressed as

$$\begin{aligned} C(t) &= C(0) + \{C(\infty)-C(0)\}\{1-\exp(-t/\tau)\} \\ &= C(0) + \Delta C \{1-\exp(-t/\tau)\} \end{aligned} \qquad (2.15)$$

where $C(0)$ is the capacitance at $t=0$, i.e., just after applying the bias V_B, $C(\infty)$ the capacitance at $t=\infty$ and τ the transient

time constant.

2.4 Deep Level Transient Spectroscopy (DLTS)[1)]

The basic idea of DLTS is the rate-window concept, which is shown in Fig.3. If the pulsed bias shown in Fig.3 (a) is applied to the Schottky or p^+n diode, the junction capacitance C(t) changes according to Eq.(2.14) as shown in Fig.3 (b). The capacitance transient is sampled at two times t_1 and t_2. DLTS signal, S(T), is defined as the difference between the capacitance at time t_1 and the capacitance at time t_2

$$S(T) = C(t_2) - C(t_1). \qquad (2.16)$$

In the case that $N_D \gg N_T$, S(T) can be written from Eq.(2.15) as

$$S(T) = \Delta C\{ \exp(-t_1/\tau) - \exp(-t_2/\tau) \}. \qquad (2.17)$$

According to Eq.(2.5), the transient time constant, τ, isvery large for low temperatures and becomes smaller as the temperature is increased. It is clear from Fig.3 (c) that S(T) goes through a maximum when τ is on the order of t_2-t_1. The relationship between τ_{max}, which is the value of τ at the maximum of S(T), and t_1 and t_2 is simply determined by differentiating

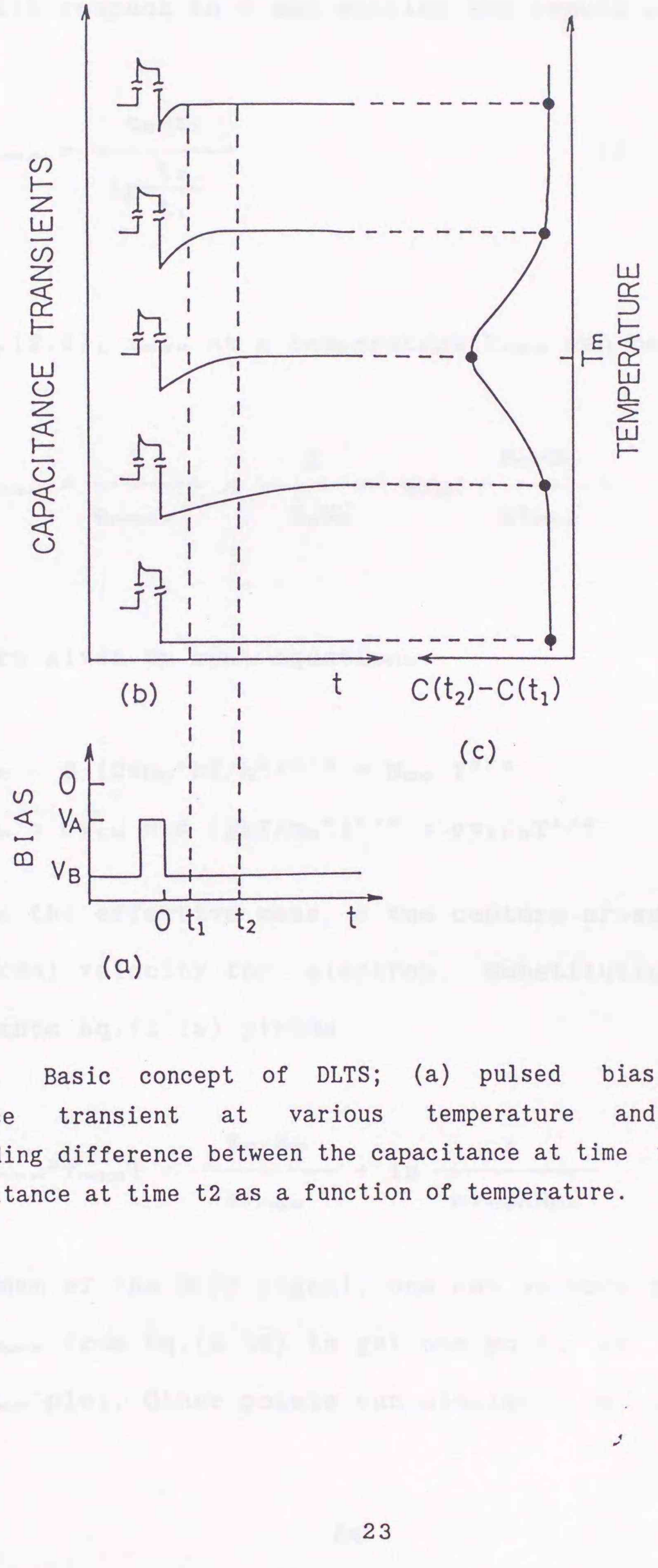

Figure 3. Basic concept of DLTS; (a) pulsed bias, (b) capacitance transient at various temperature and (c) corresponding difference between the capacitance at time t1 and the capacitance at time t2 as a function of temperature.

Eq.(2.17) with respect to τ and setting the result equal to zero.

$$\tau_{max} = \frac{t_2 - t_1}{\ln \frac{t_2}{t_1}} \qquad (2.18)$$

From Eq.(2.5), τ_{max} at a temperature T_{max} can be given as

$$\tau_{max} = \frac{1}{e_{nmax}} = \frac{g}{C_n N_C} \exp\left(\frac{E_C - E_T}{kT_{max}}\right). \qquad (2.19)$$

N_C and C_n are given by next equations.

$$N_C = 2\,(2\pi m_n^* kT/h^2)^{3/2} = N_{Co}\,T^{3/2} \qquad (2.20)$$

$$C_n = \sigma v_{th} = \sigma\,(3kT/m_n^*)^{1/2} = \sigma v_{tho} T^{1/2} \qquad (2.21)$$

where m_n^* is the effective mass, σ the capture cross section and v_{th} the thermal velocity for electron. Substituting Eqs.(2.20) and (2.21) into Eq.(2.19) yields

$$\ln(T_{max}^2 \tau_{max}) = \frac{E_C - E_T}{kT_{max}} + \ln \frac{1}{\sigma v_{tho} N_{Co}} \qquad (2.22)$$

At the maximum of the DLTS signal, one can measure the T_{max} and calculate τ_{max} from Eq.(2.18) to get one point of $\ln(T_{max}^2 \tau_{max})$ versus $1/T_{max}$ plot. Other points can similarly be obtained from

other scans made with different window settings, and thus different values of τ_{max} and differnt peak temperature. Therefore, one can easily get the energy level, E_T, and the capture cross section, σ, from Eq.(2.22). The magnitude of peak maximum of the DLTS signal can be related to the capacitance change, ΔC, by Eq.(2.17).

$$S_{max} = \Delta C\{ \exp(-t_1/\tau_{max}) - \exp(-t_2/\tau_{max}) \}. \qquad (2.23)$$

Just after applying the bias V_B (t=0), the deep level in the region $x_A<x<w(0)-\lambda$ is filled with electrons as shown in Fig.2 and we have

$$\frac{\varepsilon(V_D+V_B)}{q} = \int_0^{x_A} N_T x dx + \int_0^{w(0)} N_D x dx. \qquad (2.24)$$

When t=∞, the deep level in the region metioned above is ionized and the depletion width is decreased to the value of w(∞).

$$\frac{\varepsilon(V_D+V_B)}{q} = \int_0^{w(\infty)-\lambda} N_T x dx + \int_0^{w(\infty)} N_D x dx \qquad (2.25)$$

It is assumed that the bias voltage V_B is constant during the transient, then the next expression is obtained,[3]

$$N_T = \frac{\{\frac{w(0)}{w(\infty)}\}^2 - 1}{\{1- \frac{\lambda}{w(\infty)}\}^2 - \{\frac{w_A-\lambda}{w(\infty)}\}^2} N_D \qquad (2.26)$$

From Eq.(2.14), Eq.(2.26) reduces to

$$N_T = \frac{\frac{2C(\infty)\Delta C - \Delta C^2}{\{C(\infty)-\Delta C\}^2}}{\{1- \frac{\lambda}{w(\infty)}\}^2 - \{\frac{w_A-\lambda}{w(\infty)}\}^2} N_D \qquad (2.27)$$

where w_A and $w(\infty)$ are the steady depletion width under the bias V_A and V_B, respectively, and are obtained from the corresponding values of the capacitance. In the case that $N_D \gg N_T$ ($C(\infty) \gg \Delta C$) and w_A, $\lambda \ll w(\infty)$, Eq.(2.27) reduces to the well-known expression as follows:

$$N_T = \frac{2\Delta C}{C(\infty)} N_D \qquad (2.28)$$

When the concentration of the deep level approaches or exceeds that of the shallow donor, the DLTS signal has a tendency to lower the peak height and to shift the peak temperature. These effects will be discussed in the Appendix.

Figure 4 shows the block diagram of the DLTS measurement system. DLTS is mainly carried out by 1 MHz capacitance meter

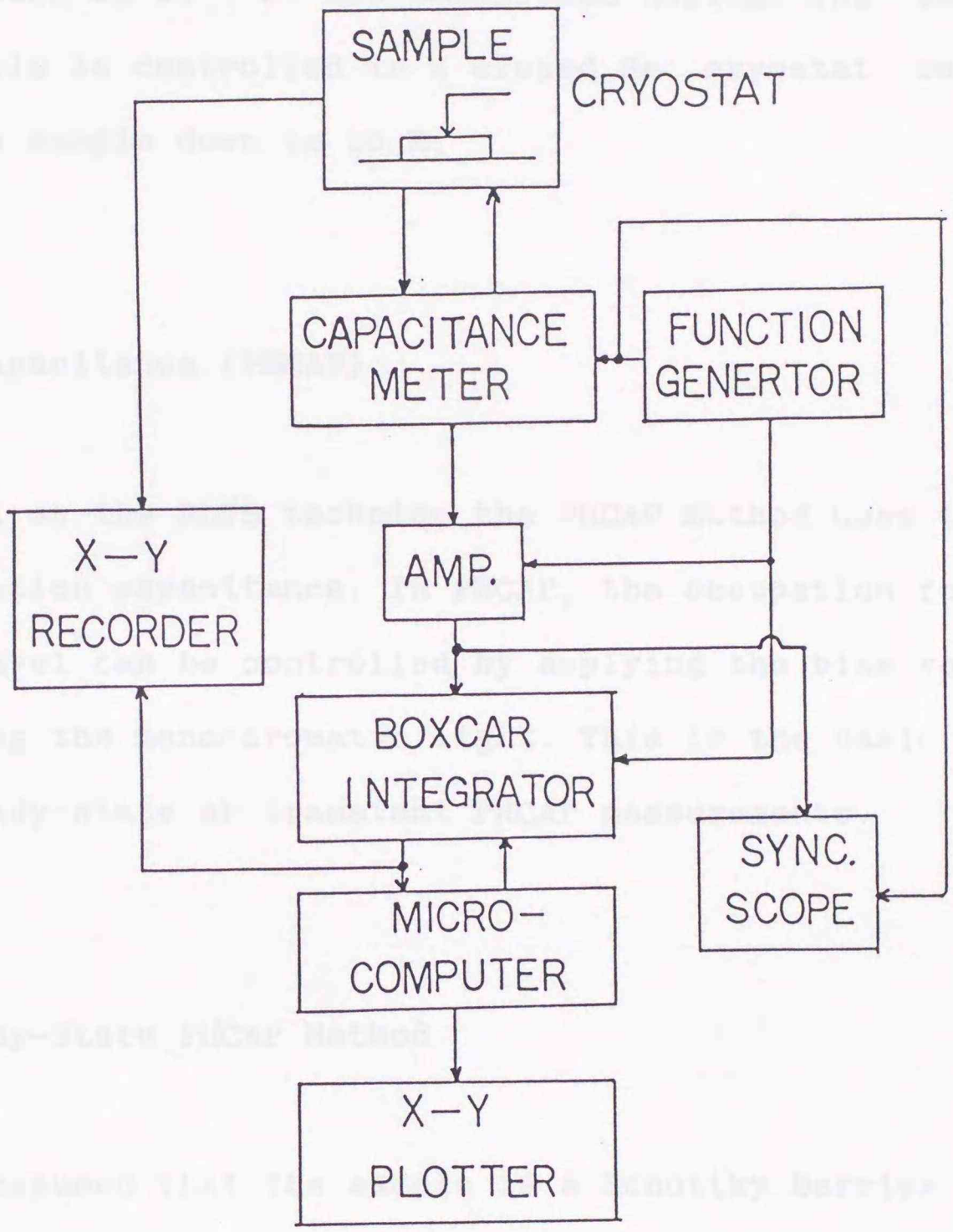

Figure 4. Block diagram of experimantal set-up used for DLTS.

with a responce time of 20 μs and a digital boxcar integrator. The detection limit of the concentration of the deep level in the present system is 10^{-4} of the background doping. The temperature of the sample is controlled in a closed He cryostat capable of cooling the sample down to 20 K.

2.5 Photocapacitance (PHCAP)

As well as the DLTS techniqe the PHCAP method uses the change of the junction capacitance. In PHCAP, the occupation function at the deep level can be controlled by applying the bias voltage and illuminating the monochromatic light. This is the basic idea of either steady-state or transient PHCAP measurements.

2.5.1 Steady-State PHCAP Method

It is assumed that the sample is a Schottky barrier in an n-type semiconductor with a donor-like deep level in the upper half of the bandgap (Fig.5 (a)). The sample is cooled from room temperature to low temperatures under a forward bias in the dark. This makes the deep level filled with a majority carriers, i.e., $f_T=1$ in almost whole depletion region. Then, the bias is changed step-wise to a reverse value, and the monochromatic light with photon energy $h\nu$ is illuminated.

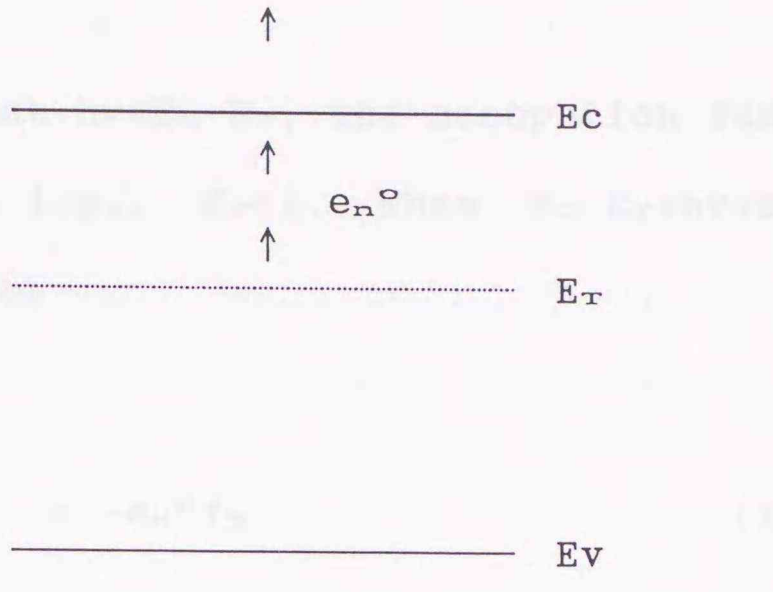

(a)

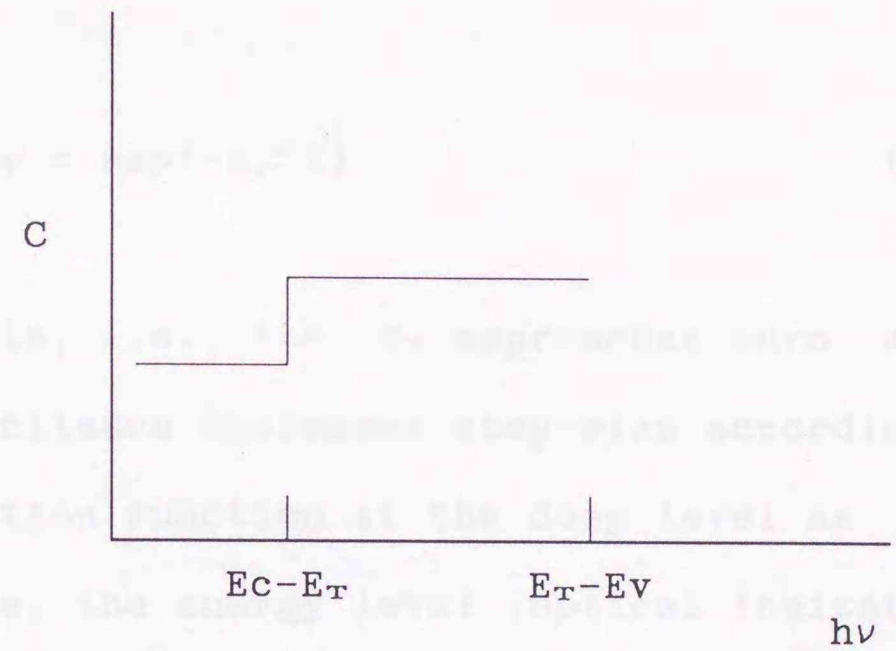

(b)

Figure 5. (a) Energy band diagram with a deep level in the upper half of the bandgap. (b) Steady state photocapacitance change. When the photon energy is chosen so that $E_C-E_T<h\nu<E_T-E_V$, the optical emission of electrons from the deep level takes place and the corresponding step-wise capacitance change can be observed.

In the case that $h\nu<E_C-E_T$, the occupation function maintains its initial state, i.e., $f_T=1$. When $E_C-E_T<h\nu<E_T-E_V$, the rate equation is given by

$$\frac{df_T}{dt} = -e_n^{\circ} f_T \qquad (2.29)$$

The solution of Eq.(2.29) with the initial condition $f_T(t=0)=1$ gives

$$f_T = \exp(-e_n^{\circ} t) \qquad (2.30)$$

In steady state, i.e., $t=\infty$, f_T approaches zero. At $h\nu\simeq E_C-E_T$ the junction capacitance increases step-wise according to the change of the occupation function at the deep level as shown in Fig.5 (b). Therefore, the energy level (optical ionization energy) of the deep state can be determined from the photon energy by which the step-wise capacitance change takes place.

2.5.2 Transient PHCAP Method

The optical emission rate is correlated to the optical cross section by the relation

$$e^{\circ} = \sigma^{\circ}\Phi \qquad (2.31)$$

where Φ is the photon flux. Since the optical cross sections provide information about their relation with the conduction and valence band, they contribute to physical syudies of the deep level.

Since the time constant of the PHCAP transient can be large, it is difficult to reach the steady state condition. So, the steady state PHCAP spectrum is a complex function of the $h\nu$-sweeping rate. This makes it difficult to obtain absolute photoionization cross sections. Absolute values of optical cross sections can generally be obtained from the time constant of the capacitance transient.

At low temperature, the rate equation of the occupation function at the deep level in the depletion region is given as

$$\frac{df_T}{dt} = -e_n^{\circ} f_T + e_p^{\circ}(1-f_T) \qquad (2.32)$$

Choosing the initial condition such that $f_T(0)=1$ by applying forward bias, the solution of Eq.(2.32) can be written as

$$f_T = \frac{e_p^{\circ}}{e_n^{\circ}+e_p^{\circ}} \{ 1 + \frac{e_n^{\circ}}{e_p^{\circ}} \exp[-(e_n^{\circ}+e_p^{\circ})t] \} \qquad (2.33)$$

Therefore, the charge density due to optical ionization of the deep level, $N_T^+(t)$, is

$$N_T^+(t) = N_T - f_T N_T = \frac{e_n^\circ N_T}{e_n^\circ + e_p^\circ} \{ 1 - \exp(-t/\tau) \} \qquad (2.34)$$

where

$$\tau = \frac{1}{e_n^\circ + e_p^\circ} = \frac{1}{\Phi(\sigma_n^\circ + \sigma_p^\circ)} . \qquad (2.35)$$

From a double integration of Poisson's equation over the depletion region and from Eq.(2.14), the junction capacitance can be expressed as follows:

$$C(t) = \sqrt{\frac{q\varepsilon}{2(V_D + V_B)}} \sqrt{N_D + N_T^+(t)} . \qquad (2.36)$$

In the case that $N_D \gg N_T$, Eq.(2.36) reduces to

$$C(t) = C(0)\{1 + \frac{N_T}{2N_D} \frac{\sigma_n^\circ}{\sigma_n^\circ + \sigma_p^\circ} [1 - \exp(-t/\tau)]\}. \qquad (2.37)$$

Equations (2.35) and (2.37) show that the time constant of the capacitance transient is generally related to the sum of two

optical cross sections. If one can choose the photon energy range where one of the two terms is negligible, the remaining optical cross section is simply determined by measuring the time constant. However, this does not avoid the trouble rising from the mixing between σ_n^o and σ_p^o for the deep level lying in the vicinity of midgap.

Chantre et al.[4] proposed new method to evaluate the optical cross sections independently. If, at t=0, the deep level is filled with electrons, the concentration of electrons trapped at the deep level, n_T, can be expressed as

$$\left(\frac{dn_T}{dt}\right)_{t\to o} = -e_n^o N_T = -\sigma_n^o \Phi N_T \qquad (2.38)$$

This means that the initial time constant of photoionization of the deep level can be governed by the optical cross section for electron emission. The initial derivative of the capacitance transient is given by Eq.(2.37) as follows:

$$\left.\frac{\Delta C(t)}{dt}\right|_{t\to o} = \frac{1}{\tau_{ini}} \Delta C(\infty) \qquad (2.39)$$

where $\Delta C(t) = C(t)-C(0)$, $\Delta C(\infty)=C(\infty)-C(0)$ and τ_{ini} is the value of τ at the initial state. Thus, the optical cross section of the deep level for electron emission is obtained by measuring the

initial derivative of the capacitance transient just after the biginning of the illumination. On the other hand, if, at t=0, the deep level is emptied, then the same measurement will lead to the value of the optical cross section for hole emission.

References

1) D.V Lang, J.Appl.Phys., 45, 3023(1974)

2) A.G.Milnes, *Deep Impurities in Semiconductors* (John Wiley & Sons, New York, 1973), p.11

3) Y.Zohta and M.O.Watanabe, J.Appl.Phys.,53,1809(1982)

4) A Chantre,G.Vincent and D.Bois, Phys.Rev.B,23,5335(1981)

CHAPTER 3

CHARACTERIZATION OF DEEP ELECTRON LEVELS IN GaAs GROWN BY THE LIQUID ENCAPSULATED CZOCHRALSKI METHOD

3.1. Introduction

Semi-insulating (SI) GaAs substrate grown by the liquid encapsulated Czochralsky (LEC) method has been considered to be a key material to improve the performance of compound semiconductor integrated circuits (ICs) or optoelectronic ICs (OEICs). The quality of the substrate is greatly influenced by the nature of the native defects and chemical impurities in the material, which are associated with the thermodynamic growing conditions and the chemical composition of the starting melt. These defects and impurities, or their complex have a tendency to introduce the deep energy states in the band gap. In LEC undoped GaAs, it has been shown that there are two dominant native defects: one is a well-known donor state called EL2 and the other is a double acceptor state with activation energies of 78 and 200 meV .[1,2]

The reason that undoped LEC GaAs grown from stoichiometric or

As-rich melt has a semi-insulating property has been considered to be that EL2 mainly compensates the residual carbon acceptor. Thus, much work has been reported on the EL2 state.[3-13] Moreover, the microscopic structure of the native defects and their complex in GaAs has been theoretically investigated,[10,14,15] and some atomic models of EL2 such as isolated As_{Ga} (antisite aresenic),[7] As_{Ga}-V_{As} (As vacancy) pair,[16-18] As cluster,[6] As_{Ga}-divacancy pair[19] and As_{Ga}-As_I (As interstitial) pair[20] have been proposed.

A double acceptor state has been considered to act as a main defect level in the compensation mechanism in undoped LEC GaAs grown only from Ga-rich melt.[1] However, von Bardeleben et al[21] recently suggested that the double acceptor exists in concentrations of 10^{15}-10^{16} cm^{-3} even in materials grown from stoichiometric or As-rich melts ($0.45 \leqq As/(As+Ga) \leqq 0.52$). This indicates that, in LEC SI GaAs, a new compensation system including both EL2 and the double acceptor state will be needed.

By comparison, relatively little has been reported on the other electron traps in GaAs, in spite of the fact that they often have almost the same concentration as EL2 in bulk materials. Recently, Terashima et al[22] and Washizuka et al[23] reported that the concentration of the residual carbon impurity is able to be reduced in the range of 10^{15} cm^{-3} in undoped GaAs by means of a horizontal magnetic field applied technique and the

use of an AlN hot zone furnace. They suggested that the reduction of carbon impurity can improve the thermal stability and the uniformity of resistivity distribution in the SI substrate. However, the reduction of carbon impurity would produce an effect on the compensation mechanism in LEC GaAs and cause a decrease in the resistivity of undoped material, i.e. the semi-insulating properties of the materials cannot be maintained due to the electron traps in the upper half of the band gap. To overcome this problem, it is of importance to clarify the properties of the electron traps in LEC GaAs.

The purpose of this chapter is, therefore, to investigate the electrical properties of electron traps in n-type LEC GaAs, especially focusing on the traps other than EL2. Temperature-dependent Hall measurement indicates that the electron trap with an activation energy of about 0.2 eV plays an important role in the compensation mechanism in as-grown material which has a low content of carbon impurity. The effect of face-to-face annealing on the electron traps is also discussed.

3.2 Samples

The GaAs crystal used in this investigation was grown in the (100) direction from As-rich melt using a PBN crucible. Dry

B_2O_3 was used as an encapsulant and the pressure of the Ar ambient was 30 atm during growth. To achieve a low resistivity crystal, the undoped melt is intentionally synthesized with low purity arsenic and gallium. The crystal was n-type along the ingot. The resistivity of the front section of the crystal ($g<0.3$, where g is the fraction solidified) was in the range above 10^6 Ωcm, whereas the resistivity of the tail section of the crystal decreased in the range of 10^4 Ω cm to 10^{-1} Ω cm as g increased from 0.3 to 0.9. Since the concentration of carbon was distributed uniformly along the ingot, this resistivity variation seems to be due to the segregation of donor impurities contained in the starting melt and/or due to native donor-defects in the upper half of the band gap that increase with the stoichiometric change of the melt.

The n-type wafers used to characterize the properties of deep states were taken from the tail section of the crystal ($g=0.89$). The carrier concentration and mobility of the crystal, estimated from Hall measurement, are 4×10^{15} cm^{-3} and 5000 $cm^2/Vsec$, respectively. Wafers were cleaned with organic solvents and then etched in $H_2SO_4:H_2O_2:H_2O = 5:1:1$ solution for 1 minute to remove surface damage. Ohmic contacts were fabricated on the unpolished side of the wafer using indium followed by annealing at 400 C for 10 min under N_2 atmosphere. For capacitance-voltage (C-V) and DLTS measurements, 1000 A Al or Au dot Schottky diodes (diameter approximately 800 μm) were

formed.

3.3 Results and Discussion

3.3.1 Electron Traps in Undoped Materials

Figure 1 shows a typical DLTS signal observed in the tail sections of the undoped n-GaAs. The shallow impurity concentration, N_D, obtained from C-V measurement was 7×10^{15} cm^{-3}. Six levels, labelled E1 to E6, are detected. As seen, the maxima of E2, E3 and E4 are very close together. These three levels were distinguished by means of theoretical curve fitting, since this configuration might cause problems in the determination of the activation energy and concentration.

Since the concentration of deep levels in melt-grown GaAs often exceeds the net concentration of shallow impurities, DLTS signal has a tendency to increase the half width of the peak, to lower the peak height, and to shift the peak position toward lower temperatures. The reason why these effects occur is that the time dependence of the capacitance transient corresponding to trapped electron emission from deep states is no longer exponential.[24] Therefore, DLTS signal is simulated in the case $N_T \geqq N_D$. The simulation indicated that the activation energy obtained from standard DLTS measurement is almost correct, even

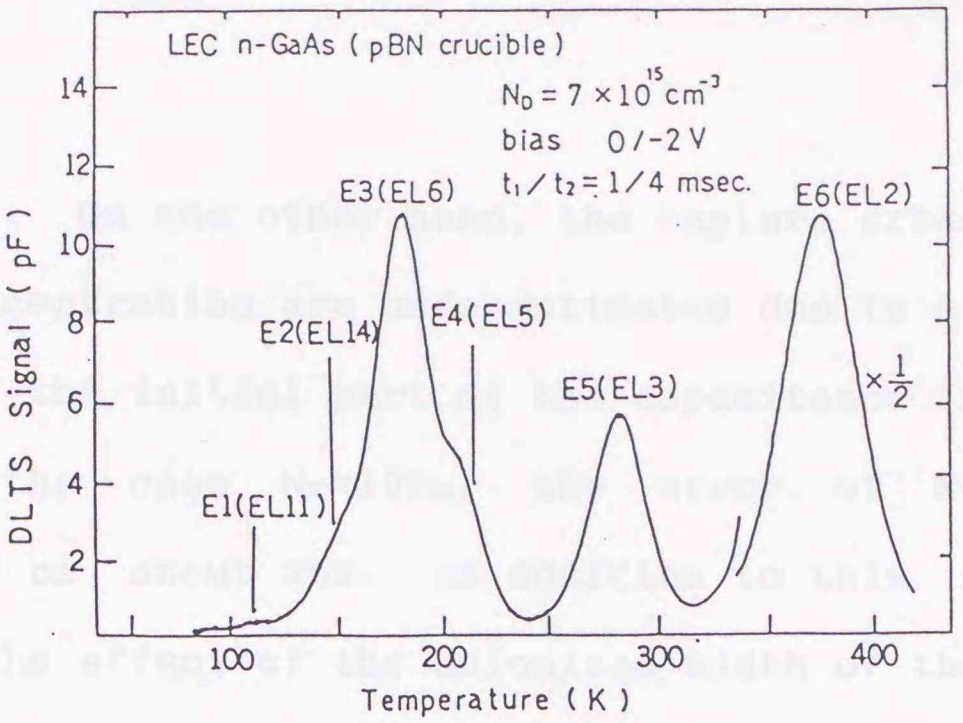

Figure 1. A typical DLTS signal from electron traps in undoped LEC n-GaAs grown from a PBN crucible.

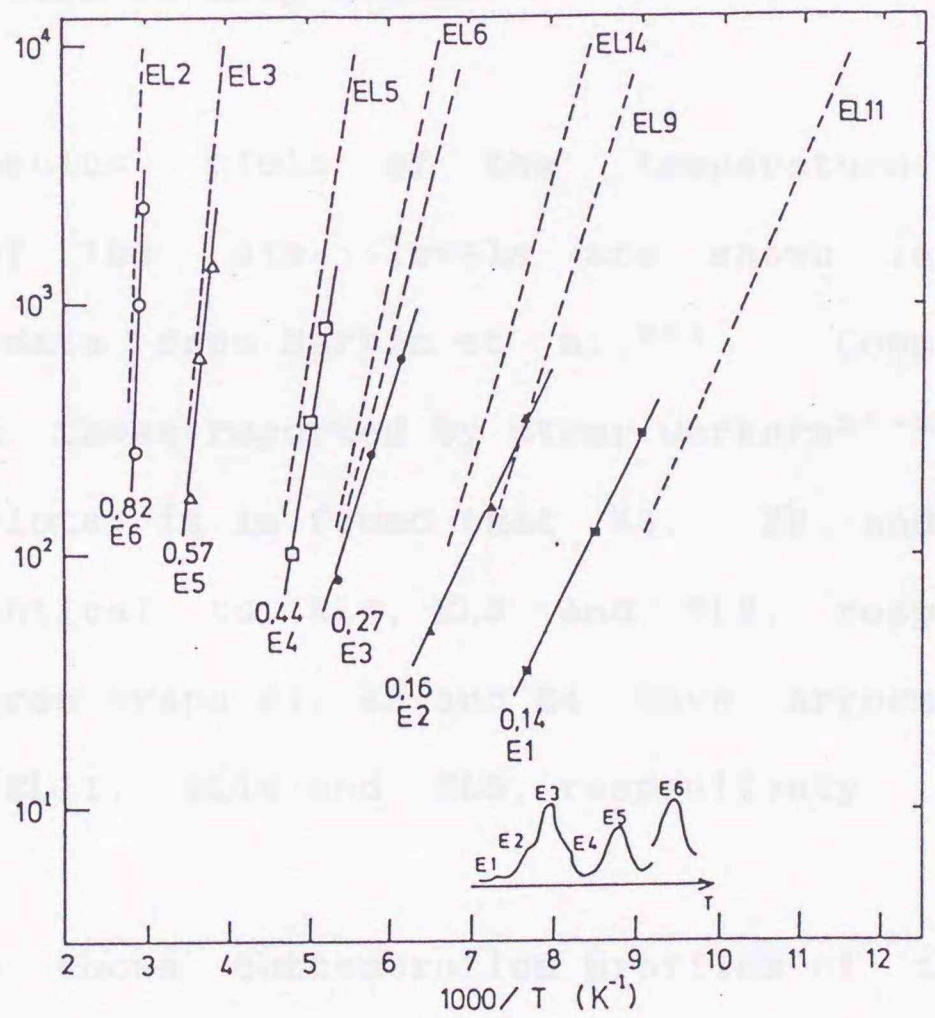

Figure 2. Arrhenius plots of six traps observed together with comparative data from Martin et al.(1979). Numbers indicate the activation energy.

when $N_T=10N_D$. On the other hand, the capture cross section and the trap concentration are underestimated due to a fast decaying component of the initial part of the capacitance transient. For example, in the case $N_T=10N_D$, the error of N_T for EL2 is estimated to be about 30%. In addition to this simulation, we considered the effect of the unionized width of the deep state in the depletion region in the estimation of N_T, that is the so-called λ effect.[25] This effect is more serious when the injection pulse height is relatively smaller than the bias voltage. These analytical methods were applied to the calculation of concentration of deep states.

The Arrhenius plots of the temperature-corrected time constants of the six levels are shown in Fig. 2 with comparative data from Martin et al.[26] Comparing our DLTS signal with those reported by other workers[27-30] and from the Arrhenius plots, it is found that E3, E5 and E6 were most probably identical to EL6, EL3 and EL2, respectively. The remaining three traps E1, E2 and E4 have Arrhenius plots close to those of EL11, EL14 and EL5, respectively.

Figure 3 shows concentration profiles of the traps. To obtain a deep level profile, the bias voltage was varied while the injection pulse height was kept constant. The concentrations of E4, E5 and E6 levels were almost uniformly distributed throughout the material, whereas E1, E2 and E3

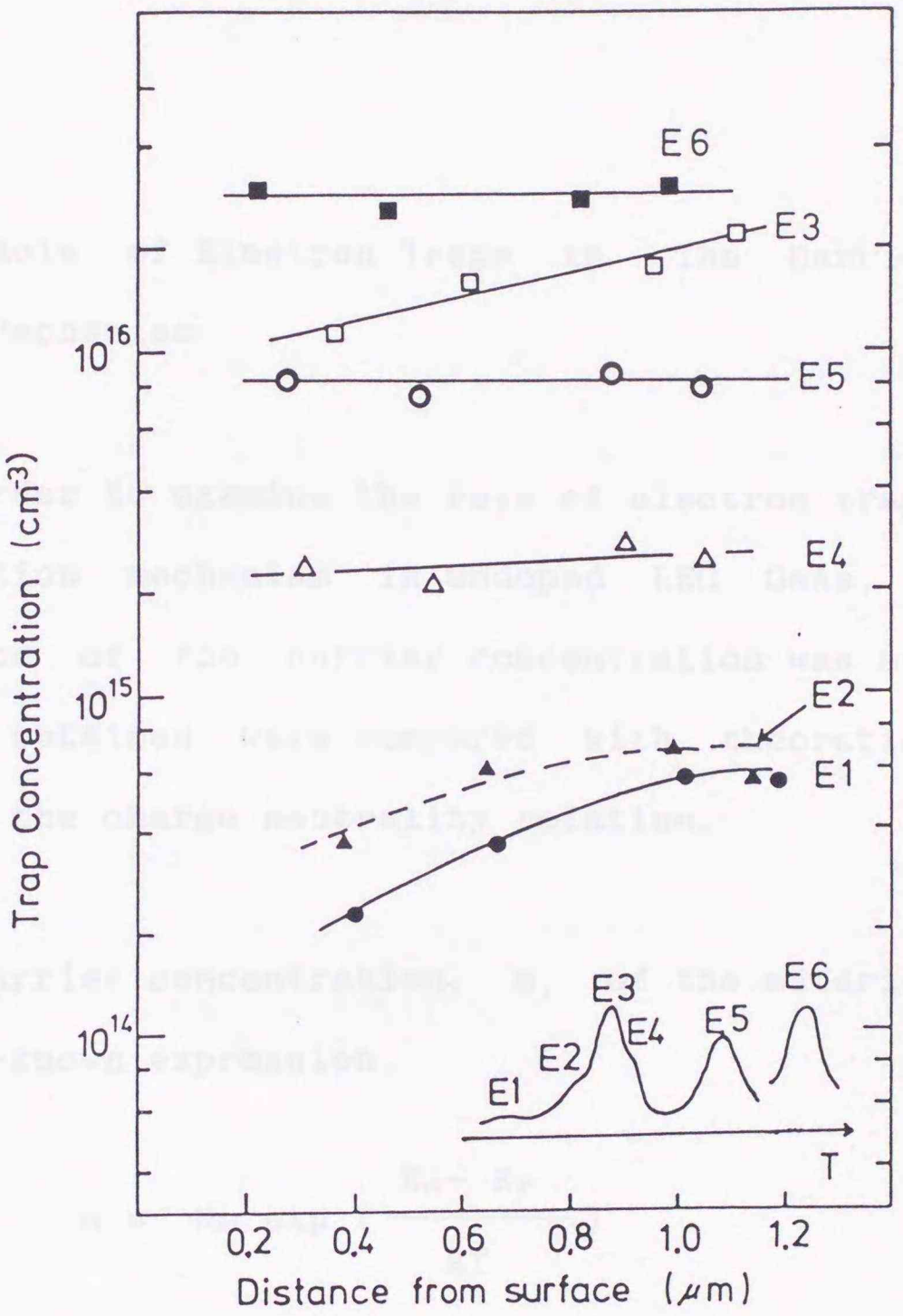

Figure 3. Concentration profiles of the electron traps.

decreased toward the Schottky barrier. This indicates that E1, E2 and E3 are related to the surface conditions or that the outdiffusion of defect elements associated with these traps occurs.

3.3.2 Role of Electron Traps in The Carrier Compensation Mechanism

In order to examine the role of electron traps in the carrier compensation mechanism in undoped LEC GaAs, the temperature dependence of the carrier concentration was measured and the results obtained were compared with theoretical calculations based on the charge neutrality relation.

The carrier concentration, n, of the material is governed by the well-known expression.

$$n = N_C \exp\left(\frac{E_G - E_F}{kT}\right) \qquad (3.1)$$

where N_C is the effective density of state in the conduction band, E_G the energy gap, E_F the Fermi level, k the Boltzmann's constant, and T the absolute temperature. The computation is carried out by determining the Fermi level position from the neutrality condition,

$$n + N_{Ai}^{-} = p + N_{Dj}^{+} \qquad (3.2)$$

where N_{Ai}^- and N_{Dj}^+ are the ionized acceptor- and donor concentrations, respectively.

$$N_{Ai}^- = N_{Ai}\left[1+\frac{1}{g}\exp\left(\frac{E_{Ai}-E_F}{kT}\right)\right]^{-1} \qquad (3.3)$$

$$N_{Dj}^+ = N_{Dj}\left[1+g\exp\left(\frac{E_{Dj}+E_F-E_G}{kT}\right)\right]^{-1} \qquad (3.4)$$

where N_{Ai} and N_{Dj} are the total acceptor- and donor concentrations, respectively, E_F is the Fermi-level, and E_{Ai} and E_{Dj} are the acceptor- and donor ionization energies, respectively. Each energy level is taken from the top of the balence band with a correction due to a possible temperature dependence of the capture cross section.[31] The degeneracy factor, g, is 4 for the shallow acceptor due to the fourfold degeneracy of the valence band, but, in the case of the deep acceptor the value of 2 is used as well as in the case of donors.[32] E_G can be written as a function of temperature,

$$E_G(T) = E_{Go} - aT^2/(b+T). \qquad (3.5)$$

For GaAs, the values of E_{Go}, a and b are 1.519, 5.405×10^{-4} and 204, respectively.[32]

Figure 4 shows the energy level model of undoped LEC GaAs. In calculation, it is considered that level E6 (EL2) acts as the carrier compensator and level E3 (EL6) as the donor

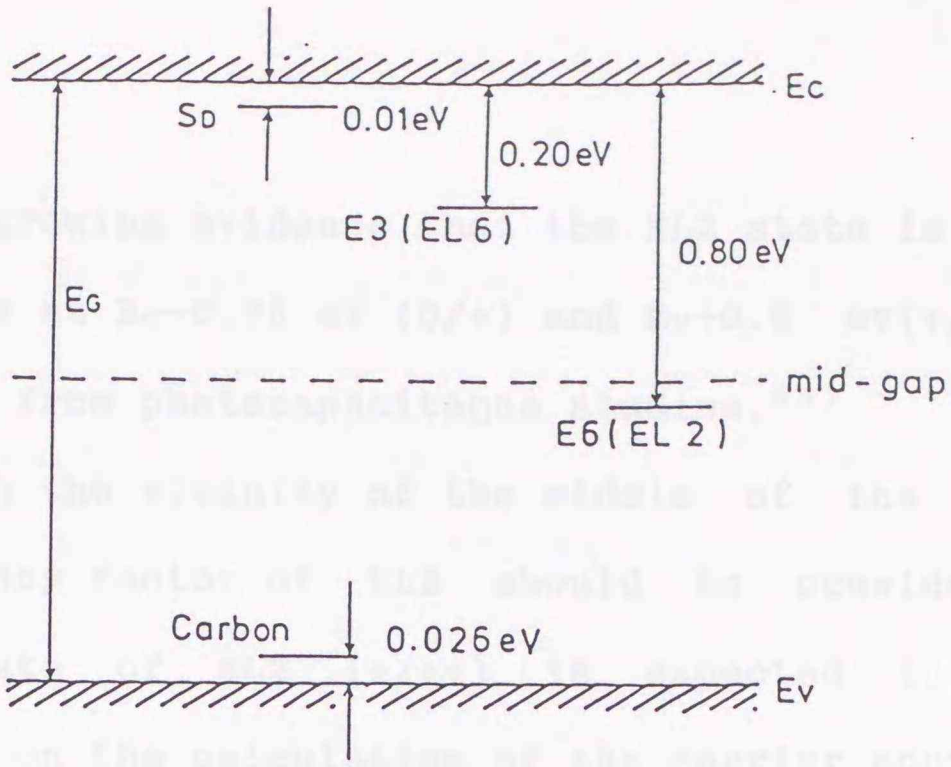

Figure 4. Band energy model of the dominant electron traps and residual impurities in undoped LEC n-GaAs.

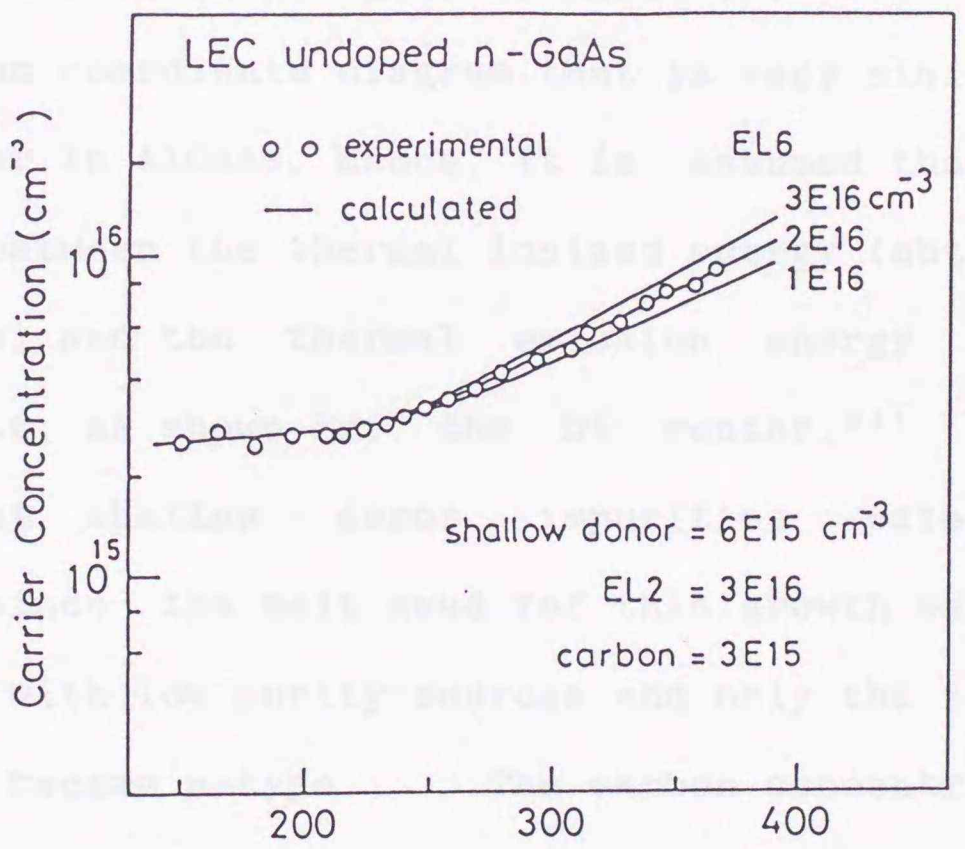

Figure 5. Temperature dependence of carrier concentration for as-grown GaAs. The solid curves represent theoretical calculations using the charge neutrality relation for assuming a shallow donor level in addition to the three-level (EL2, EL6 and carbon) model.

state. There is growing evidence that the EL2 state is a double donor with levels at E_C-0.75 eV (0/+) and E_V+0.5 ev(+/++). This has been derived from photocapacitance studies.[33] When the Fermi level is in the vicinity of the middle of the band gap, where the occupancy factor of EL2 should be considered, the second donor state of EL2 (+/++) is expected to have an important effect on the calculation of the carrier concentration. However, in n-type conductive material, EL2 is in its neutral state. Therefore, the first state of EL2 is took into account in the calculation. Chantre et al[31] reported that EL6 has the large Frank-Condon shift value of about 0.6 eV, suggesting the configuration coordinate diagram that is very similar to that of the DX center in AlGaAs. Hence, it is assumed that there was a difference between the thermal ionized energy (obtained from Hall measurements) and the thermal emission energy (obtained from DLTS) for EL6, as shown for the DX center.[34] It is also assumed that shallow donor impurities exist in this material, since the melt used for this growth was intentionally synthesized with low purity-sources and only the tail sections of the crystal became n-type. The carbon concentration, 3 x 10^{15} cm^{-3}, was determined by Fourier transform infrared spectroscopy (FTIR) using the calibration constant of 7 x 10^{15} cm^{-3} for the local vibrational mode (LVM) absorption, 1 cm^{-2}, reported by Kadota et al.[35]

Both the experimental results and the theoretical

calculations of the temperature-dependent carrier concentration of LEC n-GaAs are shown in Fig. 5. Experimental data are excellently fitted by the theoretical calculation based on the model illustrated in Fig.4. This suggests that the shallow donor impurities introduced by starting sources mainly cause the decrease in the resistivity of the crystal. Furthermore, E3 (EL6) seems to act as the donor state and to produce a strong effect on the carrier compensation mechanism in LEC GaAs in the temperature range above 250 K. The thermal ionized energy of EL6 is probably smaller than the thermal emission energy obtained by DLTS measurement, which is associated with the large Frank-Condon shift of this state.[31] Look and Walter[36] reported that native defects from 0.13 to 0.20 eV below the conduction band can dominate the electrical properties of several as-grown HB and LEC GaAs. From the results obtained from Hall analysis, EL6 might be one of the candidates for these levels.

Here, we will discuss in more detail the decrease in the resistivity of undoped crystal. Figure 6 illustrates the variations of the densities of the total positive charge (holes and ionized donors) and the total negative charge (electrons and ionized acceptors) as a function of the position of the Fermi level. For the samples used in the present work, the positive- and negative charges are represented by the heavy solid curves, and their intersection, E_F, gives the Fermi level needed to

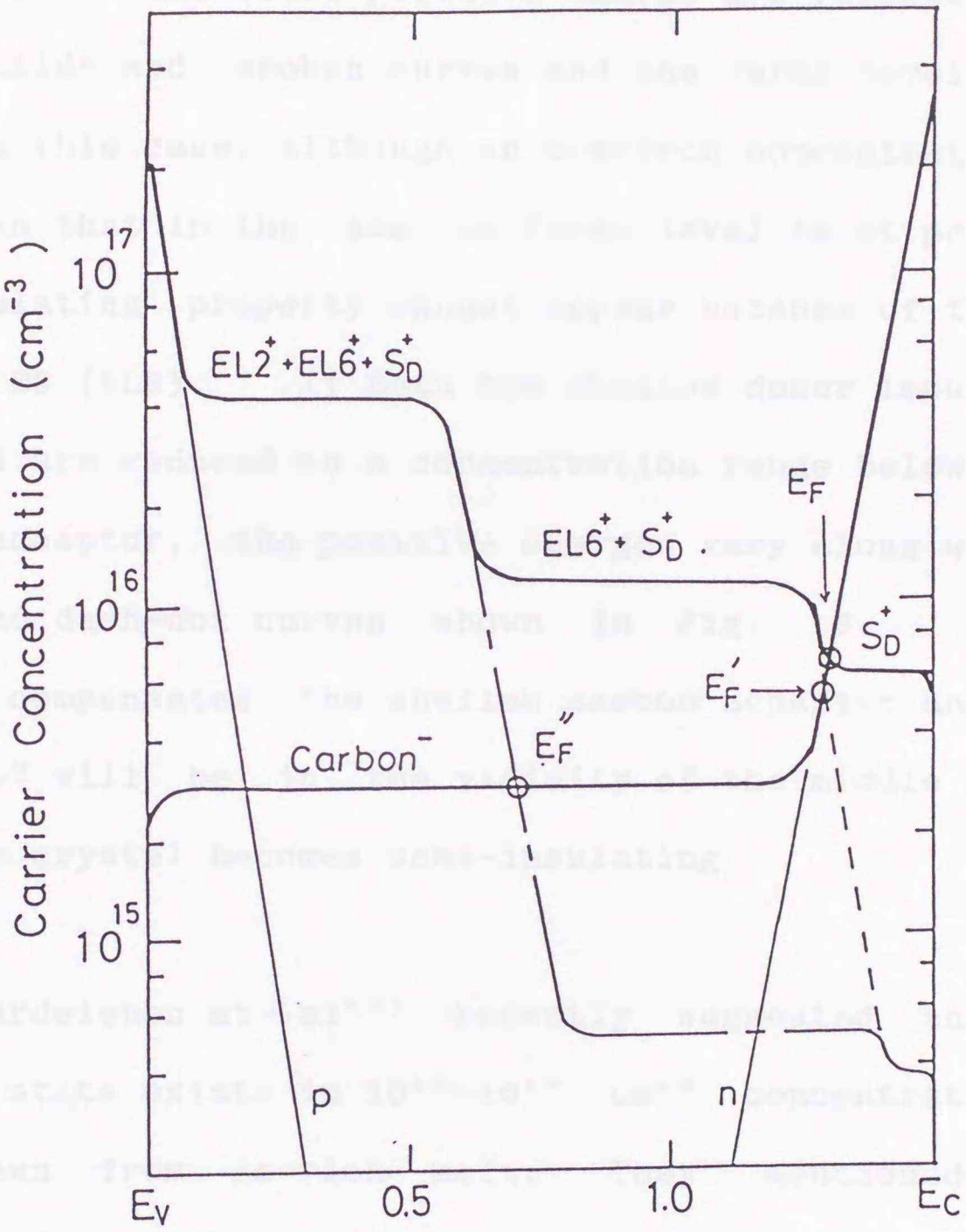

Figure 6. Graphic representation of the variations of the positive- and negative charges in LEC GaAs as a function of the position of the Fermi level.

satisfy charge neutrality [Eq.(3.2)]. When the concentration of the shallow donor (S_D) is below that of the carbon acceptor, the variations of the total positive charge are represented by the heavy solid- and broken curves and the Fermi level is at point E_F'. In this case, although an electron concentration has lower value than that in the case the Fermi level is at point E_F, the semi-insulating property cannot appear because of the existence of level E3 (EL6). If both the shallow donor impurity (S_D) and level E3 are reduced to a concentration range below that of the carbon acceptor, the positive charges vary along with the heavy solid- and dash-dot curves shown in Fig. 6. Since level E6 (EL2) compensates the shallow carbon acceptor and the Fermi level E_F" will be in the vicinity of the middle of the band gap, the crystal becomes semi-insulating.

Von Bardeleben et al[21] recently suggested that a double acceptor state exists in 10^{15}-10^{16} cm^{-3} concentrations in LEC GaAs grown from As-rich melt. They mentioned that low concentration of the residual acceptor ($\leqq 5 \times 10^{15}$ cm^{-3}) was inconsistent with the concentration of ionized EL2 studied by EPR in LEC SI GaAs. Therefore, further study on the characterization of the double acceptor state seems to be needed. For the material used in the present work, the effect of the double acceptor state on the compensation mechanism is less likely because of the annealing properties of the states (see next section); i.e. the decrease of electron states other than EL2 did

not cause the material to convert to one with semi-insulating property.

Recent improvements in the LEC growth technique have made it possible to reduce the carbon impurity to the concentration range of 10^{15} cm^{-3} in the undoped crystal,[22,23] as well as in the samples used in the present work. Thus, as mentioned above, the increase of the carrier concentration in undoped LEC crystal attributed to the deep donor states that are positioned in the upper half of the band gap may cause problems in the stability of the SI GaAs substrate. Therefore, it is necessary to reveal the properties of these states and to decrease their concentrations below that of the shallow acceptor.

3.3.3 Annealing Properties of Electron Traps

It is very important to evaluate the annealing properties of electron traps and clarify the relationship between their origins and the growth process or technique. Heat treatment was performed using face-to-face proximity capping by GaAs wafers in high purity H2 gas for 1 hour. After this, a thermal damage layer about 10 μm thick is removed from the surface to examine the annealing effect in the bulk.

DLTS signals of LEC GaAs before and after annealing at 800 C

are illustrated in Fig. 7, while Fig. 8 shows the concentration variations of the five electron traps versus the annealing temperature. Note that 400 C is the annealing temperature during ohmic contact fabrication and that the concentration shown in Fig. 8 is in the region about 1 μm from the Schottky contact. The concentrations of the observed traps were almost unchanged by 600 C heat treatment, whereas Auret et al.[28] reported that the concentration of EA8 (E1), EA4 (E3) and EA3 (E5) increased by a factor of 2 to 5 with 600 C annealing. One possible explanation of the difference may be that their results involve the effects of surface damage layer. Fang et al[30] indicated that EL2 becomes low in concentration in the surface region (about 1.7 μm under their annealing conditions).

After 800℃ annealing, the concentration of E1, E3 and E5 were reduced by more than an order of magnitude compared with that of the as-grown sample, whereas E2 and E4 remained more or less the same, as shown in Figs. 7 and 8. A similar result has been reported in undoped LEC material by Kitagawara et al[29] and in HB material by Fang et al.[30] It has been reported that the passivation of defect levels in GaAs is performed by both hydrogen plasma at 300 C[18,37] and H_2 ambient at 850 C with SiO_2 cap.[38] However, this effect appeared only in the surface region within several microns. Since the deep level probing depth in the present work is more than 10 μm from the surface, the decrease in the concentration of deep states is most likely

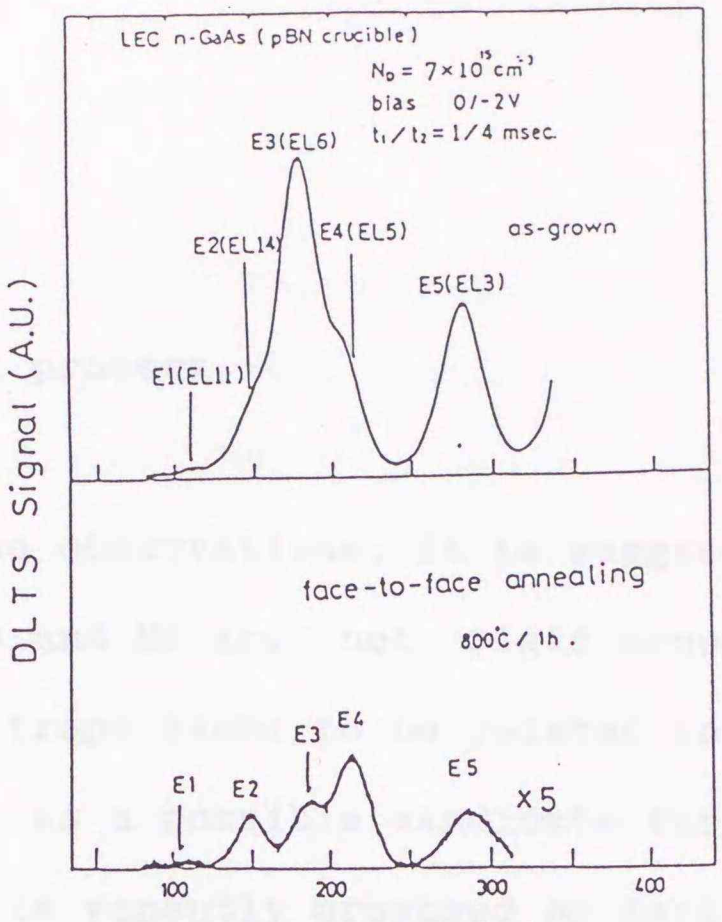

Figure 7. DLTS signals of undoped n-type LEC GaAs. The upper signal is for an as-grown sample, the lower signal is for a sample annealed by face-to-face proximity capping for 1 h at 800 C in H_2 ambient.

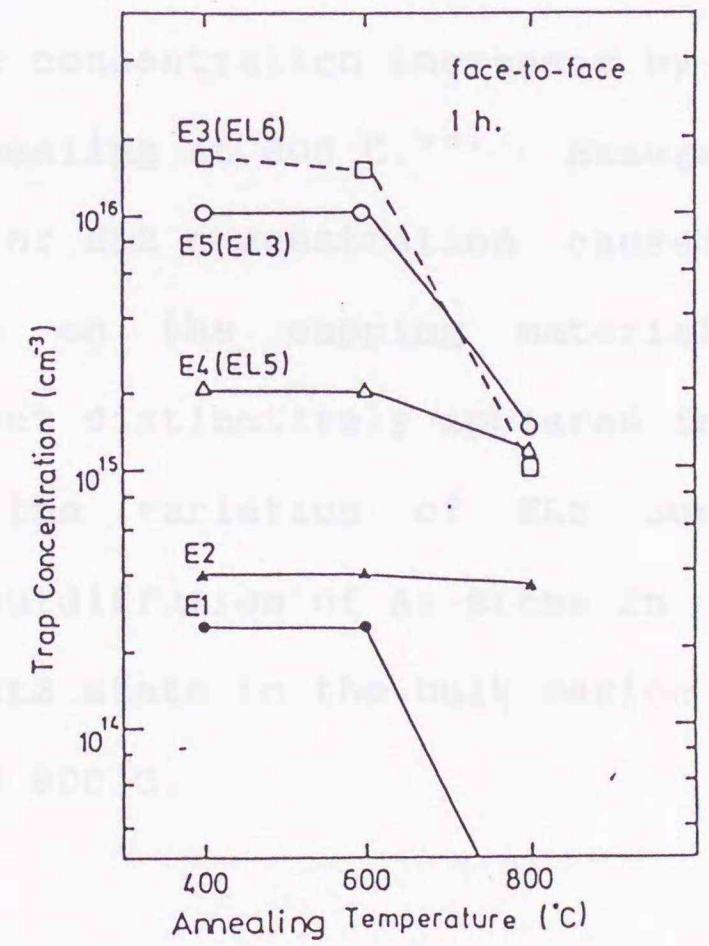

Figure 8. Variations of the concentrations of the five electron traps versus annealing temperature. The starting point, 400 C, was the temperature during ohmic contact fabrication. Heat treatment was carried out using face-to-face proximity capping by GaAs wafer.

due to a thermal process.

Based on these observations, it is suggested that the defect bonds of E1, E3 and E5 are not rigid around 800 C, i.e. the origin of these traps seems to be related to the cooling process during growth. As a possible candidate for E3(EL6), the defect complex V_{Ga}-V_{As} is recently proposed by Fang et al.[30]

Contrary to the results mentioned above, little change of the concentration of E6 (EL2) appeared as a result of face-to-face annealing in the temperature range of 600-800 C, which is almost consistent with the results reported by Kitagawara et al.[29] In HB GaAs, the EL2 concentration increases by a factor of 2.5 by face-to-face annealing at 800 C.[30] Hasegawa et al[39] showed that the change of EL2 concentration caused by heat treatment strongly depends on the capping materials and the ambient. Again, this effect distinctively appeared in the surface region, indicating that the variation of EL2 concentration could be related to the outdiffusion of As atoms in the surface region. Therefore, the EL2 state in the bulk region most likely remains stable at around 800 C.

3.4.Conclusion

The electrical properties of electron traps in LEC GaAs were investigated by DLTS and temperature-dependent Hall measurements. Six electron traps were detected in as-grown samples . Level E3 (EL6), with almost the same concentration as that of EL2, plays a significant role in the compensation mechanism in LEC GaAs which has a low concentration of carbon impurity. By 800 C heat treatment in H2 for 1 h, three levels (E1, E3 and E5) were reduced in concentration by more than one order of magnitude. The formation of these levels seems to be related to the cooling process during growth.

References

1) K.R.Elliot, D.E.Holmes, R.T.Chen and C.G. Kirkpatrick, Appl.Phys.Lett., 40, 898-901(1982)

2) K.R.Elliot, Appl.Phys.Lett., 42, 274-6(1983)

3) S.Miyazawa,K. Watanabe,J. Osaka and K.Ikuta, Rev.Phys.Appl., 23, 727-38(1988)

4) Y.Mochizuki and T.Ikoma, Rev.Phys.Appl.,23,747-63(1988)

5) J.P.Fillard,Rev.Phys Appl.,23, 765-77(1988)

6) B.Dischler and U.Kaufmann, Rev.Phys.Appl., 23,779-91(1988)

7) M.Kaminska, Rev.Phys.Appl., 23, 793-802(1988)

8) D.Stievenard and H.J.von Bardeleben, Rev.Phys.Appl., 23, 803-7(1988)

9) B.K.Meyer, Rev.Phys.Appl., 23, 809-16(1988)

10) G.A.Baraff and M.Lannoo, Rev.Phys.Appl., 23, 817-31(1988)

11) G.Guillot, Rev.Phys.Appl.,23, 833-46(1988)

12) S.Makram-Ebeid and P.Boher, Rev.Phys.Appl., 23, 847-62(1988)

13) J.C.Bourgoin and M.Lannoo, Rev.Phys.Appl., 23, 863-9(1988)

14) D.J.Chadi and K.J.Chang, Phys.Rev.Lett., 60, 2187-90(1988)

15) J.Dabrowski and M.Scheffler, Phys. Rev.Lett., 60, 2183-6 (1981)

16) J.Lagowski,M.Kaminska,J.M.Parsey,H.C.Gatos and W.Walukiewicz Int.Symp.GaAs and Related Compounds 1982 (Albuquerque) (Inst.Phys.Conf.Ser.No.65), pp41-8(1983)

17) J.Lagowski,M.Kaminska,J.M.Parsey,H.C.Gatos and M. Lichtensteiger, Appl.Phys.Lett., 41, 1078-80(1982)

18) J.Lagowski,H.C.Gatos,C.H.Kang,M.Skowronski,K.Y.Ko and D.G. Lin, Appl.Phys.Lett., 49, 892-4(1986)

19) J.F.Wagner and J.A.Van Vechten, J.Appl.Phys., 62,4192-5(1987)

20) H.J.Von Bardeleben, D.Stievenard,D.Deresmes,A.Huber and J.C.Bourgoin, Phys.Rev.B, 34, 7192-202(1986)

21) H.J.Von Bardeleben, J.C.Bourgoin and D.Stievenard, Appl.Phys.Lett., 53, 1089-91(1988)

22) K.Terashima, S.Washizuka, J.Nishio, H.Shimada, S.Yasuami and M. Watanabe, *Semi-Insulating III-V Materials* (OHMUSHA,Tokyo, 1986),pp59-64

23) S.Washizuka,J.Nishio,K.Terashima and M.Watanabe, *Semi-Insulating III-V Materials* (OHMUSHA,Tokyo,1986),p65-70

24) A.C.Wang and C.T.Sah, J.Appl.Phys., 55, 565-70(1984)

25) Y.Zohta and M.O.Watanabe, J.Appl.Phys., 53, 1809-11(1982)

26) G.M.Martin,A.Mitonneau and A.Mircea, Electron.Lett.,13, 191-3(1977)

27) M.Taniguchi and T.Ikoma, J.Appl.Phys., 54, 6448-51(1983)

28) F.D.Auret, A.W.R.Leitch and J.S.Vermaak, J.Appl.Phys., 59, 158-163(1986)

29) Y.Kitagawara,N.Noto,T.Takahashi and T.Takenaka, Appl.Phys. Lett., 48, 1664-5(1986)

30) Z.Q.Fang,T.E.Schlesinger and A.G.Milnes, J.Appl.Phys.,61, 5047-50(1987)

31) A.Chantre, G.Vincent and D.Bois, Phys. Rev. B,23, 5335-59 (1981)

32) S.M.Sze, *Physics of Semiconductor Devices,* 2nd.Ed.,(John

Wiley & Sons,New York), Chap.1

33) T.Wosinski, Appl.Phys.A, 36, 213-6(1985)

34) D.V.Lang and R.A.Logan, Phys.Rev.B, 19, 1015-30(1979)

35) Y.Kadota,K.Sakai,T.Nozaki,Y.Itoh and Y.Ohkubo,
Semi-Insulating III-V Materials (OHMUSHA,Tokyo,1986),p201-6

36) D.C.Look and D.C.Walter, Solid State Commun.,42, 745-8(1982)

37) S.J.Pearton,E.E.Haller and A.G.Elliot, Electron.Lett., 24,
1052-3(1983)

38) B.Hughes and C.Li, *GaAs and Related Compounds*
(Albuquerque,1982), Inst.Phys.Conf.Ser.No.65, p57-64(1983)

39) F.Hasegawa,N.Yamamoto and Y.Nannichi, Appl.Phys.Lett., 45,
461-3(1984)

CHAPTER 4

DEEP LEVELS IN UNDOPED EPITAXIAL GaAs

4.1 Introduction

The recent remarkable progress in the technology of molecular beam epitaxy (MBE) and metalorganic vapor phase epitaxy (MOVPE) allows an achievement of high quality heterostructures, which have been applied to the development of new semiconductor devices such as high electron mobility transistor (HEMT), heterojunction bipolar transistor (HBT), semiconductor lasers (LD), optical devices and quantum electron devices. The main features of MBE are slow growth rate, precise control of layer thickness and low growth temperature. Hence, MBE makes possible abrupt doping profile and abrupt hetero-interface, resulting in the high electron mobility because of the nearly ideal spatial separation between electrons and ionized donors. MOVPE can also achieve the abrupt hetero-interface comparable with that grown by MBE. In addition, MOVPE has an excellent uniformity of the grown layer and a suitability for large scale production, which are the most attractive features for optoelectronic devices.

The deep level characterization of the epitaxial layer is

an important indicator of the layer quality as well as the characterization of the carrier concentration and mobility, since deep levels provide direct effects on device performance. Additionally, deep levels are also related to the growth mechanism, which is not fully understood at present, and thus they may be able to be used as a tool to reveal the growth mechanism.

This chapter describes the characterization of deep levels in GaAs grown by MBE and MOVPE. Deep level transient spectroscopy (DLTS) was used to investigate deep levels in grown layers.

Deep levels in MOVPE GaAs examined by several workers[1-6] showed some common features, such as the dominant electron trap with an activation energy of 0.80 eV which is the so-called EL2. Other levels, however, seem to depend on the growth system, substrate and starting material. In the present work, deep electron traps in undoped MOVPE GaAs grown with two different trimethylgallium (TMG) sources are investigated.

Lang et al.[7] have first reported that nine electron traps with activation energies ranging from 0.08 to 0.85 eV exist in GaAs layers grown by MBE. Then, the effect of growth conditions such as growth temperature, As/Ga ratio, source materials, etc., on deep levels in MBE GaAs have been investigated by many workers. In this chapter, the properties of deep levels in

undoped MBE GaAs are characterized. Moreover, variation of deep level concentration and change of reflection high energy electron diffraction (RHEED) pattern with a coincident Pb flux are investigated in order to probe into growth mechanism.

4.2 Electron States in Metalorganic Vapor Phase Epitaxy Grown GaAs

The epitaxial layers were grown on undoped semi-insulating or Si doped n^+-GaAs substrate oriented (100)$\pm$ 0.5. TMG and arsine (10% AsH_3 in H_2) were used as the source for gallium and aresenic, respectively. A standard MOVPE growth system used in the present work is shown in Fig.1. Two different TMG sources (TMG-A and TMG-B), which were obtained from different suppliers, were used to estimate the effect of TMG source on the deep levels of grown layers. TMG-A is supposed to be higher quality than TMG-B. Growth was done under atmospheric pressure at temperatures ranging from 670 to 760 ℃ . Mole fraction ratio of AsH_3 to TMG (V /Ⅲ ratio) used in the present work was in the range 30-60, which resulted in n-type layers. Typical growth rate was about 400 A/min and typical thickness of the epitaxial layers was 4 μm. Two different series of GaAs layers from the two different source TMGs were grown under these same conditions. Typical samples measured are listed in Table 1.

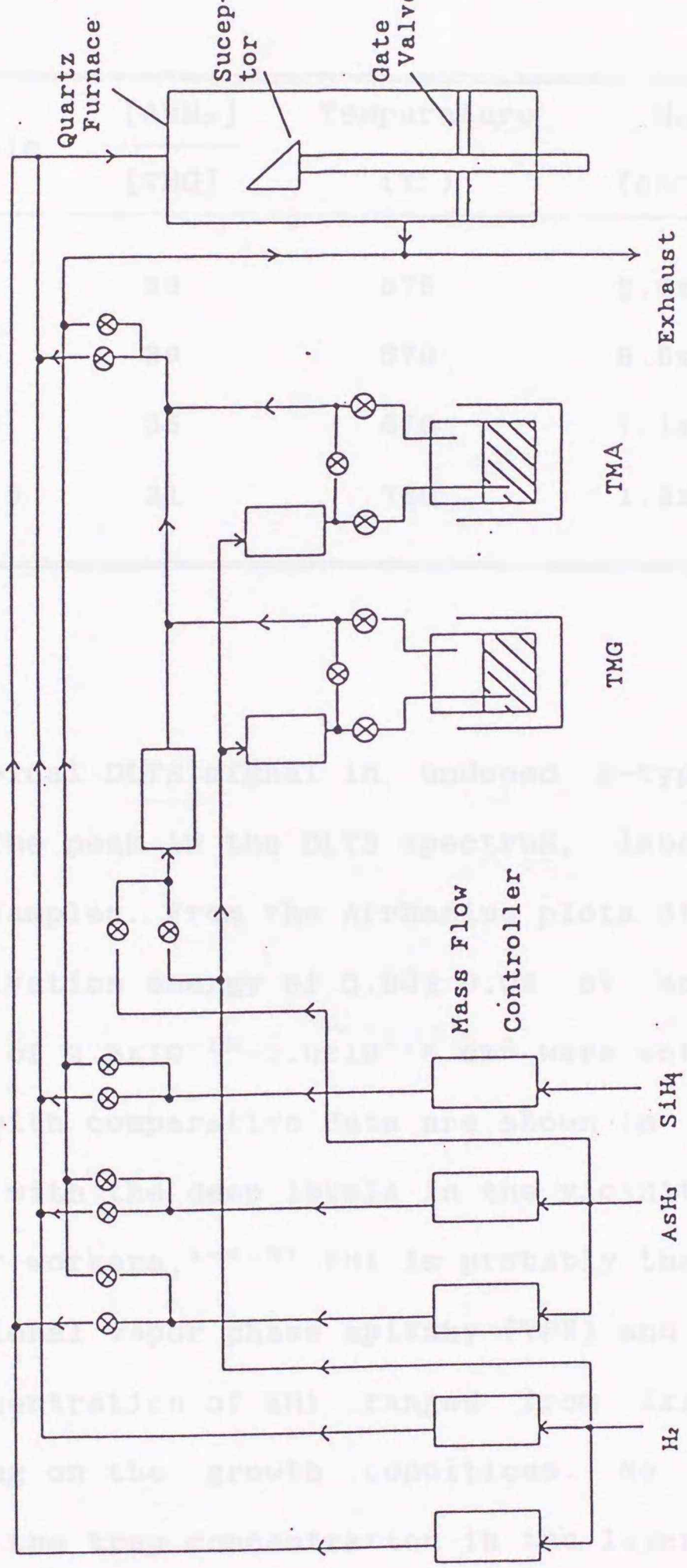

Figure 1. Schematic diagram of the MOVPE growth system used in the present work.

Table 1 Samples and typical growth conditions.

Sample	$\frac{[AsH_3]}{[TMG]}$	Temperature (℃)	N_D (cm^{-3})	TMG
MO1	38	675	$2.0x10^{16}$	TMG-A
MO5	39	670	$8.5x10^{15}$	TMG-B
MO8	35	670	$7.1x10^{16}$	TMG-A
MO15	31	760	$1.2x10^{16}$	TMG-A

A typical DLTS signal in undoped n-type GaAs is shown in Fig.2. The peak in the DLTS spectrum, labelled EH1, was found in all samples. From the Arrhenius plots of $T^2\tau$ versus 1000/T, the activation energy of 0.80 ± 0.02 eV and the capture cross section of $2.5x10^{-13}$-$1.0x10^{-12}$ cm^2 were obtained. Arrhenius plots of EH1 with comparative data are shown in Fig.3. Comparing our results with the deep levels in the vicinity of midgap reported by other workers,[1-6,8] EH1 is probably the same level as EL2 in conventional vapor phase epitaxy (VPE) and in MOVPE GaAs layer. The concentration of EH1 ranged from $2x10^{14}$ to $4x10^{15}$ cm^{-3}, depending on the growth conditions. No difference was found between the trap concentration in the layer grown with TMG-A and that with TMG-B. The concentration profile of this level was

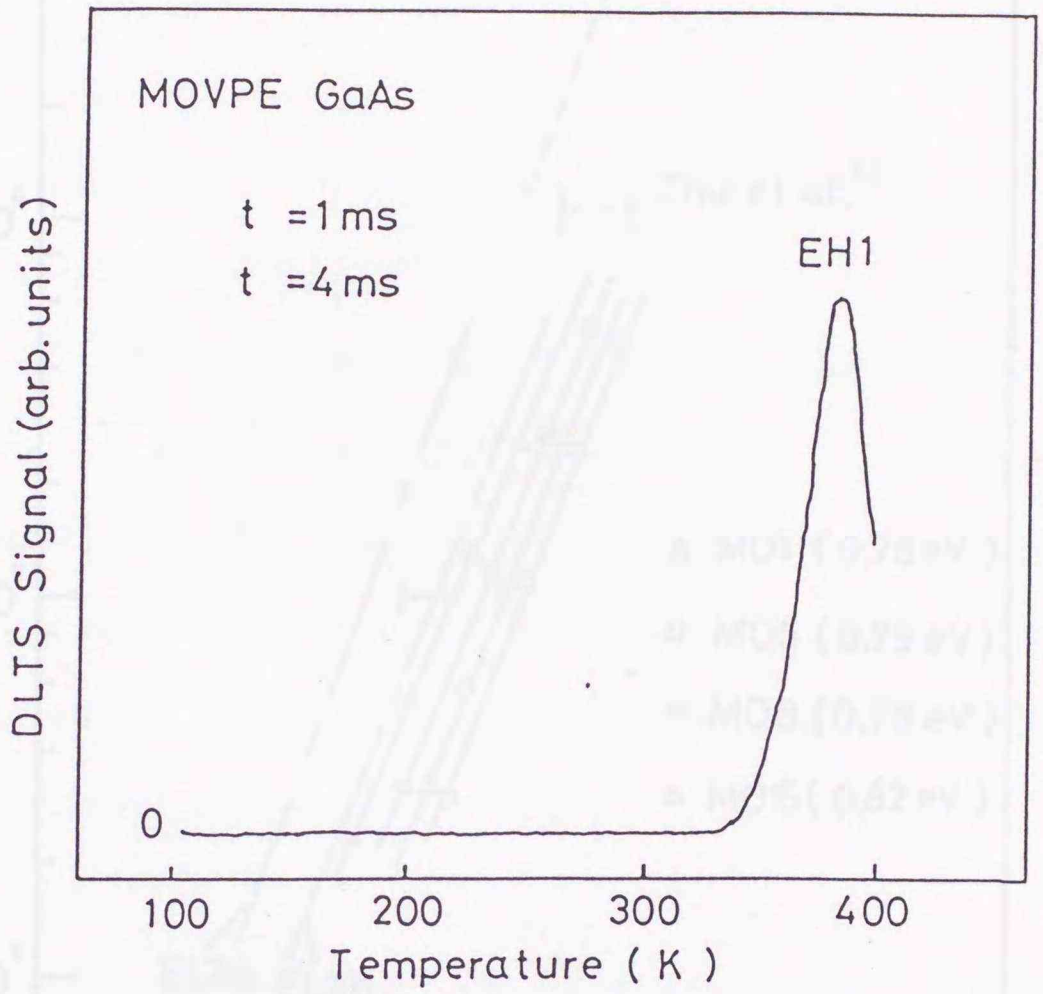

Fig.2 Typical TLTS spectrum in undoped n-type GaAs layers grown with TMG-A.

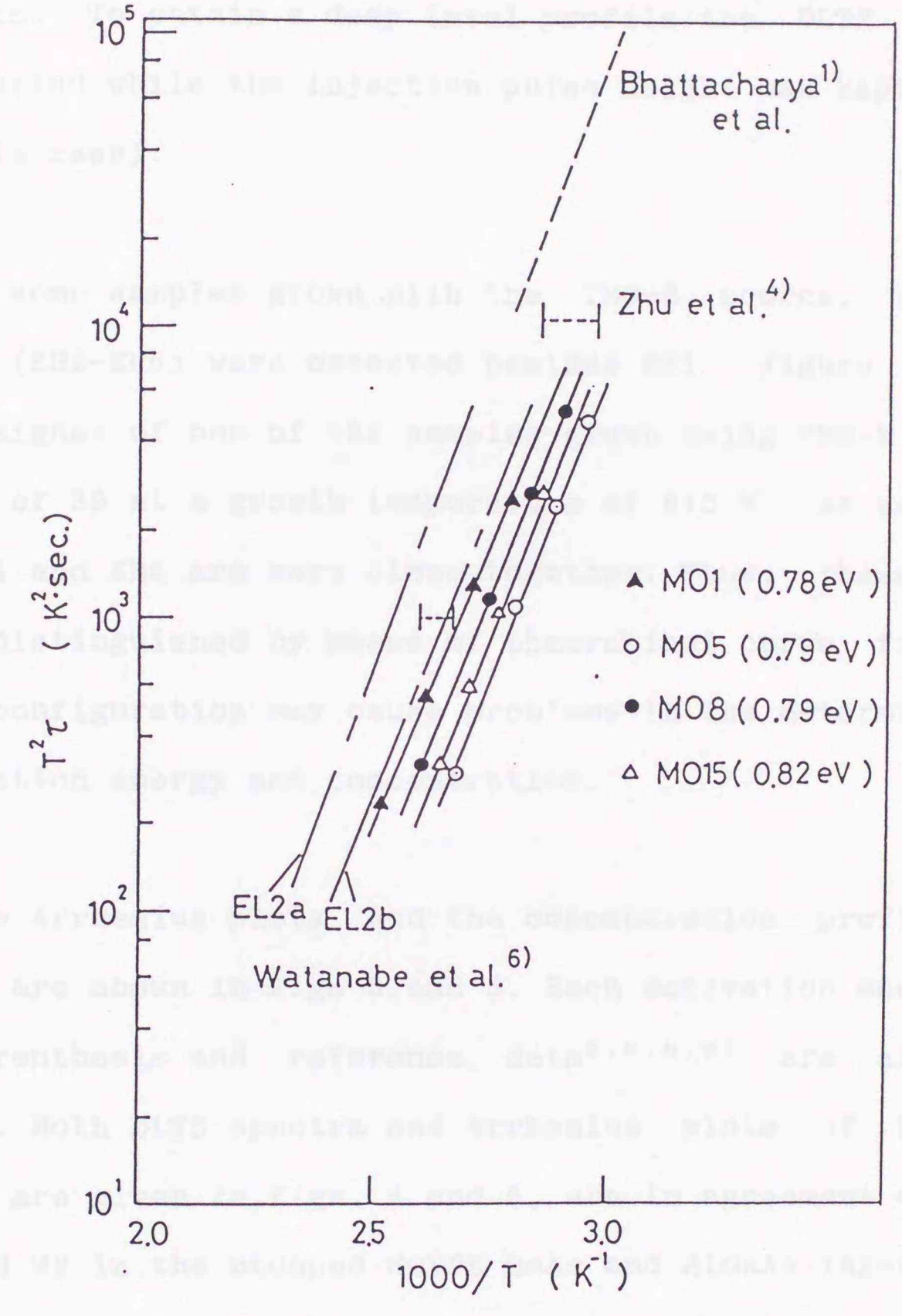

Fig.3 Arrhenius plots of the EH1 level in various samples. Also shown is the comparative data of the dominant deep level in MOVPE GaAs.

constant throughout the grown layer and nearly the same for all samples. To obtain a deep level profile the DLTS bias voltage was varied while the injection pulse height was kept constant (2V in this case).

In some samples grown with the TMG-B source, four electron traps (EH2-EH5) were detected besides EH1. Figure 4 shows the DLTS signal of one of the samples grown using TMG-B with a V/III ratio of 39 at a growth temperature of 670 ℃. As seen, the peaks of EH4 and EH5 are very close together. Thus, these two levels were distinguished by means of theoretical curve fitting, since this configuration may cause problems in the determination of the activation energy and concentration.

The Arrhenius plots and the concentration profiles for the traps are shown in Figs 5 and 6. Each activation energy is given in parenthesis and reference data[2,6,8,9] are also shown in Fig.3. Both DLTS spectra and Arrhenius plots of EH4 and EH5, which are given in Figs. 4 and 5, are in agreement with those of W1 and W2 in the undoped MOVPE GaAs and AlGaAs layers reported by Wagner et al.[2] In their results, the sum of the concentration of both levels increased in the range of 10^{12} to 10^{17} cm^{-3} as aluminum content increased 0 to 0.35. Therefore, they concluded that W1 and W2 were introduced to epitaxial layers by timethylaluminum (TMA) or by the impurities carried by TMA, which remained even during growth of unintentionally doped GaAs. W1 and

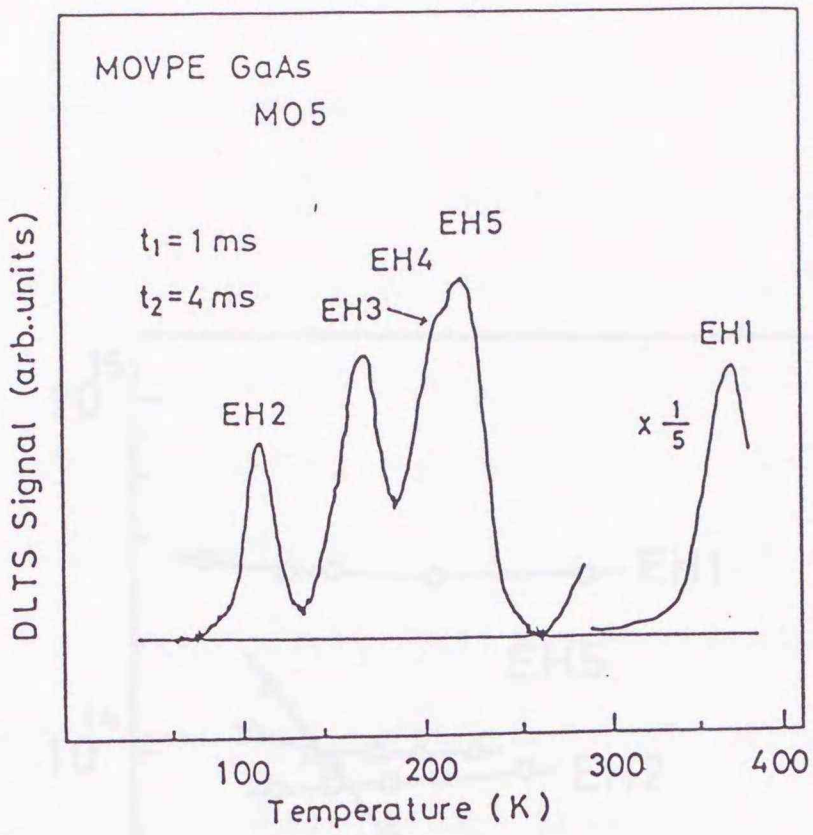

Fig.4 DLTS spectrum in particular samples grown with TMB-B.

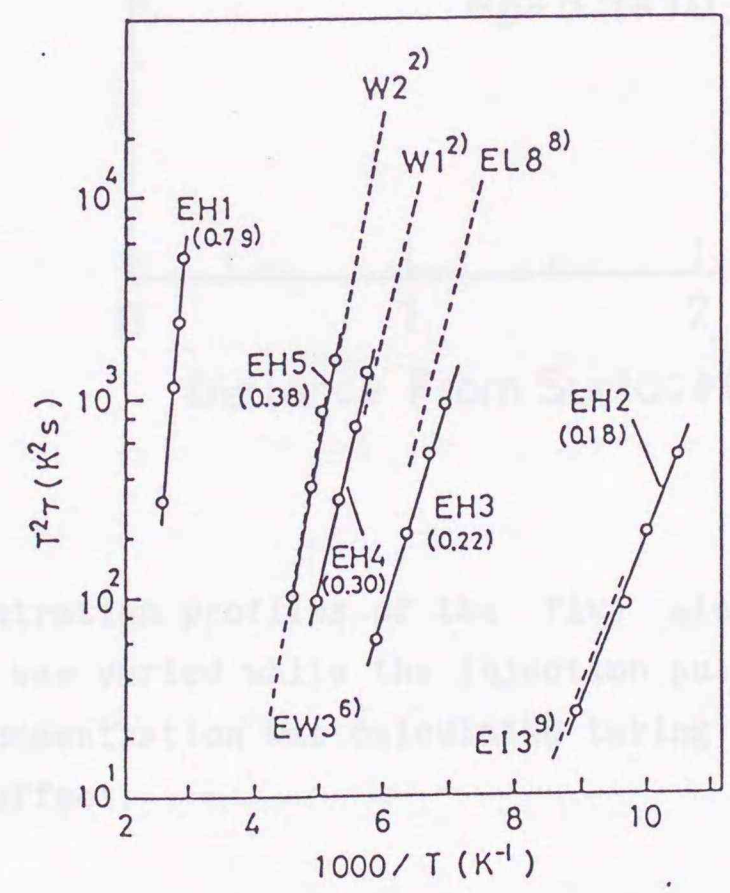

Fig.5 Arrhenius plots of the five electron traps shown in Fig.4 with comparative data from Wagner et al. (W1 and W2), Watanabe et al. (EW3), Martin et al. (EL8) and Lefevre and Schulz (EI3). Each activation energy is given in parenthesis in eV.

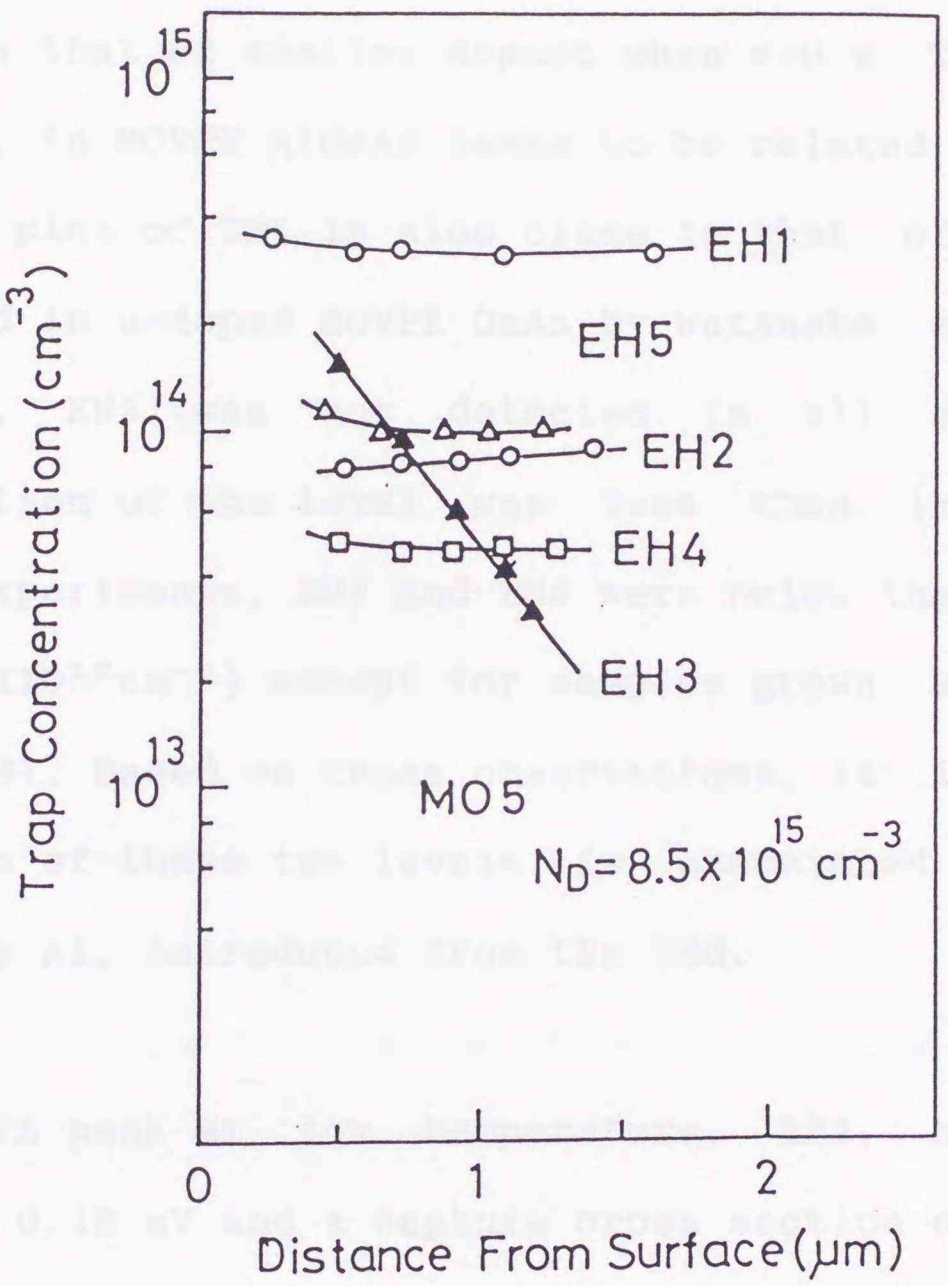

Fig.6 Concentration profiles of the five electron traps. The bias voltage was varied while the injection pulse height was kept in 2V. The concentration was calculated taking into account the so-called λ effect.

W2 are very similar to the well-known deep level called DX center[10,11] in $Al_xGa_{1-x}As$ in many respects-the Arrhenius plots, the DLTS spectrum composed of several centers, the concentration as high as that of shallow dopant when x>0.2. Thus, these levels, W1 and W2, in MOVPE AlGaAs seems to be related to DX center. The arrhenius plot of EH5 is also close to that of EW3, which has been found in undoped MOVPE GaAs by Watanabe et al.[8] As they described, EW3 was not detected in all samples and the concentration of the level was less than $1x10^{12}cm^{-3}$. In the present experiments, EH4 and EH5 were below the detection limit ($5x10^{11}$-$5x10^{12}cm^{-3}$) except for samples grown with a particular TMG (TMG-B). Based on these observations, it is concluded that the origin of these two levels is associated with impurities, especially Al, introduced from the TMG.

The DLTS peak at low temperature, EH2, has an activation energy of 0.18 eV and a capture cross section of $3.3x10^{-14}cm^3$. By comparison with the data given by Lefevre and Schultz,[9] it is probably identical with EI3 which has been seen in VPE layers. From the deep level profile, they claimed that EI3 was related to the temperature fluctuation during the growth of the epitaxial layer. In the present results, however, EH2 was only detected in the particular samples grown with TMG-B, indicating that EH2 is caused by impurities in the TMG source. The fifth electron trap EH3 with an activation energy of 0.22eV, gives the close Arrhenius plot with EL8 which was reported by Martin et al.[8] A

distinctive feature was that the concentration of EH3 extremely decreased with increasing depth from the surface, as shown in Fig.5. The shape of the depth profile could be due to traps being annealed out during the epitaxial growth. It is also concluded that the origin of EH3 is seems to be related to the impurities in TMG by the same argument as for EH2, EH4 and EH5.

4.3 Electron States in Molecular Beam Epitaxy Grown GaAs

4.3.1 Growth of Undoped GaAs

The MBE apparatus used in the present work is shown in Fig.7. The chamber was the stainless-steel type and consists of the growth chamber and the vacuum interlock exchanging chamber to avoid disturbing the vacuum integrity.

The growth system was mainly pumped by a ion pump and the background pressure of the growth chamber was about 2×10^{-7} Pa. Titanium sublimation pumps with liquid nitrogen-cooled surfaces and sorption pumps were also used. The growth chamber was equipped with quadrupole mass spectrometer (QMS) for analyzing residual gasses and molecular beam. Reflection high energy electron diffraction (RHEED) was also equipped for monitoring the surface. The RHEED is an effective *in-situ* facility because it is of great use to optimize the growth condition and is very

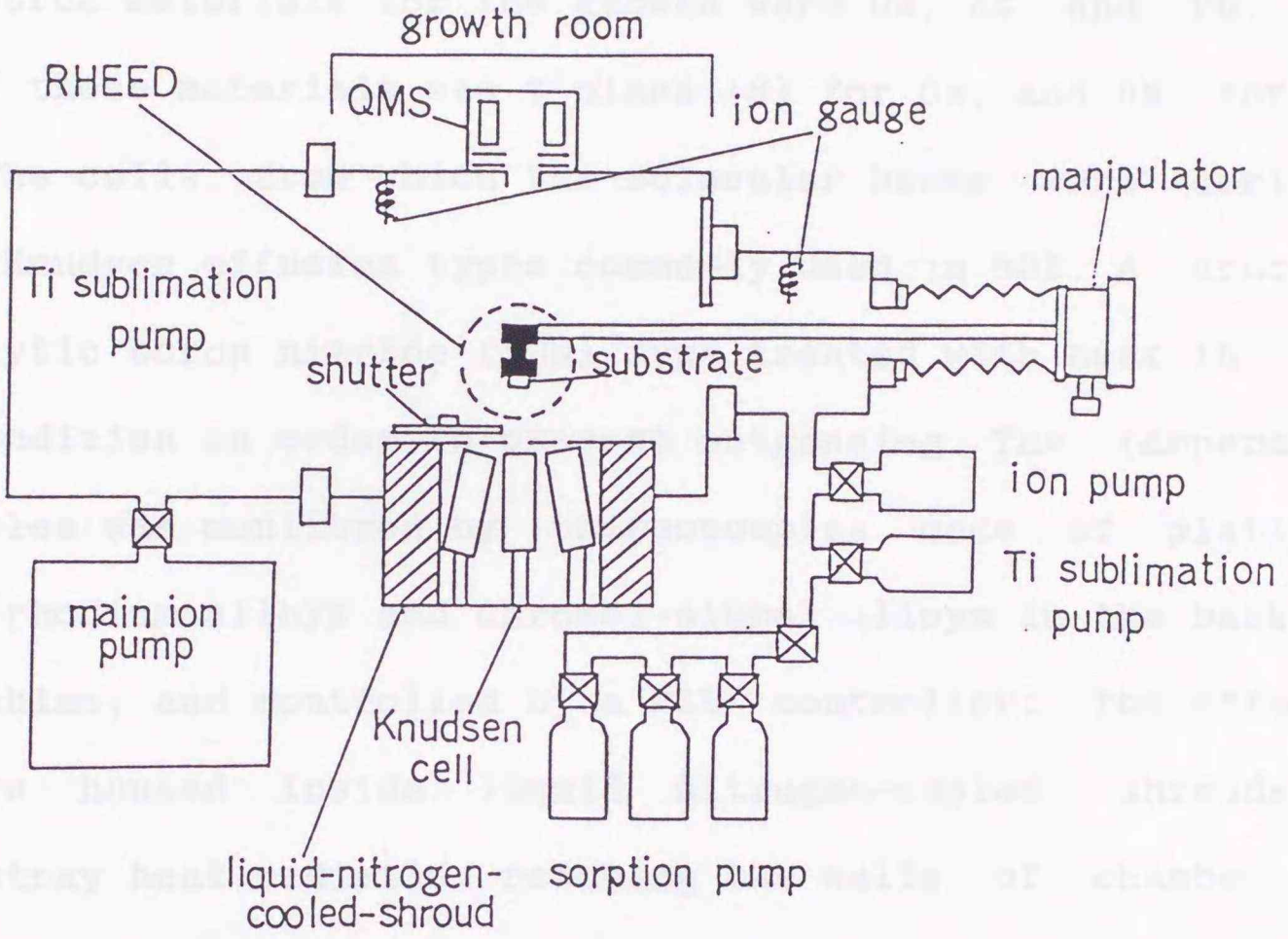

Fig.7 Schematic diagram of the MBE system used in the present work.

sensitive yet simple tool which can be used while the film is growing.

The source materials for the growth were Ga, As and Pb. The purity of these materials was 7 nines (N) for Ga, and 6N for As and Pb. The cells, from which the molecular beams were derived, were the Knudsen effusion types commonly used in MBE. A crucible was pyrolytic boron nitride (PBN) type treated with heat in high vacuum condition in order to prevent outgassing. The temperature of crucibles was monitored by thermocouples made of platinum-platinum/rhodium alloys and chromel-alumel alloys in the back of the crucibles, and controlled by a PID controller. The effusion cells were housed inside liquid nitrogen-cooled shrouds to prevent stray heat radiation reaching the walls of chamber and causing outgassing problems.

The substrate used in the present work were undoped LEC SI (100) GaAs and Si doped HB n^+-type GaAs. The growth procedure can be simply summarized as following:the substrate was first cleaned ultrasonically with acetone and methanol, then etched in etchant for 1 min (H_2SO_4:H_2O_2:H_2O = 7:1:1), rinsed in deionized water and mounted on the Mo block. The cells were heated and when the cell temperature reached the required temperature, the effusion of molecular beam was confirmed by QMS. The substrate temperature was raised to remove the surface oxide monitored by RHEED. Note that the As cell shutter was opened to prevent the desorption of

As from the substrate when the substrate temperature reached approximately 400 ℃. The substrate temperature was then reduced to the required growth temperature. The growth was started by opening the Ga cell shutter. The growth temperature range was from 500 to 580 ℃ and the growth were done under (2x4) arsenic stabilized conditions by observation of RHEED patterns. The growth rate was in the range of 0.8-1.0 μm/h.

Undoped GaAs layers were all n-type, which is probably due to residual donor-type atoms previously used in this chamber. The mobility and electron concentration were measured by the Van der Pauw technique. Figure 8 shows the electron mobility at 77K as a function of electron concentration in undoped grown layers. The numbers indicate the growth times and the solid curves represent lines of constant compensation ratio[12] defined as N_A^-/N_D^+, where N_A^- and N_D^+ are the concentration of ionized acceptors and donors, respectively. The highest mobility value achieved in the present work was 6100 $cm^2V^{-1}sec^{-1}$ with $n=3.0x10^{16}cm^{-3}$ at 77K, and the lowest compensation ratio obtained was about 0.4. These results indicate that the relatively high concentration of residual acceptors as well as donors remain in growth chamber.

4.3.2 Electron Traps in Undoped GaAs

Typical DLTS signals in undoped GaAs layers are shown in Fig.9. Little deference of the electron mobility and

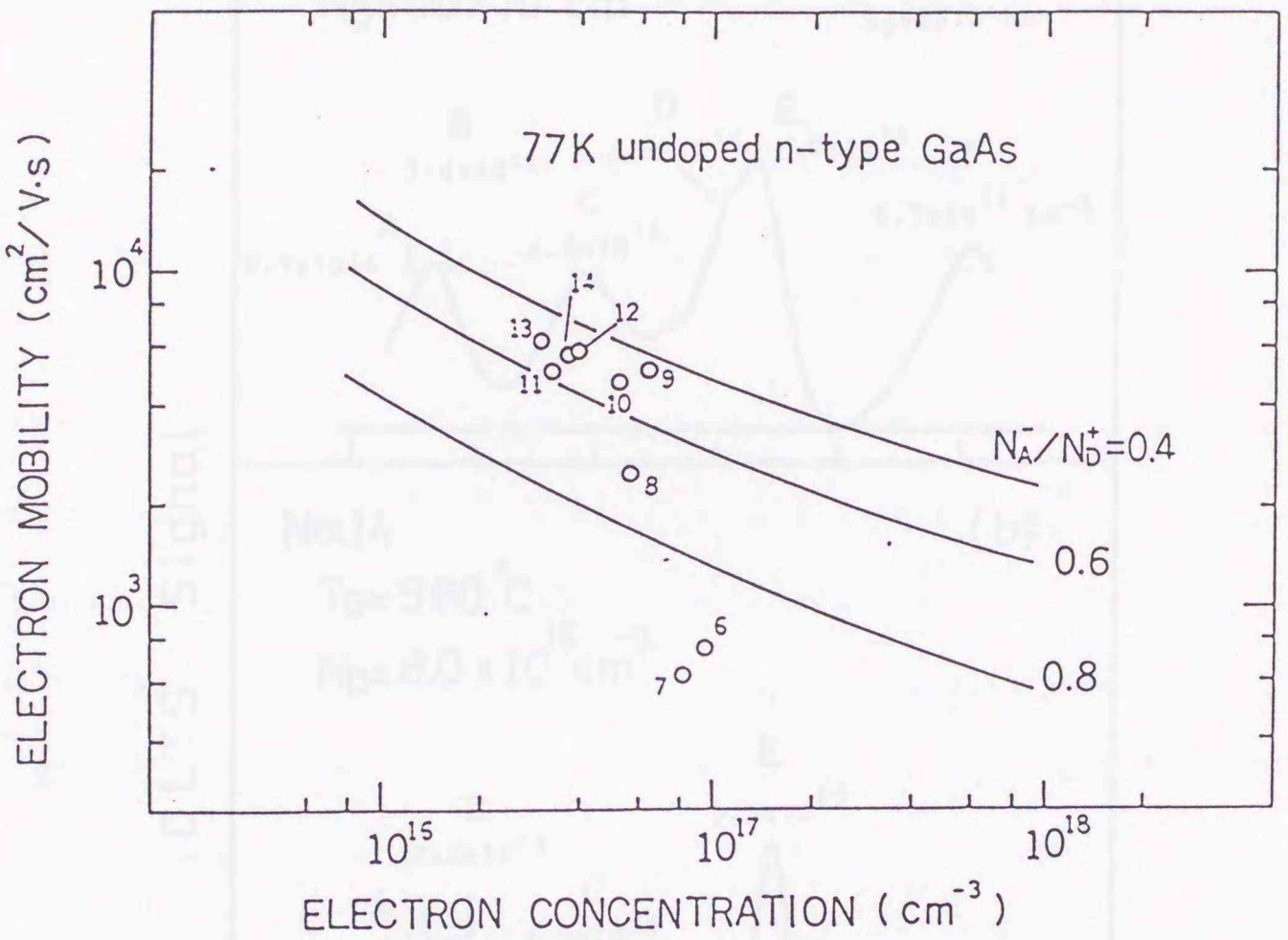

Fig.8 Hall mobilities at 77K as a function of electron concentration in undoped GaAs layers. The numbers indicate the growth time. The solid curves represent the calculated lines (Ref.12) for various compensation ratios.

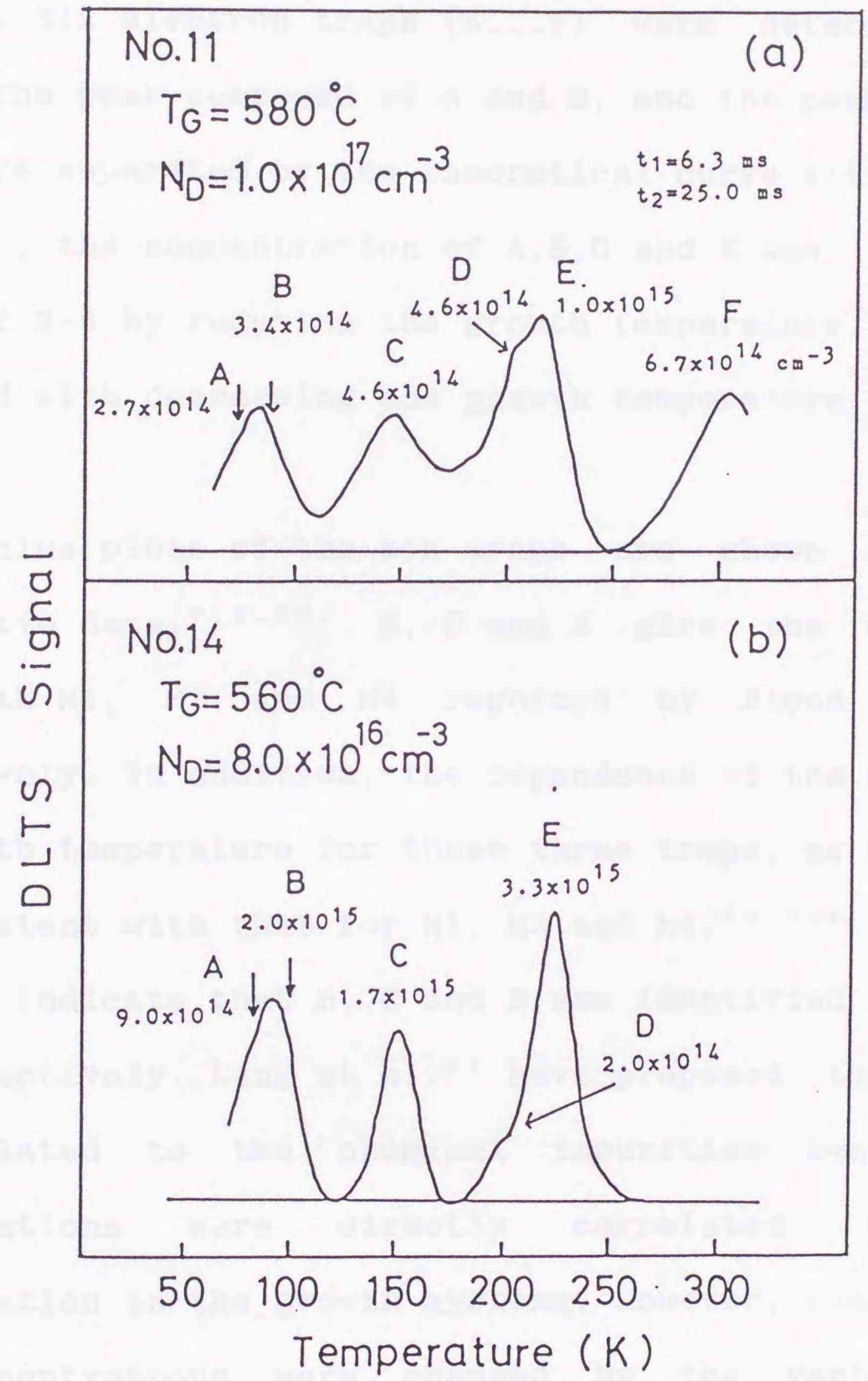

Fig.9 Typical DLTS spectra of the electron traps obtained from undoped GaAs layers grown at (a) 580°C and (b)560°C. Curve fitting was used to separate A, B, D and E levels.

concentration between these two samples (No.11 and No.14) was observed. Six electron traps (A...F) were detected in undoped layers. The peak composed of A and B, and the peak composed of D and E were separated by the theoretical curve fitting. As shown in Fig.9., the concentration of A,B,C and E was increased by a factor of 3-5 by reducing the growth temperature. Only D trap was decreased with decreasing the growth temperature.

Arrhenius plots of the six traps are shown in Fig.10 with comparative data.[7,8,13] B, C and E give the close Arrhenius plots with M1, M3 and M4 reported by Blood and Harris,[13] respectively. In addition, the dependence of the concentration on the growth temperature for these three traps, as mentioned above, is consistent with that for M1, M3 and M4.[13,14] These results strongly indicate that B, C and E are identified as M1, M3 and M4, respectively. Lang et al.[7] have proposed that these traps were related to the chemical impurities because the trap concentrations were directly correlated with spurious contamination in the growth systems. However, the fact that the trap concentrations were changed by the variation of As/Ga ratio[13,15] or by the modification of surface process during growth[16] seems to suggest that the origin of these traps are associated with native defects, possibly Ga vacancy, and/or complexes created by As overpressure.[13,14]

From the Arrhenius plots, A trap seems to be identical with

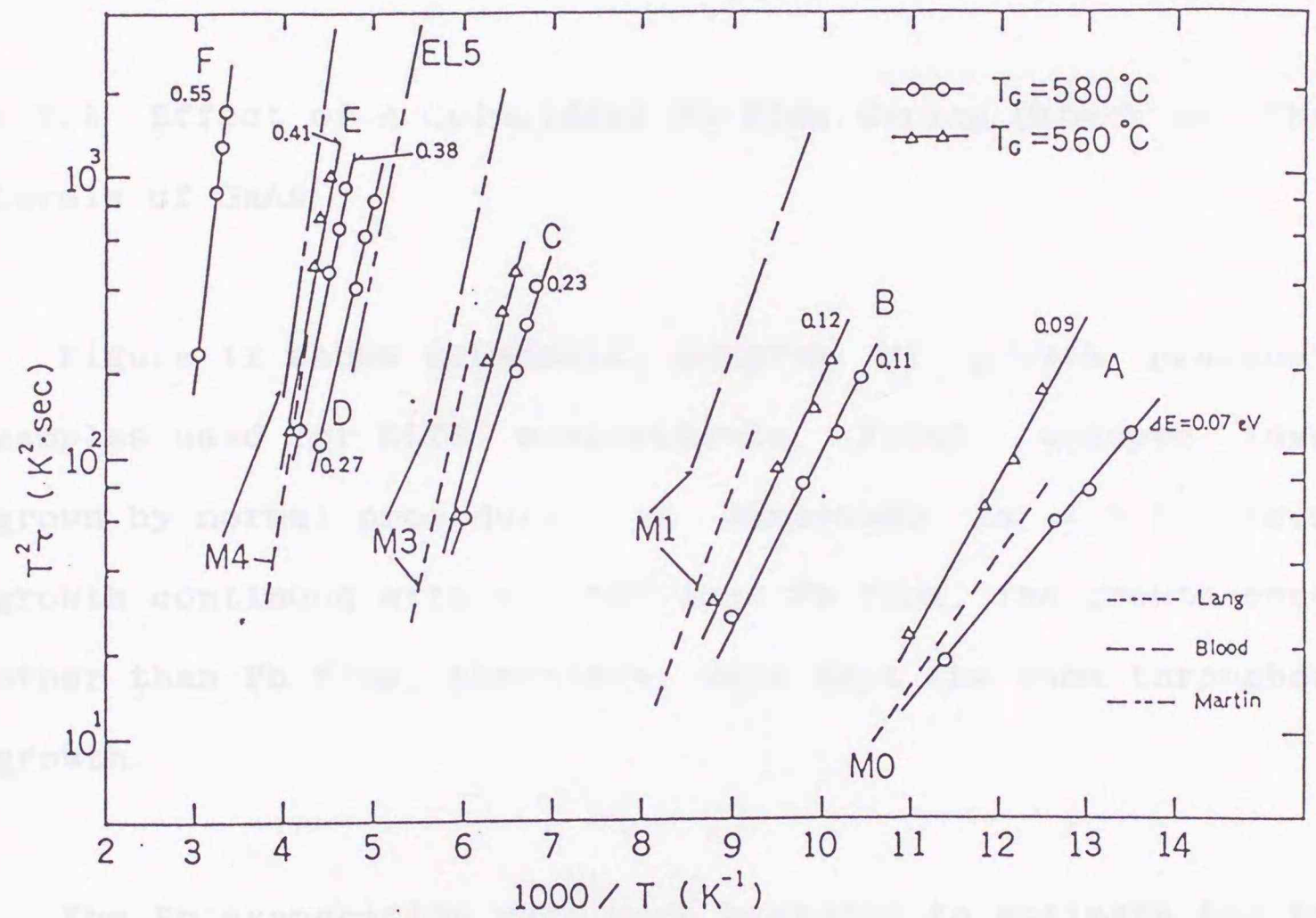

Fig.10 Arrhenius plots of five electron traps with comparative data. Numbers indicate the activation energy.

MO. The D trap gives the close Arrhenius plot with EL5 reported by Martin et al.[8] in VPE layer. Since only this trap was decreased in concentration by reducing the growth temperature, as shown in Fig.9, the origin of the trap seems to be different from that of other traps.

4.3.3 Effect of A Coincident Pb Flux during Growth on The Deep Levels of GaAs

Figure 11 shows schematic diagram of growth procedure and samples used for DLTS measurements. First, undoped layer was grown by normal procedure, as described in 4.3.1. Then, the growth continued with a coincident Pb flux. The growth conditions other than Pb flux, therefore, were kept the same throughout the growth.

The Pb evaporation rate were measured to estimate the Pb flux intensity. Figure 12 shows the Pb evaporation rate as a function of reciprocal temperature of the Pb cell. The upper solid line in Fig.11 reprensents the vapor pressure of Pb versus $1/T_{Pb}$. It appeared that the line of the vapor pressure was parallel to the experimental line, i.e., the Pb flux intensity was proportional to the Pb vapor pressure. The Pb flux intensity, J_{Pb}, used in the present work was from $1x10^{14}$ to $1x10^{15}$ $cm^{-2}s^{-1}$.

The surface lifetime τ of Pb is given by

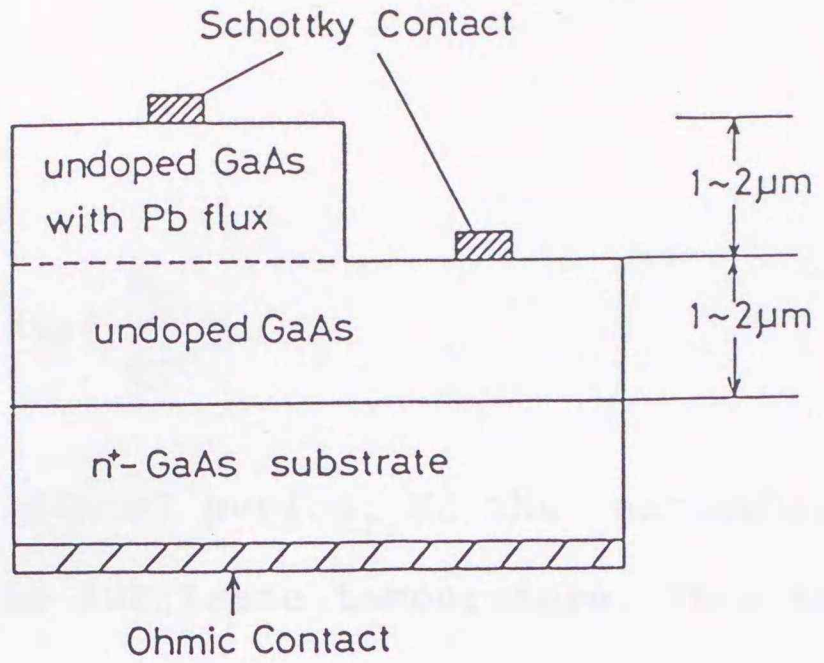

Fig.11 Layer structure of undoped GaAs grown by normal procedure and grown with a coincident Pb flux.

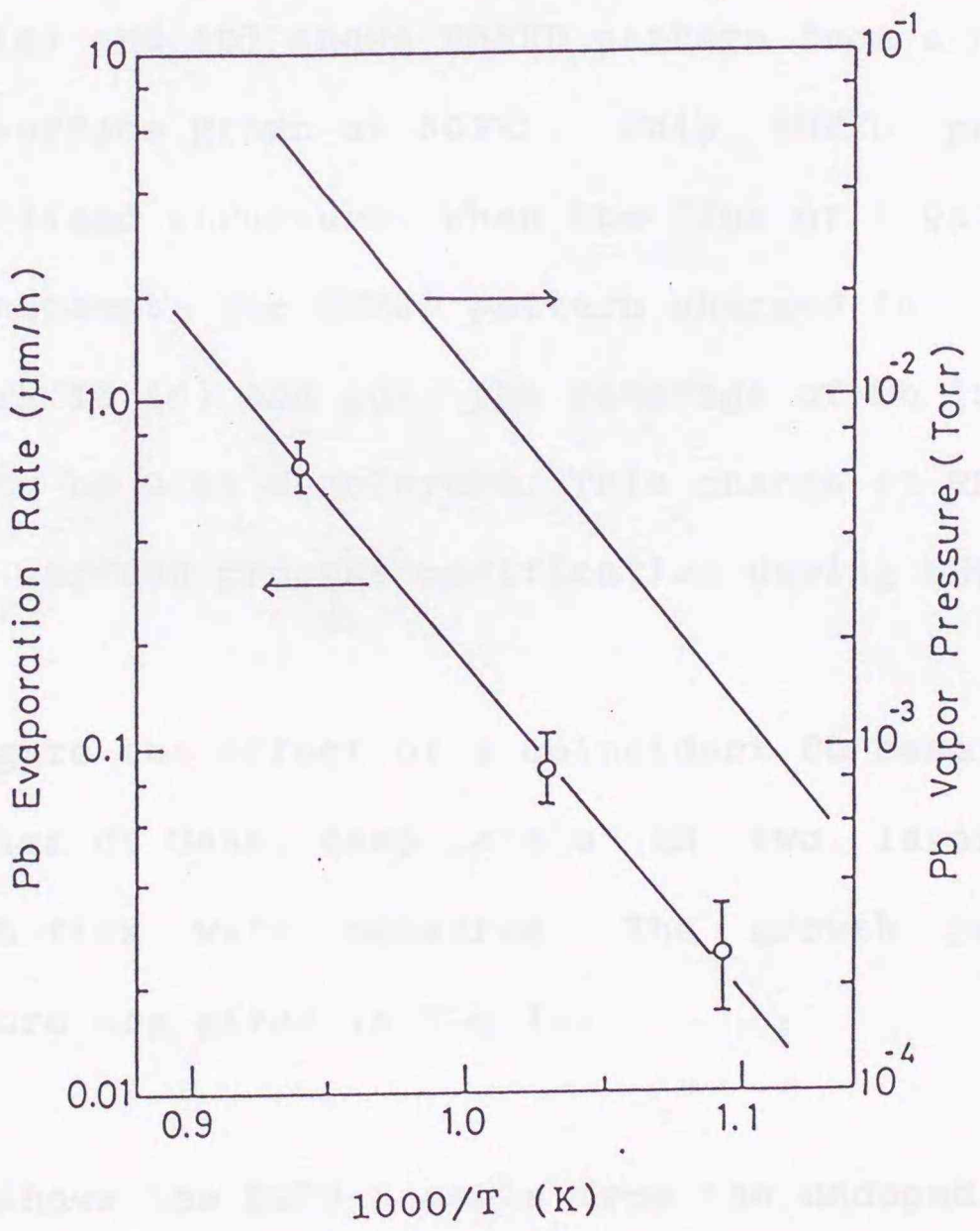

Fig.12 Pb evaporation rate as a function of reciprocal temperture of Pb cell. The upper solid line represents the vapor pressure of Pb.

$$\tau = \tau_o \exp(\frac{E_D}{kT}) \qquad (4.1)$$

where τ_o is a vibrational period, E_D the activation energy for adsorption and T the substrate temperature. Then the coverage is equal to $J_{Pb} \cdot \tau / 4x10^{14}$. Whitehouse et al.[17] reported that $E_D = 1.4 \pm 0.2$ eV, $\tau_o = 2x10^{-11}$s for Pb atoms. From these data, the flux of $1x10^{15}$ Pb atoms $cm^{-2}s^{-1}$ corresponds to 0.05 monolayers at T=560℃ .

Figure 13 (a) and (b) shows RHEED pattern from a normal (001) undoped GaAs surface grown at 505℃ . This RHEED pattern gives (2x4) As stabilized structure. When the flux of $1.9x10^{15}$ Pb atoms $cm^{-2}s^{-1}$ was incident, the RHEED pattern changed to vague (2x3), as shown in Fig.13 (c) and (d). The coverage of Pb in this case is estimated to be 0.11 monolayers. This change of RHEED pattern indicates the surface process modification during MBE growth.

To investigate the effect of a coincident Pb beam on the MBE growth mechanism of GaAs, deep levels in two layers with and without the Pb flux were measured. The growth procedure and sample structure are given in Fig.11.

Figure 14 shows the DLTS signals from the undoped layers with and without Pb flux. The carrier concentration of both layers estimated from C-V measurement at room temperature was 1 x 10^{17}

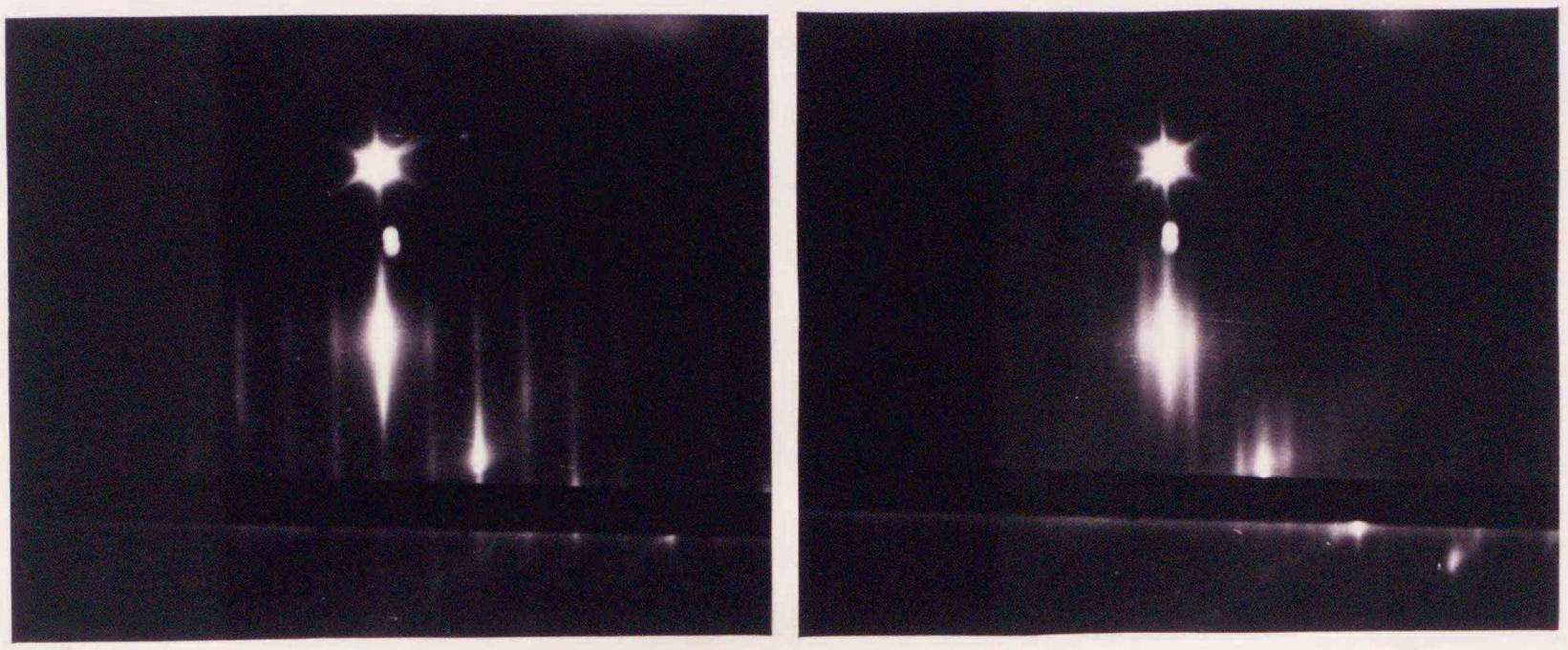

(a)

(b)

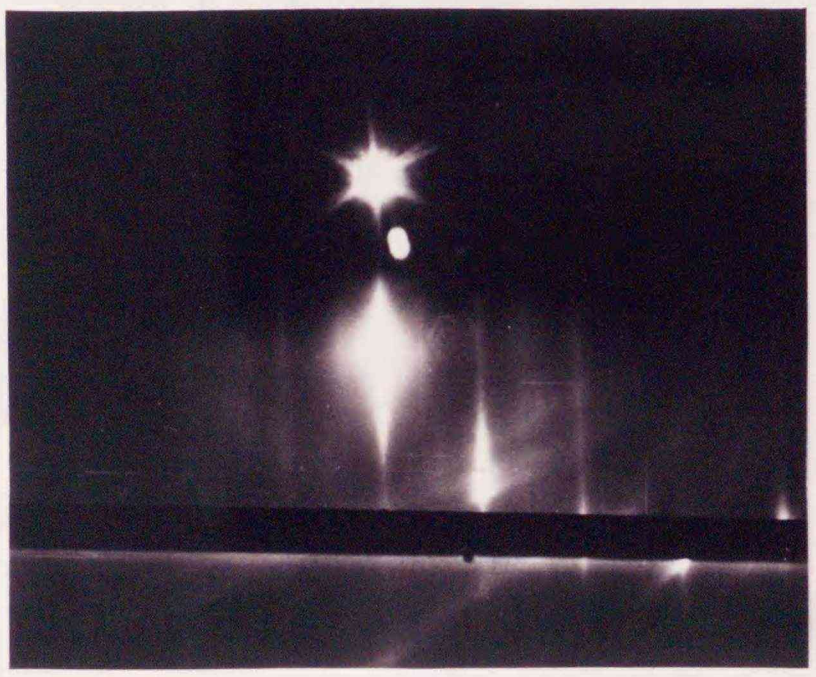

(c)

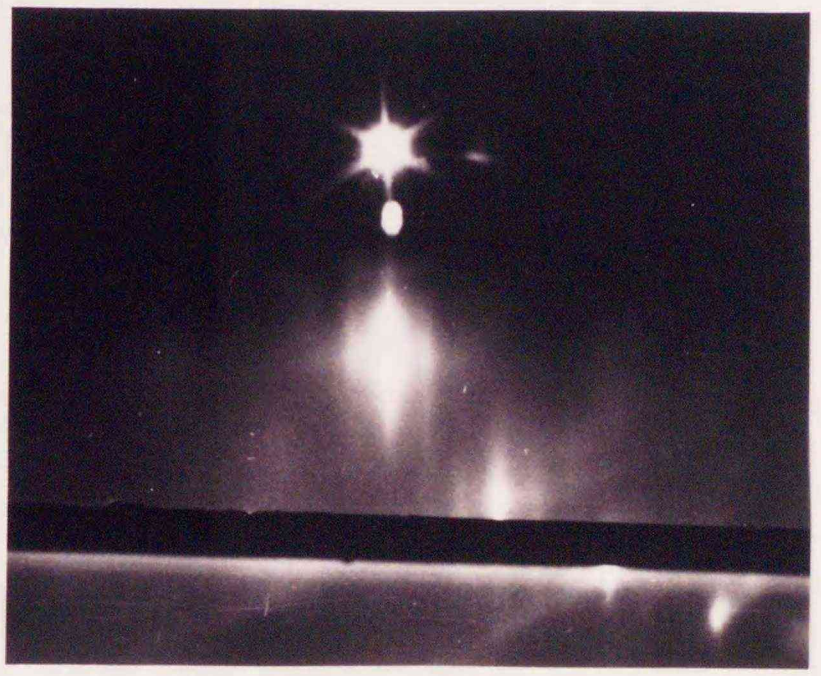

(d)

Fig.13 RHEED patterns from the (001) undoped GaAs grown at 505℃ (a) [$\bar{1}$10] azimuth and (b) [110] without Pb flux, (c) [110] and (d) [$\bar{1}$10] with the flux of 1.9×10^{15} Pb atoms $cm^{-2}s^{-1}$.

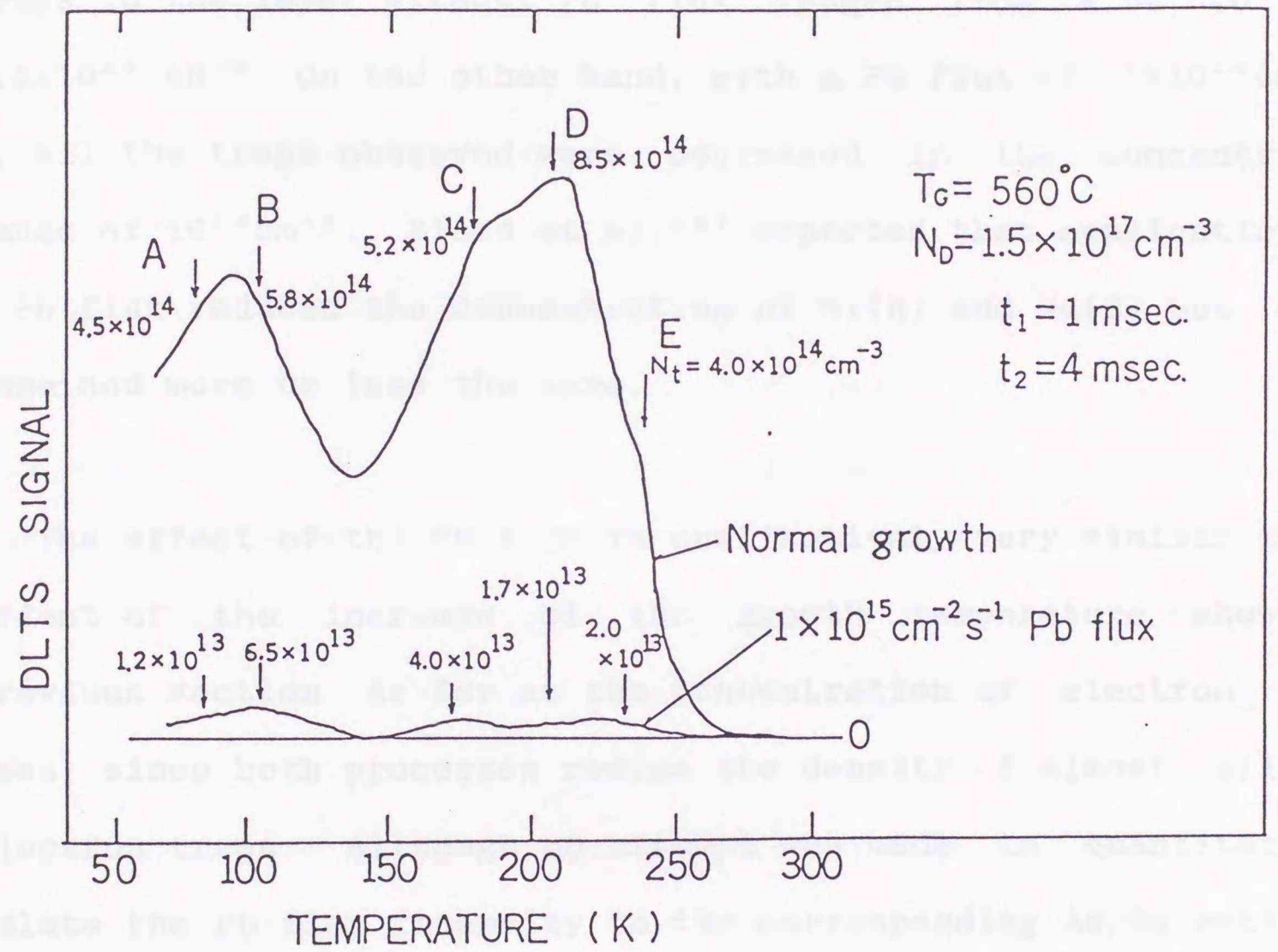

Fig.14 DLTS spectra from the undoped layers with and without Pb flux.

cm^{-3}. In addition, XPS studies[18] have shown that there is little chemical interaction between the Pb overlayer and GaAs substrate. These observations may indicate that Pb atoms are not incorporated in epitaxial GaAs layer. Five traps, as described in 4.3.2, were detected in both layers. The concentrations of the traps in the layer without Pb flux ranged from $4.0x\ 10^{14}$ to $8.5x10^{14}$ cm^{-3}. On the other hand, with a Pb flux of $1x10^{15}cm^{-2}s^{-1}$, all the traps observed were decreased in the concentration range of $10^{13}cm^{-3}$. Blood et al.[16] reported that application of a Pb flux reduced the concentration of M1(B) and M4(E) but M3(C) remained more or less the same.

The effect of the Pb flux is qualitatively very similar to the effect of the increase of the growth temperature shown in previous section as far as the concentration of electron traps goes, since both processes reduce the density of almost all the electron traps. Although no attempt was made to quantitatively relate the Pb flux intensity to the corresponding As/Ga ratio in terms of deep level concentration, a coincident Pb flux seems to change the effective As/Ga ratio at the surface. Because of the change of the RHEED pattern as described in the previous section, the surface process modification of growing layer is probably responsible for the reduction of deep level concentration in GaAs.

4.4 Conclusion

Deep levels in undoped MOVPE and MBE layers were investigated.

Five electron traps were detected by DLTS in n-type undoped MOVPE GaAs. The dominant trap is EH1 with an activation energy of 0.80±0.02eV, that is probably the same level with EL2 in conventional VPE and MOVPE GaAs layers. The four remaining traps (EH2-EH5) appeared only in the samples grown with a particular TMG source (TMG-B) obtained from a different supplier. Several speculations have been proposed on the origin of these traps,[2,8] however, based on the present results, it is concluded that they are due to impurities introduced with the TMG source.

Six electron traps (A-F) were detected in undoped n-type MBE layers. The concentration of the four traps was increased by a factor of 3-5 by reducing the growth temperature from 580 to 560 ℃. To investigate the effect of a coincident Pb flux on the growth mechanism, deep levels in two layers with and without the Pb flux were measured. With a Pb flux of $1x10^{15}cm^{-2}s^{-1}$, all the traps observed were decreased in the concentration range of $10^{13}cm^{-3}$. The change of RHEED pattern indicates that the Pb flux can cause the surface process modification, e.g., the change in surface stoichiometry, resulting in the reduction of deep level

concentration in GaAs.

References

1) P.K.Bhattacharya,J.W.Ku,S.J.T.Dwen,V.Aebi,C.B.Cooper and R.L.Moon,Appl.Phys.Lett.,36,304(1980)

2) E.E.Wagner,D.E.Mars,G.Hom and G.B.Stringfellow,J.Appl.Phys., 51,5434(1980)

3) N.M.Johnson,R.D.Burnham,D.Fekete and R.Yingling,*Defects in Semiconductors* (North-Holland,Amsterdam,1981),p.481

4) H.Z.Zhu,Y.Adachi and T.Ikoma,J.Cryst.Growth,55,154(1981)

5) L.Samuelson,P.Omling,H.Titze and H.G.Grimmeiss,J.Cryst.Growth, 55,164(1981)

6) M.O.Watanabe,A.Tanaka,T.Udagawa,T.Nakanisi and Y.Zohta,Jpn.J. Appl.Phys,22,923(1983)

7) D.V.Lang,A.Y.Cho,A.C.Gossard,M.Ilegems and W.Wiegmann,J.Appl. Phys.,47,2558(1976)

8) G.M.Martin,A.Mitonneau and A.Mircea,Electron.Lett.,13,191 (1977)

9) H.Lefevre and M.Schultz,Appl.Phys.,12,45(1977)

10) D.V.Lang,R.A.Logan and M.Jaros,Phys.Rev.B,19,1015(1979)

11) P.M.Mooney,J.Appl.Phys.,67,R1(1990)

12) W.Walukiewicz,J.Lagowski and H.C.Gatos,J.Appl.Phys.,53,375 (1982)

13) P.Blood and J.J.Harris,J.Appl.Phys.,56,993(1984)

14) R.A.Stall,C.E.C.Wood,P.D.Kirchner and L.F.Eastman,Electron. Lett.,16,171(1980)

15) Y.Akatsu,H.Ohno,H.Hasegawa and T.Hashizume,J.Cryst.Growth,

81,319(1987)

16) P.Blood,J.J.Harris,B.A.Joyce and J.H.Neave,J.De Physique 43,C5-351(1982)

17) S.B.Whitehouse,C.T.Foxon and B.A.Joyce,Appl.Phys.A,26,27 (1981)

18) J.F.van der Veen,L.Smit,P.K.Larsen,J.H.Neave and B.A.Joyce, J.Vac.Sci.Technol.,21,375(1982)

CHAPTER 5

MIDGAP STATES IN $Al_xGa_{1-x}As$ GROWN BY METALORGANIC VAPOR PHASE EPITAXY

5.1. Introduction

The $Al_xGa_{1-x}As$ alloys grown by the metalorganic vapor phase epitaxy (MOVPE) are technologically important for device applications such as heterostructure field effect transistors (FETs), heterojunction bipolar transistors (HBTs), laser diodes (LDs), light emitting diodes (LEDs) and high efficiency solar cells. However, not much is known about the deep levels in these materials.

Previous deep level transient spectroscopy (DLTS) studies[1-3] of MOVPE $Al_xGa_{1-x}As$ alloys detected deep levels lying near the midgap in addition to the well-known DX center. The DX center causes serious instability problems in modulation-doped heterostructure FETs, whereas near-midgap deep levels behave as recombination centers and affect the operating characteristics of minority carrier devices such as HBTs, LDs, LEDs and solar

cells.[4] However, neither the energy positions of the midgap levels nor their electrical and optical properties have not been clarified so far.

The purpose of this chapter is to study the electrical properties of the midgap levels in the MOVPE $Al_xGa_{1-x}As$ alloys by detailed DLTS and photocapacitance (PHCAP) measurements.

In the case of x=0, i.e., GaAs, the dominant deep level is the well-known midgap state called EL2. Owing to both basic and scientific interests, a great deal of experimental[5] and theoretical[6-8] work has been reported on this deep state. There exist various models concerning the microscopic origin of EL2, including isolated antisite arsenic (As_{Ga})[9], As_{Ga}-As vacancy pair (As_{Ga}-V_{As})[10], As cluster[11], As_{Ga}-As interstitial pair (As_{Ga}-As_I)[12], As_{Ga}-divacancy pair[13] and As_{Ga}-interstitial transition.[8] However, its origin is not completely understood except for a consensus that the EL2 is associated with excess As.

An interesting question is whether EL2-related states exist in the GaAs related alloy system such as $Al_xGa_{1-x}As$. In fact, Omling et al.[14] and Samuelson[15] have investigated the properties of deep levels in the $GaAs_{1-x}P_x$ alloy system, and have identified the presence of an EL2-related state. In so doing, they have paid a particular attention to the metastable photoquenching behavior of the state, since this is considered

to be a characteristic property of the EL2 in GaAs. For the $Al_xGa_{1-x}As$ alloy systems, however, there has been no report on the metastable property of EL2-related states.

In the present study, a particular attention is therefore paid on the photoquenching behavior of the midgap states as well as on the chemical trend of their energy positions with the alloy composition. Two deep levels were detected in MOVPE $Al_xGa_{1-x}AS$ alloys, and it is shown that one of them is closely related to the EL2 in GaAs.

5.2. Experimental

The samples used in the present work were undoped n-type MOVPE $Al_xGa_{1-x}As$ with x=0, 0.05, 0.22, 0.33 and 0.47. The MOVPE growth were performed at atmospheric pressure in a vertical reactor system.[16] Trimethylgallium (TMG), trimethylaluminum (TMA) and 10% arsine (AsH_3) in H_2 were used to grow undoped n-type $Al_xGa_{1-x}As$ layers on n^+ or semi-insulating (100) GaAs substrates. The growth temperature was 720°C and the III to V mole ratio ranged from 50 to 70. The carrier concentration of the epitaxial layer was 1-3 x 10^{16} cm^{-3} and the typical thickness was in the range of 2 to 3 μm.

The AlAs mole fraction, x, of $Al_xGa_{1-x}As$ was determined by

double crystal X-ray diffraction measurements with CuKα radiation as the X-ray source. The value of x was calculated from the difference of the diffraction angle between the $Al_xGa_{1-x}As$ epitaxial layer and the GaAs substrate.

Deep states in the undoped $Al_xGa_{1-x}As$ layers were detected by DLTS and PHCAP measurements on Al Schottky diodes. The DLTS system had a 1 MHz capacitance meter with a response time of 20 μsec and a digital boxcar integrator. The light source used in the PHCAP measurement was a GaAs LED with the emission wavelength of 0.94 μm and the FWHM of 40 nm.

5.3. DLTS Study

Figure 1 shows an example of a DLTS spectrum observed in an undoped n-$Al_{0.22}Ga_{0.78}As$ sample. The spectrum exhibits two dominant peaks with activation energies of 0.30 and 0.42 eV in the low temperature range. Similar two low temperature peaks were observed in all the AlGaAs samples but not in GaAs sample in which only a high temperature EL2 peak was present.[17] Comparing the Arrhenius plots of the emission time constants with the published data,[18] these two levels at 0.42 eV and 0.30 eV were assigned to the DX center associated with Si and to that associated with a column VI donor, respectively.

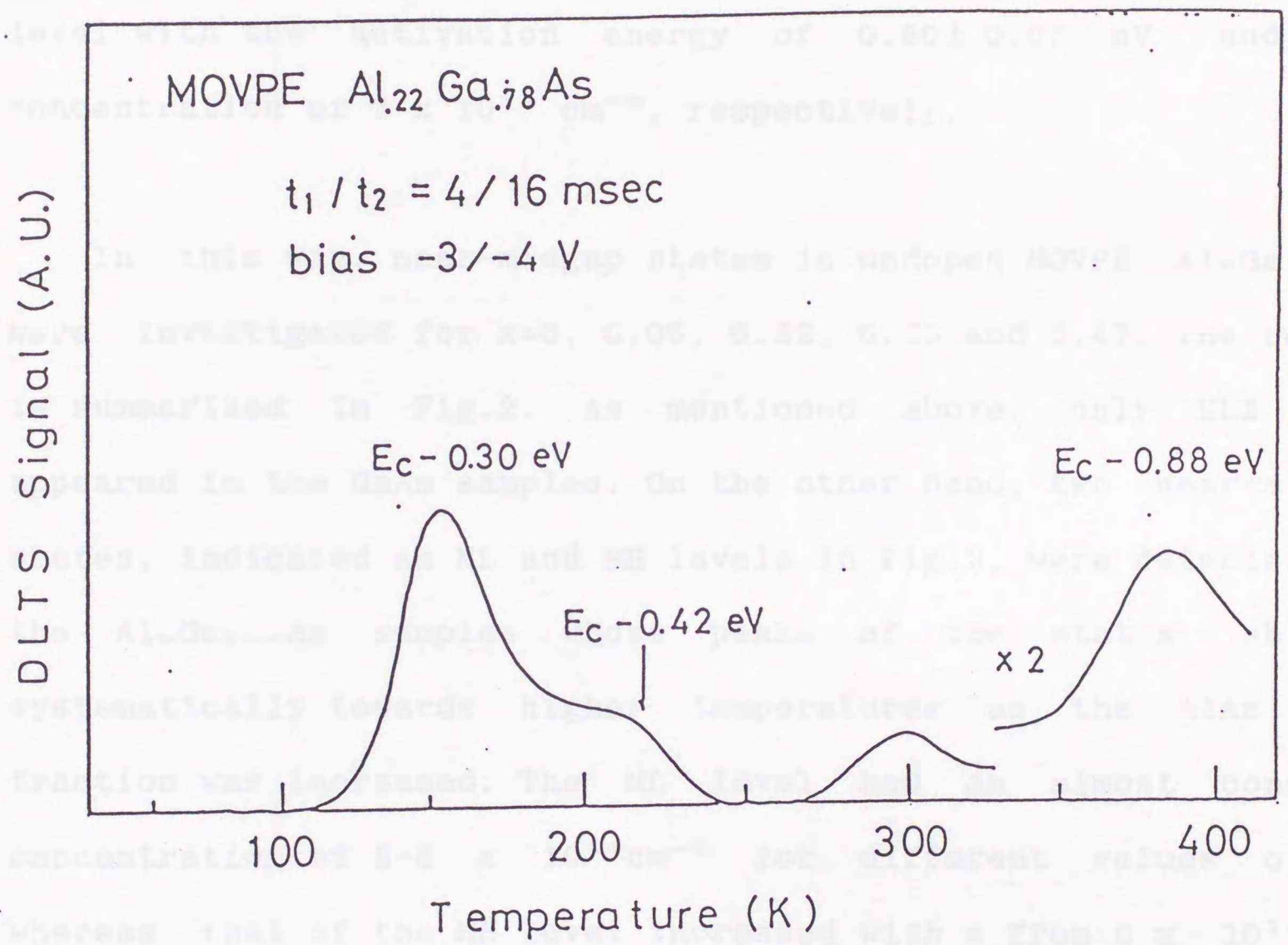

Figure 1 DLTS spectrum for a MOVPE $Al_{0.22}Ga_{0.78}As$ sample.

On the other hand, there are two peaks on the high temperature side of the DLTS spectrum. They are a lower lying midgap (ML) level with the activation energy of 0.88± 0.02 eV and the concentration of 7 x 10^{14} cm^{-3} and a higher lying midgap (MH) level with the activation energy of 0.60± 0.02 eV and the concentration of 3 x 10^{14} cm^{-3}, respectively.

In this way, near-midgap states in undoped MOVPE $Al_xGa_{1-x}As$ were investigated for x=0, 0.05, 0.22, 0.33 and 0.47. The result is summarized in Fig.2. As mentioned above, only EL2 peak appeared in the GaAs samples. On the other hand, two near-midgap states, indicated as ML and MH levels in Fig.2, were detected in the $Al_xGa_{1-x}As$ samples whose peaks of the states shifted systematically towards higher temperatures as the AlAs mole fraction was increased. The ML level had an almost constant concentration of 6-8 x $10^{14}cm^{-3}$ for different values of x, whereas that of the MH level increased with x from 6 x $10^{13}cm^{-3}$ for x=0.05 to 8 x$10^{14}cm^{-3}$ for x=0.47. Since two peaks were very close to each other in the cases of x=0.33 and 0.47, they were separated by curve fitting, assuming that the response is a superposition of two discrete levels. Figure 3 shows the Arrhenius plots of two midgap states for $Al_xGa_{1-x}As$ as well as those of the EL2 level (x=0). The activation energies of the ML and MH levels increased as the value of x was increased from 0.05 to 0.47. The activation energy and the cross section of the ML

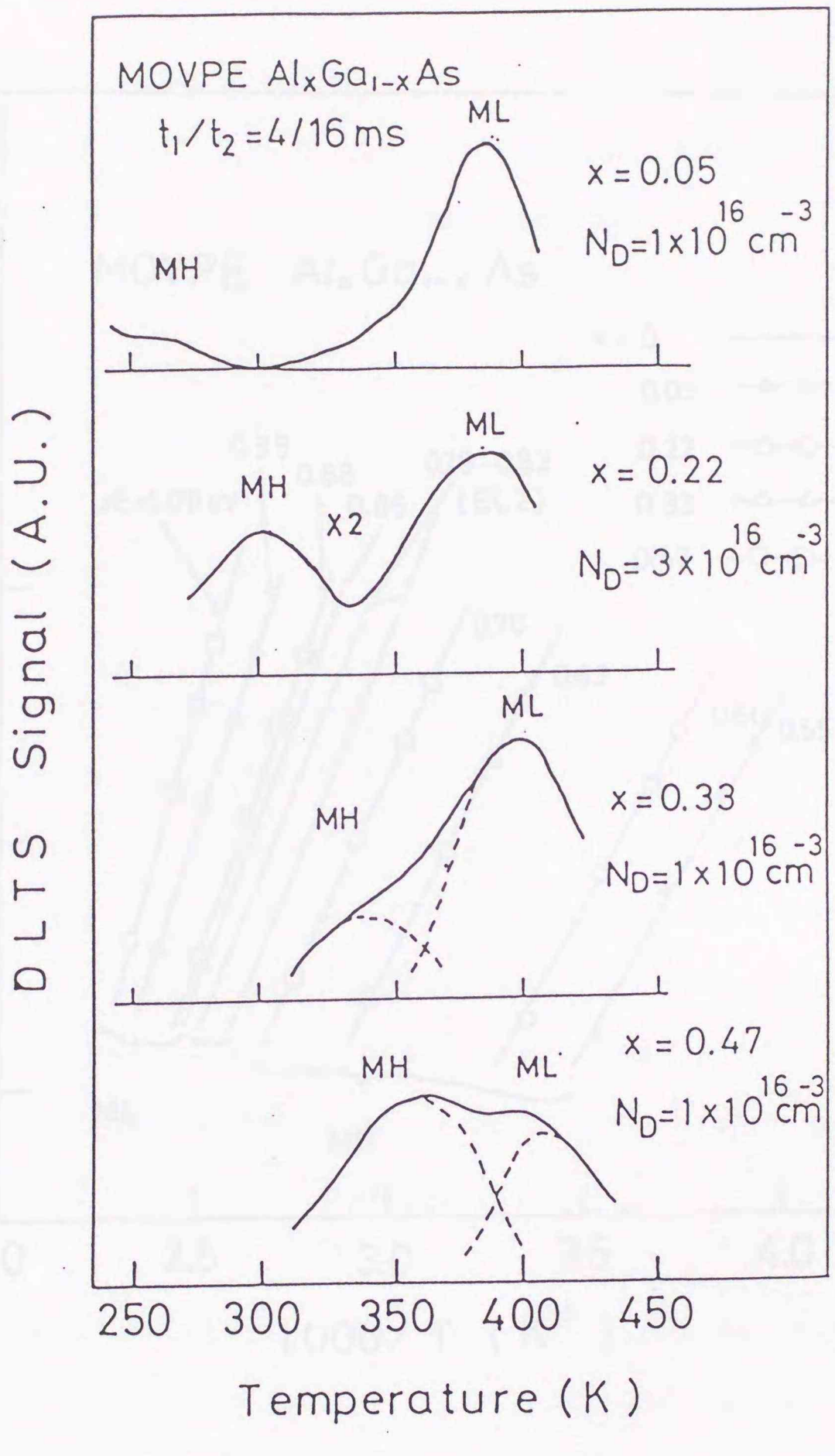

Figure 2 Summary of DLTS spectra of the midgap levels in the MOVPE $Al_xGa_{1-x}As$ system.

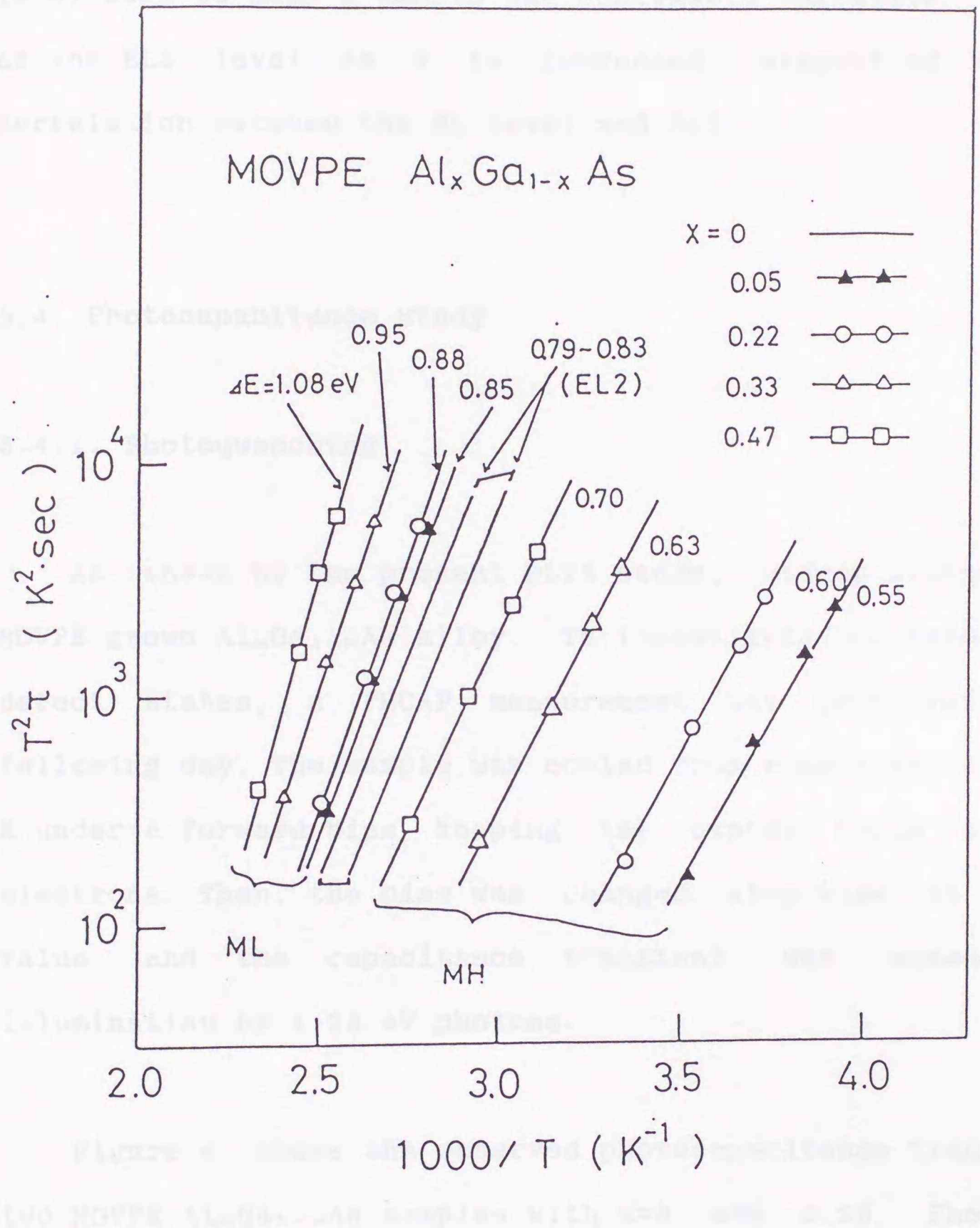

Figure 3 Arrhenius plots of the electron emission rate for the midgap levels in the MOVPE $Al_xGa_{1-x}As$ system.

level seem to make a smooth and continuous variation from those of the EL2 level as x is increased, suggesting a possible correlation between the ML level and EL2.

5.4. Photocapacitance Study

5.4.1. Photoquenching

As shown by the present DLTS study, midgap states exist in MOVPE grown $Al_xGa_{1-x}As$ alloy. To investigate the nature of these defect states, a PHCAP measurement was performed in the following way. The sample was cooled from room temperature to 70 K under a forward bias, keeping the states being occupied by electrons. Then, the bias was changed step-wise to a reverse value and the capacitance transient was measured under illumination by 1.32 eV photons.

Figure 4 shows the observed photocapacitance transients for two MOVPE $Al_xGa_{1-x}As$ samples with x=0 and 0.22. Photoquenching effects were seen in both samples, indicating the presence of the EL2-like metastable deep states in the $Al_{0.22}Ga_{0.78}As$ sample. A quantitative analysis of the amount of change involved in the quenching has indicated that the quenching is caused by the ML level, and not by the MH level. As compared with the case of GaAs, the quenching behavior in the $Al_{0.22}Ga_{0.78}As$ sample is

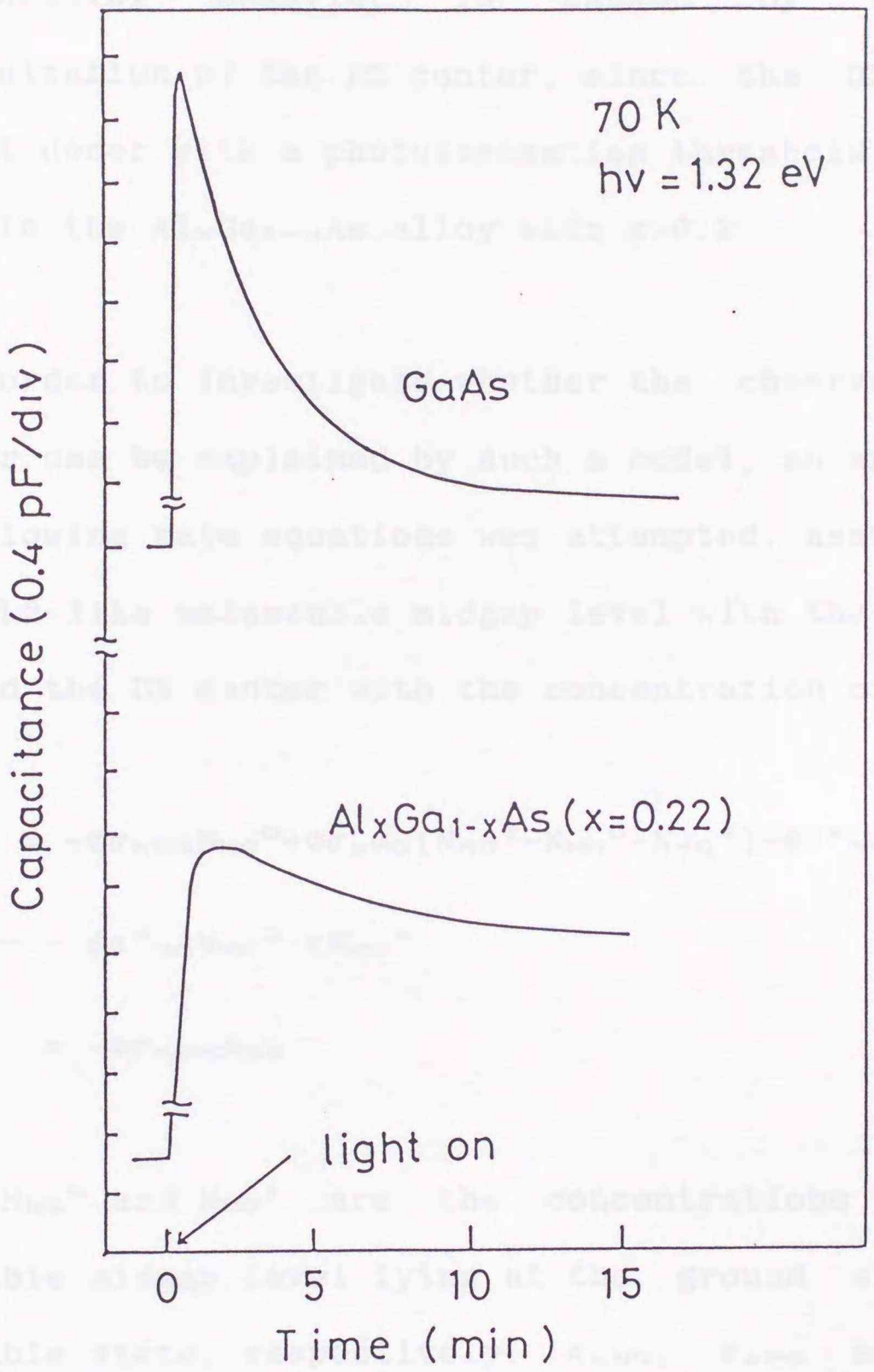

Figure 4 Observed photocapacitance transients for the $Al_xGa_{1-x}As$ samples with x = 0 and 0.22

apparently highly nonexponential. It is possible that this nonexponential behavior is caused by the simultaneous photoionization of the DX center, since the DX center is the dominant donor with a photoionization threshold energy of about 1.0 eV in the $Al_xGa_{1-x}As$ alloy with $x>0.2$.

In order to investigate whether the observed nonexponential behavior can be explained by such a model, an analysis based on the following rate equations was attempted, assuming coexistence of an EL2-like matastable midgap level with the concentration of N_{MG}^T and the DX center with the concentration of N_{DX}.

$$\frac{dN_{MG}^G}{dt} = -\phi\sigma_{nMG}N_{MG}^G+\phi\sigma_{pMG}(N_{MG}^T-N_{MG}^G-N_{MG}^*)-\phi\sigma^*_{MG}N_{MG}^G+rN_{MG}^* \quad (5.1)$$

$$\frac{dN_{MG}^*}{dt} = \phi\sigma^*_{MG}N_{MG}^G-rN_{MG}^* \quad (5.2)$$

$$\frac{dN_{DX}}{dt} = -\phi\sigma_{nDX}N_{DX} \quad (5.3)$$

Here, N_{MG}^G and N_{MG}^* are the concentrations of the EL2-like metastable midgap level lying at the ground state and at the metastable state, respectively. σ_{nMG}, σ_{pMG} and σ^*_{MG} are the optical cross sections of the midgap level for electron emission, hole emission and electron excitation to the metastable state, respectively. r is the thermal recovery rate from the metastable state down to the ground state of the midgap level. ϕ is the photon flux density. σ_{nDX} is the optical cross section of the DX center. Figure 5 shows the calculated normalized photoquenching

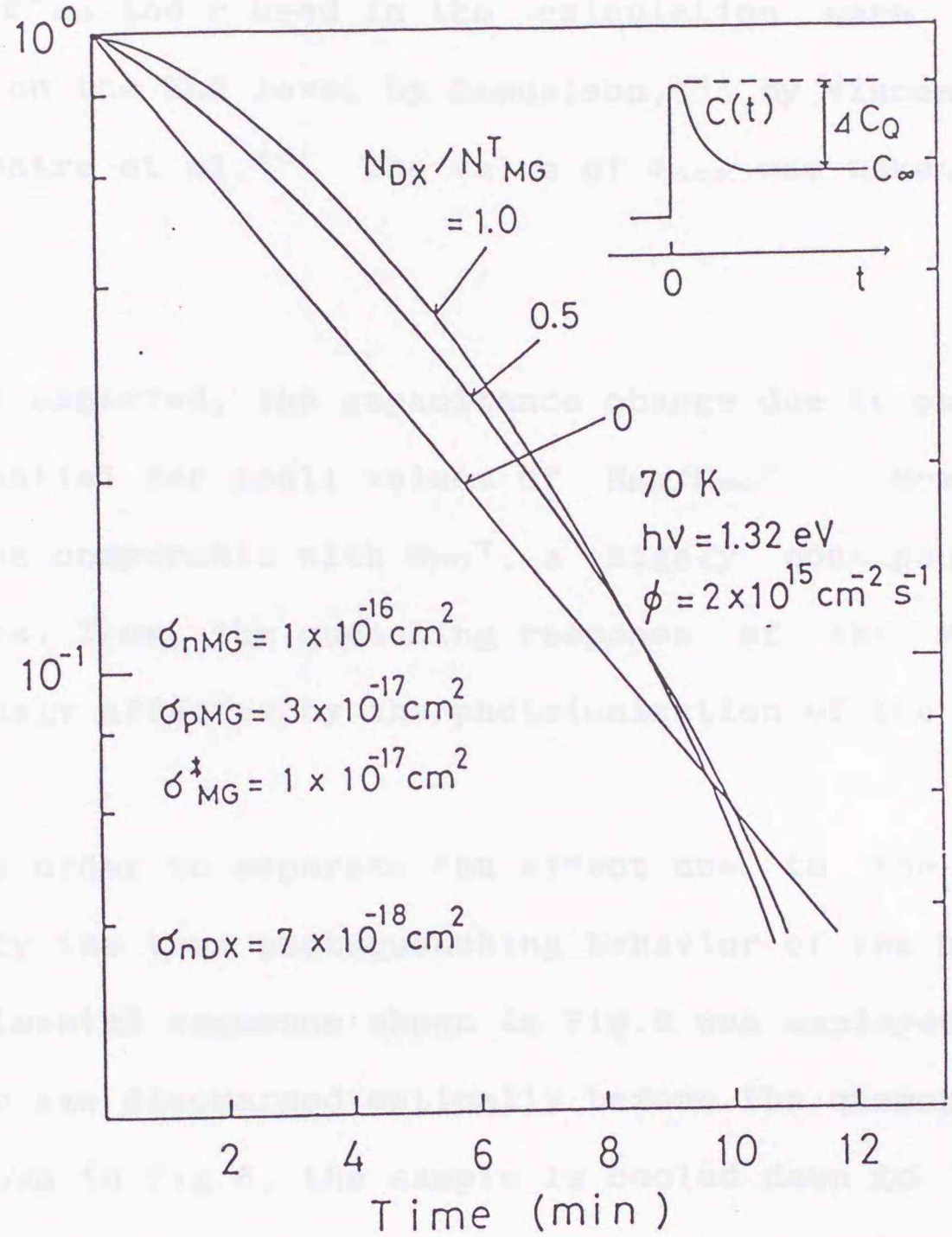

Figure 5 Calculated photoquenching transients of capacitance at 70 K for different ratios of concentration of DX center to that of the midgap level, N_{DX}/N_{MG}^{T}. The vertical scale is $(C(t)-C_{\infty})/\Delta C_Q$ where C_{∞} is the steady state value of capacitance and ΔC_Q is the total amount of capacitance quenching. The values of capture cross section are taken from refs.15,19,20 and 21.

transients at 70 K for different ratios of the concentration of DX center to that of midgap state, $N_{DX}/N_{MG}{}^{T}$. The value of σ_{nMG}, σ_{pMG}, $\sigma^{*}{}_{MG}$ and r used in the calculation were taken from the works on the EL2 level by Samuelson,[15] by Vincent et al.[19] and by Chantre et al.[20] The value of σ_{nDX} was taken from Moony et al.[21]

As expected, the capacitance change due to photoquenching is exponential for small values of $N_{DX}/N_{MG}{}^{T}$. However, when N_{DX} becomes comparable with $N_{MG}{}^{T}$, a highly nonexponential behavior appears. Thus, the quenching response of the midgap level is seriously affected by the photoionization of the DX center.

In order to separate the effect due to the DX center and clarify the true photoquenching behavior of the ML level, a new experimental sequence shown in Fig.6 was employed where the DX center was discharged optically before the quenching was studied. As shown in Fig.6, the sample is cooled down to 70 K under a forward bias. Then, it is illuminated with 1.32 eV photons under a reverse bias. Subsequently, the temperature is raised up to 120 K. In this sequence, the DX center is emptied by the first illumination. When the light is turned off and the temperature is raised to 120K, electrons can not return to the DX center due to the presence of the capture barrier, which causes the well known persistent photoconductance effect. On the other hand, electrons in the midgap state are also transferred into its matastable

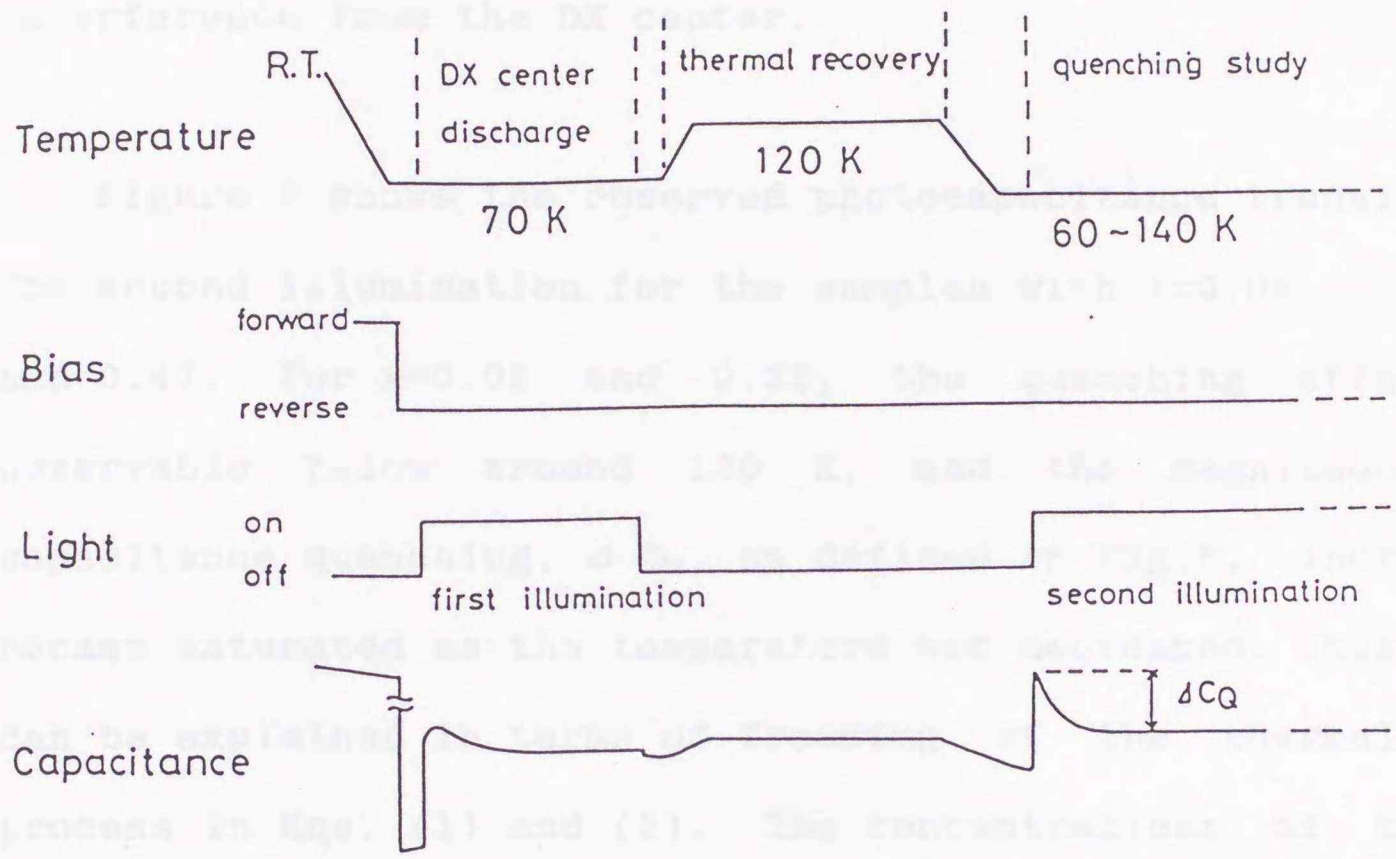

Figure 6 A new experimental procedure to separate the effect due to the DX center from the photoquenching behavior of the midgap level.

state by the first illumination. However, they can gradually return to the ground state in the dark at around 120 K due to the thermal recovery. Thus, one can examine the quenching effect of the midgap state with the second illumination without interference from the DX center.

Figure 7 shows the observed photocapacitance transient under the second illumination for the samples with x=0.05, 0.22, 0.33 and 0.47. For x=0.05 and 0.22, the quenching effect became observable below around 130 K, and the magnitude of the capacitance quenching, ΔC_Q, as defined in Fig.6, increased and became saturated as the temperature was decreased. This behavior can be explained in terms of freezing of the thermal recovery process in Eqs. (1) and (2). The concentrations of the midgap state in these samples estimated from the magnitude of ΔC_Q at 60 K was in good agreement with those of the ML level obtained from the DLTS measurements. On the other hand, no quenching effect was observed for x=0.33 and 0.47, in spite of the fact that the DLTS spectra in Fig.2 clearly indicated presence of the peak of the ML midgap level.

The photoquenching transients observed for the samples with x=0, 0.05 and 0.22 under the the new measurement procedure are plotted in Fig.8 in the normalized form. As compared with Fig.4, purely exponential behavior is seen for each sample, indicating that the present experimental procedure removes the effect due to

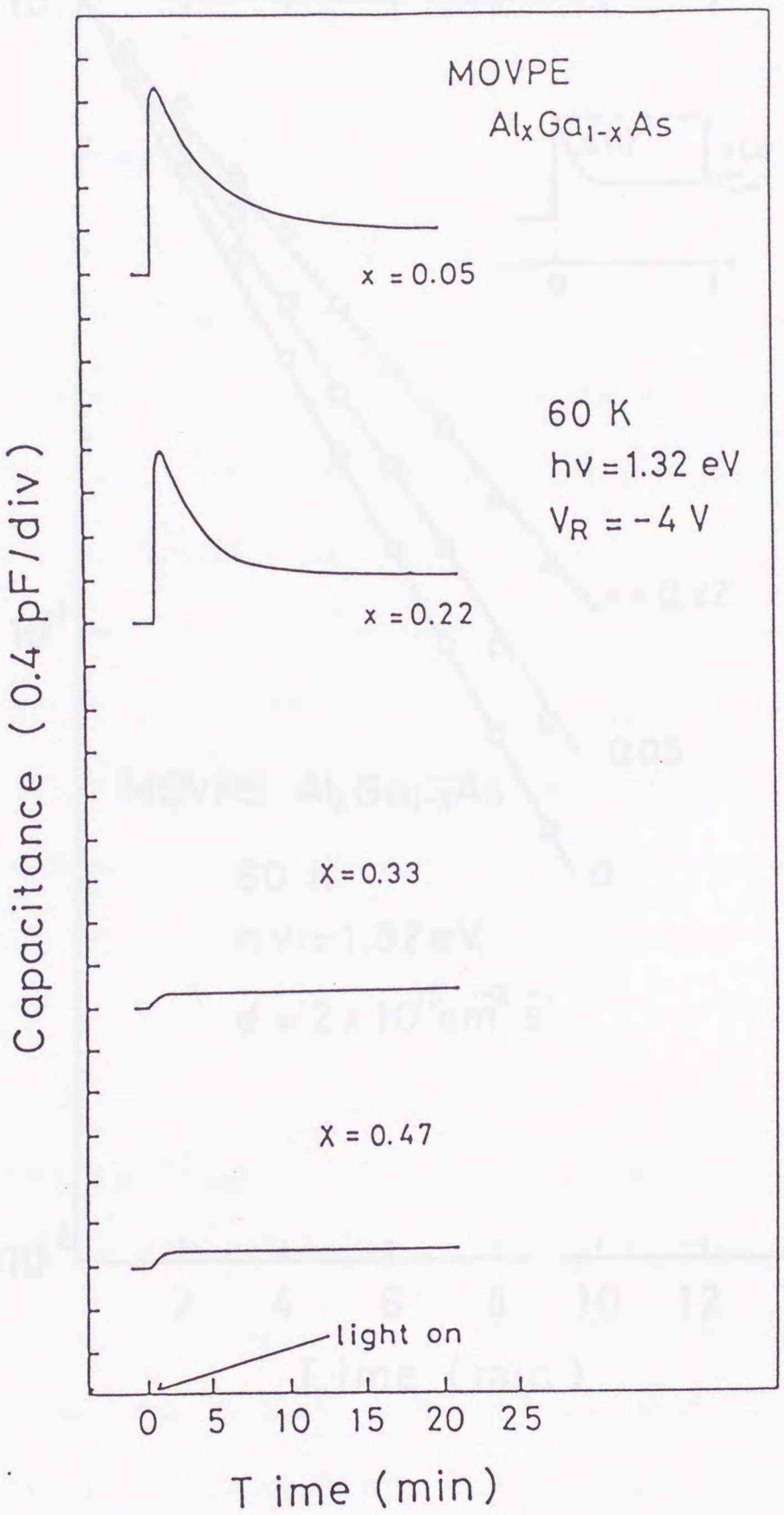

Figure 7 Photocapacitance transients at 60 K under the second illumination for MOVPE $Al_xGa_{1-x}As$ samples with x=0.05, 0.22, 0.33 and 0.47.

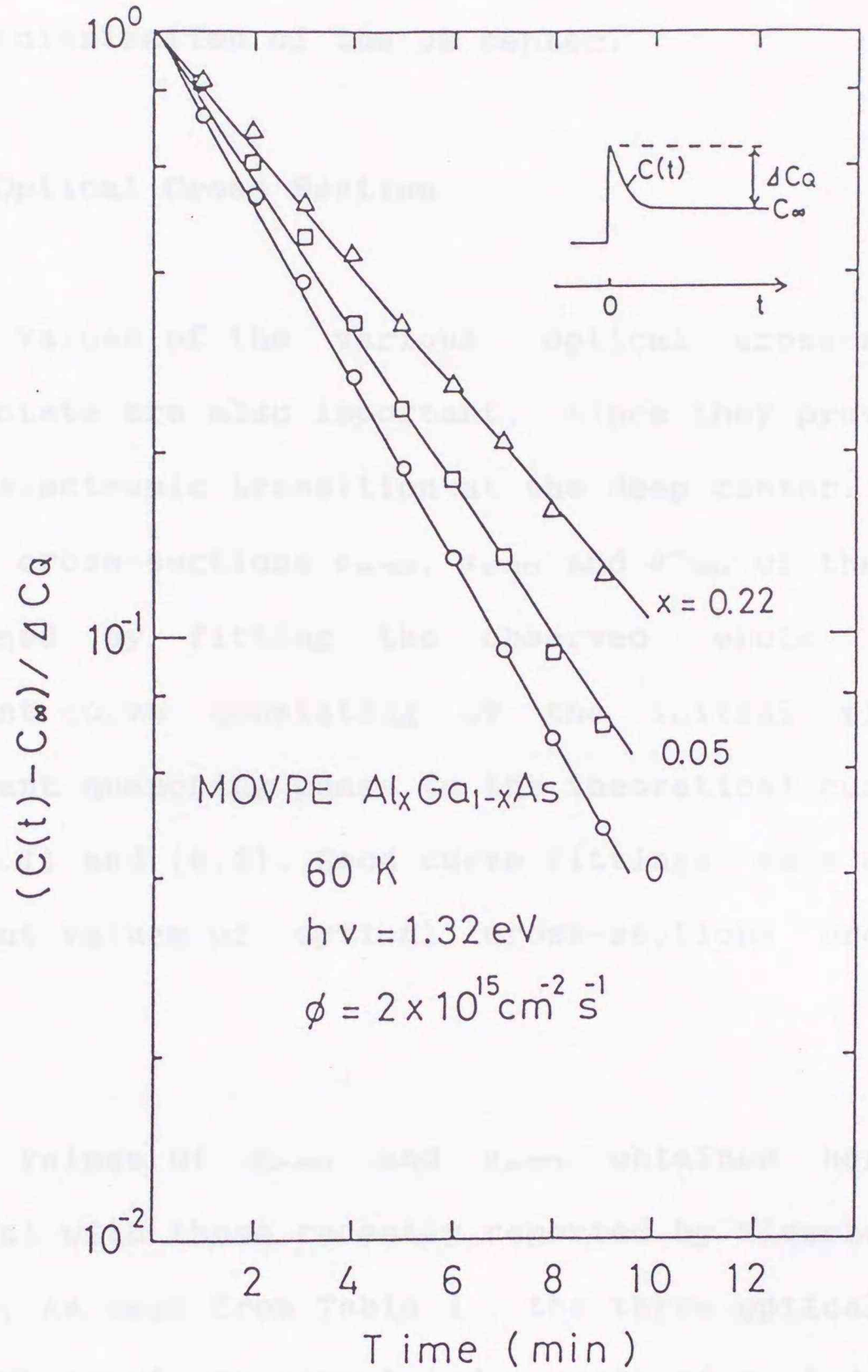

Figure 8 Normalized quenching transients in the MOVPE $Al_xGa_{1-x}As$ samples with x=0, 0.05 and 0.22.

the photoionization of the DX center.

5.4.2. Optical Cross Section

The values of the various optical cross-sections of the midgap state are also important, since they provide information on the electronic transition at the deep center. The values of optical cross-sections σ_{nMG}, σ_{pMG} and σ^*_{MG} of the ML level can be determined by fitting the observed whole photocapacitance transient curve consisting of the initial rising phase and subsequent quenching phase to the theoretical curve based on the Eqs. (5.1) and (5.2). Good curve fittings were obtained and the resultant values of optical cross-sections are summarized in Table I.

The values of σ_{nMG} and σ_{pMG} obtained here are in good agreement with those recently reported by Siverberg et al.[22] for the EL2. As seen from Table I , the three optical cross-sections of the ML level are almost independent of x, indicating that the electron transfer mechanism from the ground state to the metastable state of the ML midgap level in $Al_xGa_{1-x}As$ is similar to that of EL2 in GaAs.

Table I Values of optical cross-sections for EL2 and the ML level in the MOVPE $Al_xGa_{1-x}As$. These values were determined by the fitting the observed capacitance transient to the theoretical curve based on Eqs. (5.1) and (5.2).

composition	optical cross-section (x $10^{-17}cm^2$)		
x	σ_{nMG}	σ_{pMG}	σ^*_{MG}
0 (EL2)	12	2.1	1.5
0.05	14	1.8	1.1
0.22	12	2.2	1.4

5.4.3. Thermal Recovery

The present experimental procedure can be extended further to determine thermal recovery parameters of the metastable state. Figure 9 shows a configuration coordinate model of an EL2-like state with a metastable property. According to such a model, the thermal recovery rate, r, of the state is temperature-dependent in the following way,[19]

$$r = r_o \exp(-\Delta E_B/kT) \qquad (5.4)$$

where ΔE_B is the barrier between the ground state (MG^G) and the metastable state (MG^*) as shown in Fig.9.

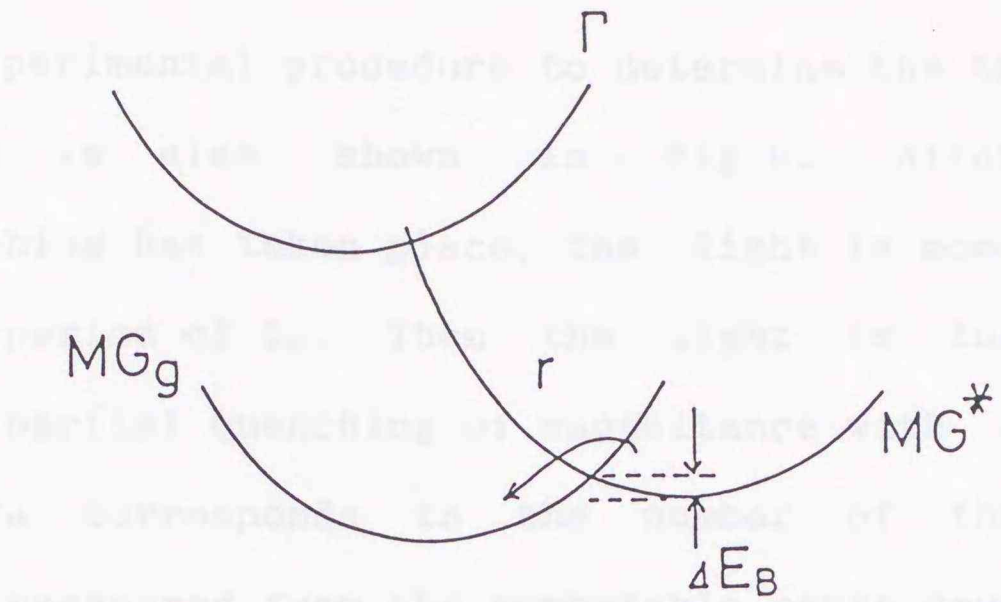

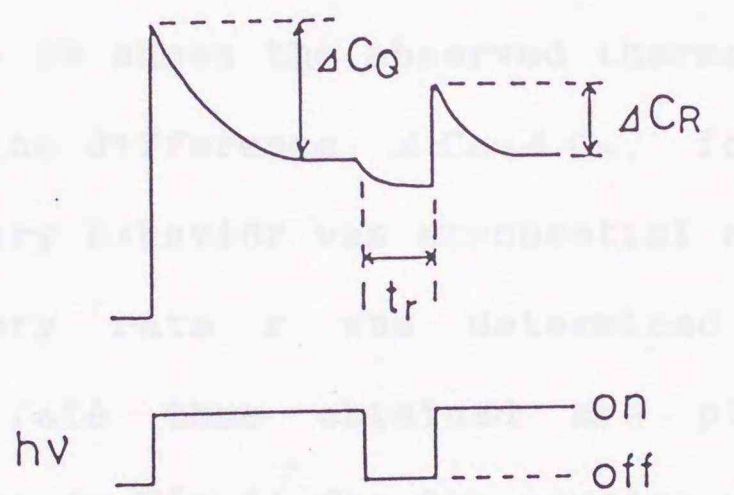

Figure 9 Configuration coordinate model of of the midgap level having a ground state (MG^G) and a metastable state (MG^*), and the experimental procedure to measure the rate, r, of the thermal recovery process from the matastable state to the ground state.

The experimental procedure to determine the thermal recovery parameters is also shown in Fig.9. After a complete photoquenching has taken place, the light is momentarily turned off for a period of t_r. Then the light is turned on again, causing a partial quenching of capacitance with a magnitude of ΔC_R. ΔC_R corresponds to the number of the midgap state thermally recovered from the metastable state down to the ground state during the time t_r.

Figure 10 shows the observed thermal recovery transients in terms of the difference, $\Delta C_Q - \Delta C_R$, for a sample with x=0.05. The recovery behavior was exponential at the initial phase and the recovery rate r was determined from this portion. The recovery rate thus obtained are plotted versus reciprocal temperature in Fig.11 for the samples with x=0, 0.05 and 0.22. The activation energy ΔE_B for GaAs was found to be 0.38 eV, which agrees well with the previous work.[19] The value of ΔE_B for the sample with x=0.05 agrees with that for GaAs above 120 K. However, the recovery rate became anomalously constant in the temperature range below 120 K. Furthermore, the recovery rate for the sample with x=0.22 was about two orders of magnitude larger than that for GaAs and ΔE_B was estimated to be 0.08 $\pm$ 0.03 eV.

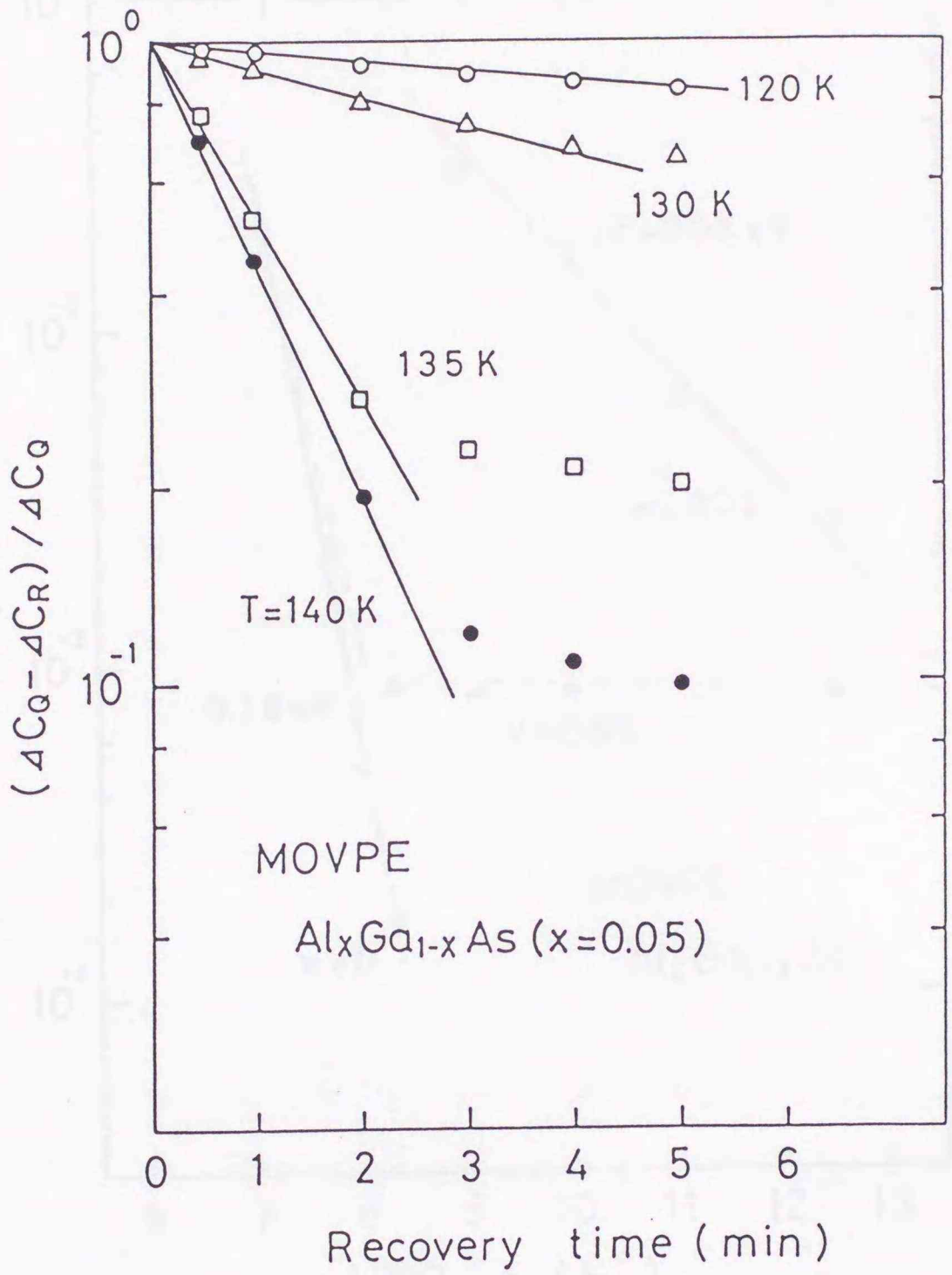

Figure 10 Plots of the observed normalized partial quenching of capacitance as a function of the time, t_r, to cause it

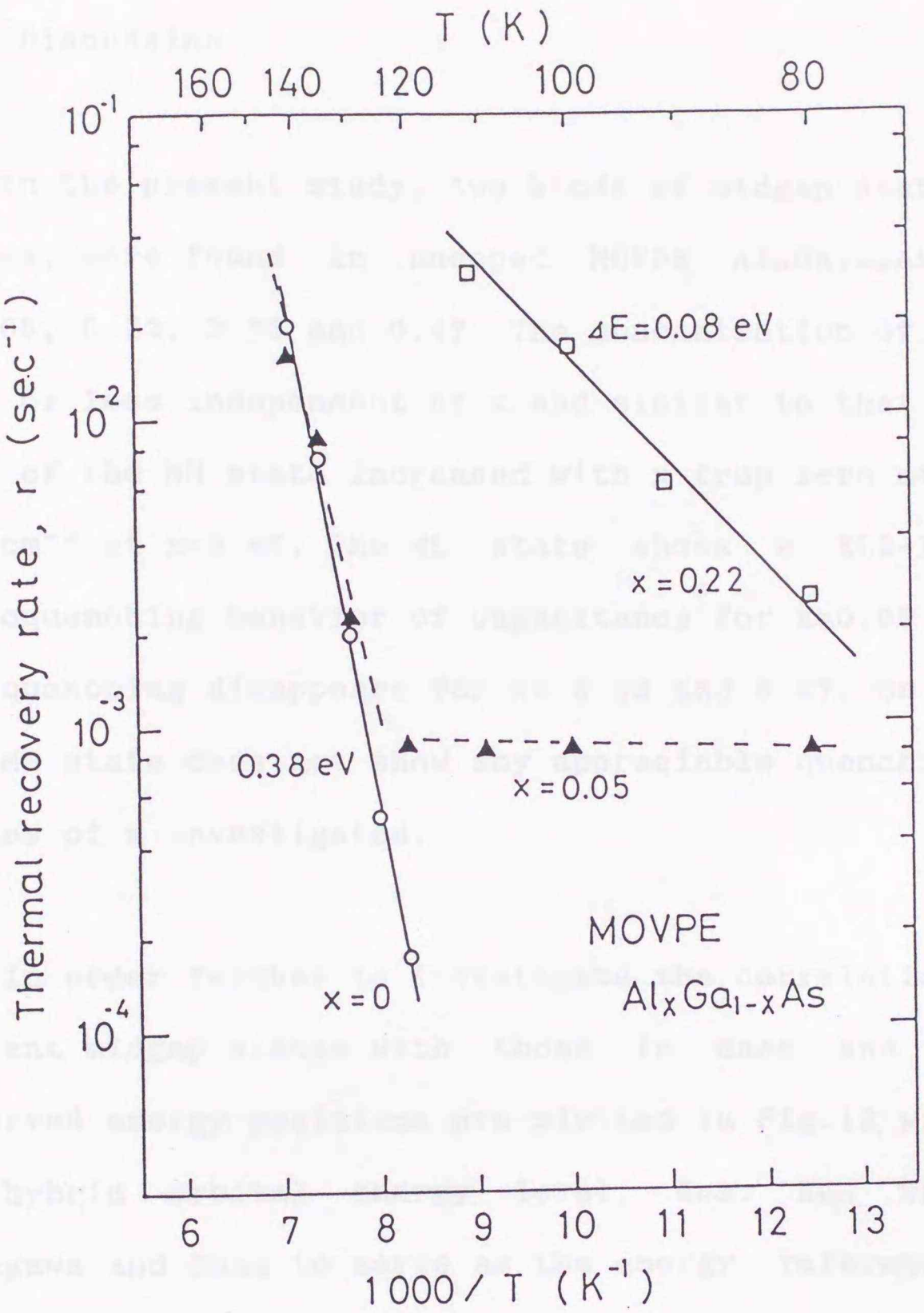

Figure 11 Arrhenius plots of the measured thermal recovery rate, r, for MOVPE $Al_xGa_{1-x}As$ with x=0, 0.05 and 0.22. r is evaluated from the linear portion of the recovery curves shown in Fig.10.

5.5. Discussion

In the present study, two kinds of midgap states, MH and ML states, were found in undoped MOVPE $Al_xGa_{1-x}As$ samples with x=0.05, 0.22, 0.33 and 0.47. The concentration of the ML state is more or less independent of x and similar to that of EL2, whereas that of the MH state increased with x from zero at x=0 to 8 x $10^{14}cm^{-3}$ at x=0.47. The ML state shows a EL2-like remarkable photoquenching behavior of capacitance for x=0.05 and 0.22, but the quenching disappears for x= 0.33 and 0.47. On the other hand, the MH state does not show any appreciable quenching for all the values of x investigated.

In order further to investigate the correlation between the present midgap states with those in GaAs and $GaAs_xP_{1-x}$, the observed energy positions are plotted in Fig.12 with respect to the hybrid orbital energy level, E_{HO}. E_{HO} was proposed by Hasegawa and Ohno to serve as the energy reference for the DX center, EL2 and transition metal levels[23,24] in major III - V compound semiconductors. It plays important roles also in the heterojunction band line-up[25] and in the interface states distributions at insulator-semiconductor and metal-semiconductor interfaces.[26] E_{HO} appears to be equivalent or closely related to the charge nuetrality level[27] or midgap energies[28,29] proposed by other authors.

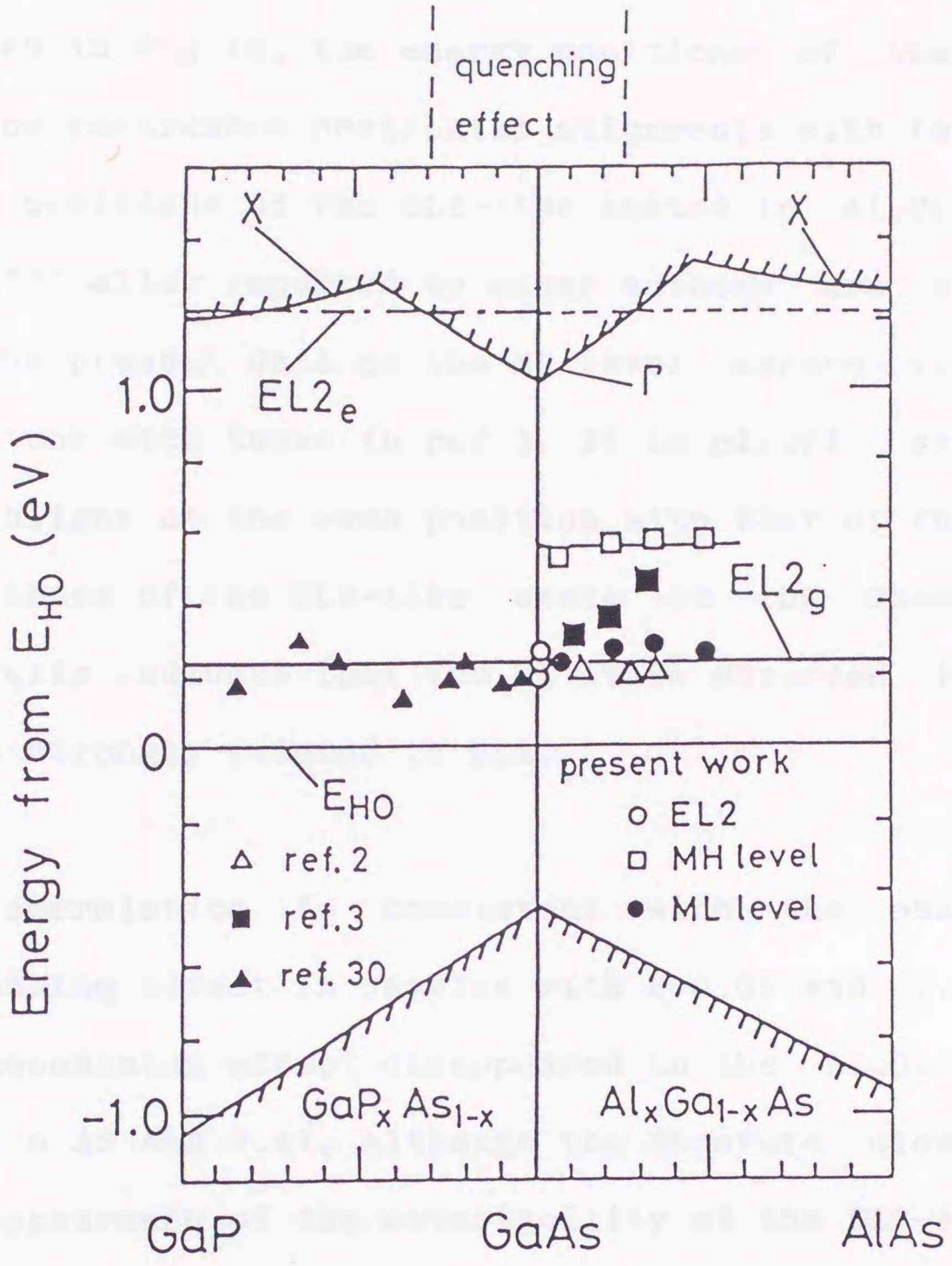

Figure 12 Alignment of the level positions of the midgap levels in $Al_xGa_{1-x}As$ and $GaAs_{1-x}P_x$ alloy systems including present ML and MH levels. E_{HO} is the hybrid orbital energy in refs.23～26 and serves as a reference energy for these levels. Data shown by closed triangles are taken from ref.30, open triangles, from ref.2 and closed squares, from ref.3, respectively. The location of the excited state of the EL2-related states is indicated by the dash-dot line ($GaAs_{1-x}P_x$) and the dashed line ($Al_xGa_{1-x}As$). The photoquenching takes place only when the excited state is resonant with the conduction band.

As seen in Fig.12, the energy positions of the MH and ML states show remarkable horizontal alignments with respect to E_{HO}. The level positions of the EL2-like states in $Al_xGa_{1-x}As$[2,3] and $GaAs_{1-x}P_x$[30] alloy reported by other authors are also shown in Fig.12. The present data on the ML level agrees with those in ref.2 but not with those in ref.3. It is clearly seen that the ML level aligns at the same position with that of the EL2 in GaAs and with those of the EL2-like state in the $GaAs_{1-x}P_x$ alloy. These results indicate that the ML state observed in $Al_xGa_{1-x}As$ system is strongly related to EL2.

Such correlation is consistent with the observation of photoquenching effect in samples with x=0.05 and 0.22. However, the photoquenching effect disappeared in the $Al_xGa_{1-x}As$ samples with x = 0.33 and 0.47, although the ML state clearly existed. Such disappearance of the metastability of the EL2-like level was previously observed in $GaAs_{1-x}P_x$ alloy by Samuelson[15] who correlated the phenomenon with the presence of an excited state of the EL2-like level. According to Samuelson, the photoquenching effect takes place by a successive transfer of electrons from the ground to the metastable state through an excited state lying at a higher energy. This transfer can only take place under the condition that the excited state remains resonant with the conduction band, resulting in considerable de-localization. As the alloy composition is varied, this excited state changes, however, its character and becomes a discrete and localized state

lying in the forbidden band for x>0.3 in the $GaAs_xP_{1-x}$ alloy. Then, the quenching transition no longer takes place.

The present study shows that a similar phenomenon takes place in the MOVPE $Al_xGa_{1-x}As$ alloy. The dash-dot line in Fig.12 shows the energy position of the excited state of EL2[9,31,32] and that of the EL2-like level in $GaAs_{1-x}P_x$ alloy.[15] The fact that the observed optical cross sections of the $Al_xGa_{1-x}As$ alloy are independent of x indicates that the excited state of the midgap level in $Al_xGa_{1-x}As$ also lies on the dashed line in Fig.12 which is an extrapolation of the dash-dot line in parallel to E_{HO}. Thus, as seen in Fig.12, the excited state of the midgap level is expected to appear in the forbidden band at or above x=0.3 in $Al_xGa_{1-x}As$. This is consistent with the observed disappearance of the photoquenching effect in the samples with x=0.33 and 0.47. Therefore, the result obtained in the present MOVPE $Al_xGa_{1-x}As$ alloy is consistent with Samuelson's suggestion, although there exists an additional hitherto undiscussed complication that the energy position of the DX center itself is almost the same as that of the excited state of the midgap level.[23]

From the above discussion, it can be concluded that the ML level in the present study is closely related to the EL2 in GaAs and originates from a certain As-related defect. It is also noted that the EL2-related state in both $Al_xGa_{1-x}As$ and $GaAs_{1-x}P_x$ alloys possess remarkably the same basic metastable behavior

with the EL2 in GaAs, not so much being affected by the way of partial substitution of whether column III atoms or column V atoms are incorporated into the host binary lattice. This seems to indicate that these defects originate from a complex defect rather than a simple pair of defects.[33] On the other hand, the origin of the MH level, whose concentration increased with x, is most probably related to Al.

Finally, a comment is made on the observed anomalous behavior of the thermal recovery rate of the ML level. Parker and Bray[34] has shown very recently that the thermal recovery rate of EL2 in oxygen doped GaAs has a very much reduced thermal activation energy of about 0.08eV. They have suggested that the presence of oxygen could modify the thermal recovery process without influencing the basic photoquenching behavior. It has also been shown that the thermal activation energy of the recovery process is sample dependent in liquid encapsulated Czochralski (LEC) GaAs.[35] Furthermore, formation of a metastable defect which behaves like EL2 has been reported in a plastically deformed GaAs.[36] Thus, the observed high thermal recovery rate in the $Al_xGa_{1-x}As$ samples seems to be caused most probably by delicate modification of the metastable state due to the different atomic surroundings.

5.6. Conclusion

The electrical properties of the midgap levels in the MOVPE $Al_xGa_{1-x}As$ alloys were studied by the DLTS and PHCAP technique. A new PHCAP measurement procedure was used to separate the effect of the photoionization of the DX center from the photoquenching of the midgap states.

Two levels, i.e., the ML and MH levels, were found to exist. Their energy positions stay constant with respect to the hybrid orbital energy level E_{HO} when the alloy composition is varied. The higher lying MH level lies at about 0.58eV from E_{HO}, and the lower lying ML level lies at about 0.24eV from E_{HO}. The concentration of the ML level was almost independent of x, whereas that of the MH level was zero in GaAs and increased with x.

The ML level exhibits an remarkable photoquenching for $x<0.3$, which disappears above $x=0.3$. The similarity of the photoquenching behavior to that in $GaAs_xP_{1-x}$ alloy as well as the energy position and the optical cross sections have led to the conclusion that the ML level is closely related to the EL2 in GaAs and originates from a certain complex defect related to As.

On the other hand, the MH level does not show photoquenching for all x, and is most probably related to Al.

References

1) E.E.Wagner,D.E.Mars,G.Hom,and G.B.Stringfellow,J.Appl.Phys. 51,5434(1980)

2) N.M.Johnson,R.D.Burnham,D.Fekete,R.Yingling,*Defects in Semiconductors* (North-Holland,Amsterdam,1981),p.481

3) T.Matsumoto and P.K.Bhattacharya,Appl.Phys.Lett.41, 662(1982)

4) P.M.Mooney,*Semi-Insulating III-V Materials* (Hilger,Bristol, 1988),p.277

5) For recent review, see for example, "Recent developments in the study of the EL2 defect in GaAs", Rev.Phys.Appl.23,727 (1988), ed. by H.J.von Bardeleben and B.Pajot, and references therein.

6) G.A.Baraff and M.Schluter,Phys.Rev.B 35,6154(1987)

7) J.Dabrowski and M.Scheffler,Phys.Rev.Lett.60,2183(1988)

8) D.J.Chadi and K.J.Chang,Phys.Rev.Lett.60,2187(1988)

9) M.Kaminska,M.Skowronski,and W.Kuszko,Phys.Lev.Lett.55,2204 (1985)

10) J.Lagowski,M.Kaminska,J.M.Persey,H.C.Gatos,and W.Walukiewicz, Inst.Phys.Conf.Ser.65,41(1982)

11) T.Ikoma and M.Mochizuki,Jpn.J.Appl.Phys.24,L905(1985)

12) H.J.von Bardeleben,D.Stievenard,D.Deresmes,A.Huber,and J.C. Bourgoin,Phys.Rev.B 34,7192(1986)

13) J.F.Wager and J.A.Van Vechten,Phys.Rev.B 35,2330(1987)

14) P.Omling,L.Samuelson,and H.G.Grimmeiss,Phys.Rev.B 29,

4534(1984)

15) L.Samuelson,Physica 117B,104(1984)

16) E.Ikeda,H.Hasegawa,S.Ohtsuka,and H.Ohno,Jpn.J.Appl.Phys. 27,180(1988)

17) T.Hashizume,E.Ikeda,Y.Akatsu,H.Ohno,and H.Hasegawa,Jpn.J. Appl.Phys.23,L296(1984)

18) O.Kumagai,H.Kawai,Y.mori,and K.Kaneko,Appl.Phys.Lett.45, 1332(1984)

19) G.Vincent,D.Bois,and A.Chantre,J.Appl.Phys.53,3643(1982)

20) A.Chantre,G.Vincent,and D.Bois,Phys.Rev.B 23,5335(1981)

21) P.M.Mooney,G.A.Northrop,T.N.Morgan,and H.G.Grimmeiss,Phys. Rev.B 37,8298(1988)

22) P.Siverberg,P.Omling, and L.Samuelson,Appl.Phys.Lett.52, 1689(1988).

23) H.Hasegawa and H.Ohno,Jpn.J.Appl.Phys.25,L319(1986)

24) H.Hasegawa,Solid State Commun.,58,157(1986)

25) H.Hasegawa and H.Ohno,J.Vac.Sci.Technol.B4,1130(1986)

26) H.Hasegawa,H.Ohno and T.Sawada,Jpn.J.Appl.Phys.,25,L265(1986)

27) F.Flores and C.Tejedor,J.Phys.C 12,731(1979)

28) J.Tersoff,Phys.Rev.B 30,4874(1984)

29) M.Cardona and N.E.Christensen,Phys.Rev.B 35,6182(1987)

30) L.Samuelson,Proc.13th Int.Conf.on Defects in Semiconductors, ed. by L.C.Kimering and J.M.Parsey Jr.(Metallurgical Soc.of AIME,1985),p.101

31) M.Kaminska,M.Skowronski,J.Lagowski,J.M.Parsey,and H.C.Gatos, Appl.Phys.Lett.43,302(1983)

32) Y.Mochizuki and T.Ikoma,*Semi-Insulating III-V Materials* (OHMUSHA,Tokyo,1986),p.323

33) M.O.Manasreh,and D.W.Fischer,Phys.Rev.B 39,3239(1989)

34) J.C.Parker and R.Bray,Phys.Rev.B 37,6368(1988)

35) D.W.Fischer,Phys.Rev.B 37,2968(1988)

36) T.Haga,M.Suezawa,and K.Sumino,Jpn.J.Appl.Phys.27,1929(1988)

CHAPTER 6

VARIATION OF DEEP LEVELS IN BULK GaAs CAUSED BY γ-IRRADIATION

6.1. Introduction

One powerful method of studying the nature of defects is to try to artificially modify the atomic configuration of the defects and to introduce other defects by irradiation. One can obtain information on their electrical and optical properties or their interactions with impurities and/or grown-in defects by a combination of complementary techniques. The midgap state, EL2 in GaAs, which plays a dominant role in growing the semi-insulating (SI) substrate, has been investigated in this procedure, and very important results on the identification of EL2 have been reported.[1] In addition, as to the defects in GaAs introduced by electron-irradiation, which are the so-called E and H traps, considerable effort has been devoted to clarifing their origin.[2] By comparison, relatively little work has been done on the effect of irradiation on the properties of other grown-in states, such as EL6, which is recently considered to play a

significant role in the compensation mechanism for liquid encapsulated Czochralski (LEC) GaAs.[3,4]

From the technological viewpoint, it is of importance to investigate the influence of irradiation on such characteristics of semiconductor devices as the decrease in transconductance and saturation current or the fluctuation of threshold voltage in the field effect transistor (FET), and the decrease in luminescence efficiency in the light emitted diode (LED) and the laser diode (LD). Furthermore, the study of defects by irradiation can provide practical data for optimizing the recovery conditions of defects in ion-implantation techniques.

The purpose of this chapter is, therefore, to present a variation of electron traps in LEC GaAs by irradiation. As an irradiation-source, we used γ-rays since they are expected to cause various kinds of damage to electronic devices exposed to radiation. LEC GaAs has been considered to be a key material for achieving high quality in compound semiconductor integrated circuits (ICs) or optoelectronic ICs. It has been reported that the degradation of GaAs FET by irradiation is greater for ion-implanted devices than for epitaxial devices.[5-7] This is, in part, explained by the non-uniform doping profiles in the FET channel.[8] However, there remains a question as to whether the degradation of the devices is governed by the different characteristics of defect states created by irradiation in

different materials. Thus, a particular attention is paid on the relationship between the behavior of grown-in traps and the creation of new traps by γ-irradiation in LEC GaAs, compared with those in epitaxial layers.

6.2. Experimental

The samples used in the present work were undoped n-type LEC GaAs grown from SiO_2 crucible with carrier concentration of about 1×10^{16} cm^{-3}. Undoped n-type GaAs on n^+-substrate grown by metalorganic vapor phase epitaxy (MOVPE) and Si-doped n-GaAs grown by molecular beam epitaxy (MBE), with almost the same carrier concentration as the LEC sample, were used as control samples. In control samples, no trap other than EL2 was detected before irradiation. Ohmic contact was fabricated by In-Sn alloy on the back sides of the samples followed by γ-irradiation. Irradiation was performed at room temperature with 60 Co γ rays at a rate of 2×10^5 Rh^{-1}. A 500 A thick Al dot Schottky diode (diameter approximately 800 μm) was formed after irradiation in order to prevent possible diffusion during this irradiation.

6.3. Results and Discussion

6.3.1. DLTS Study

Figure 1 shows typical DLTS signals in as-grown and γ-irradiated LEC GaAs. Also indicated is a signal for a MOVPE control sample in which no trap other than EL2 was detected before irradiation. Arrhenius plots of these levels are shown in Fig.2, with comparative data from Martin et al[9], and Pons and Bourgoin.[2] In both samples, little change in the carrier concentration estimated from capacitance-voltage (C-V) characteristics at room temperature appeared before and after irradiation. In the MOVPE control sample, as well as the MBE sample, the DLTS signal and the Arrhenius plots of the levels obtained were very similar to those of the so-called E traps, which were previously found in electron-irradiated GaAs.[2,10] E1 and E2 were also detected in the LEC sample after γ-irradiation, while E3, E4 and E5 seems to be masked by the high peaks of EL6, EL3 and EL2, respectively. In addition, two distinctive features of DLTS signal were obtained in γ-irradiated LEC samples. First, the peak heights of two grown-in traps, EL6 and EL3, changed in spite of the fact that the DLTS spectrum of the EL2 state did not change. With 2×10^8 R γ-rays, EL6 was reduced in concentration by a factor of 3 to 5, whereas EL3 increased about by one order of magnitude. Second, two new traps, labelled EG1 and EG2, appeared in addition to the E traps. An increase in concentration of EL3 also appeared in the sample with irradiation of 5×10^7 R.

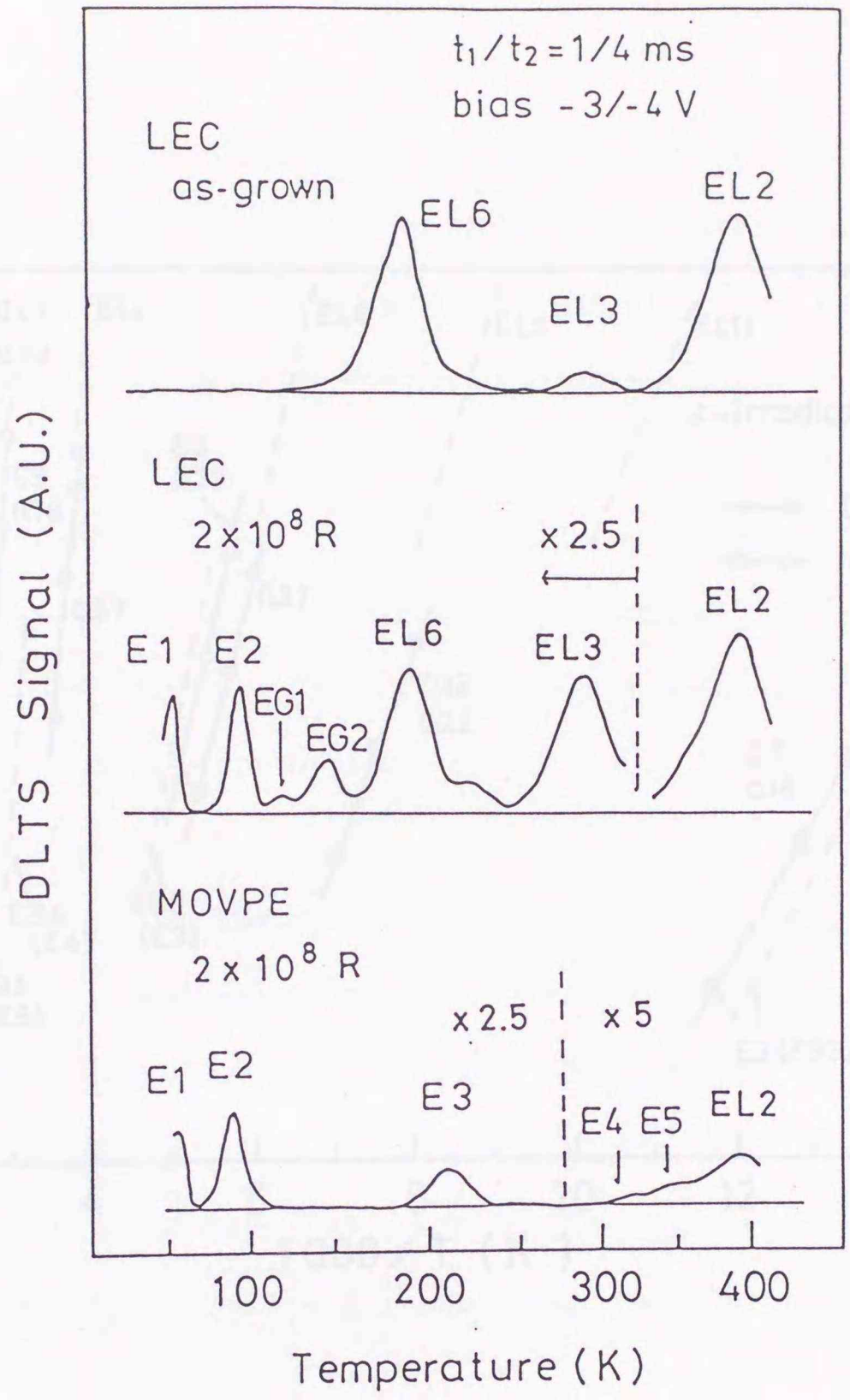

Figure 1. Typical DLTS signals of the LEC and control samples. (a) as-grown LEC sample, (b) irradiated LEC sample with γ rays of 2 x 10^8 R and (c) irradiated control sample with 2 x 10^8 R. The control sample (c) was undoped MOVPE n-GaAs in which no trap was detected before irradiation except for EL2.

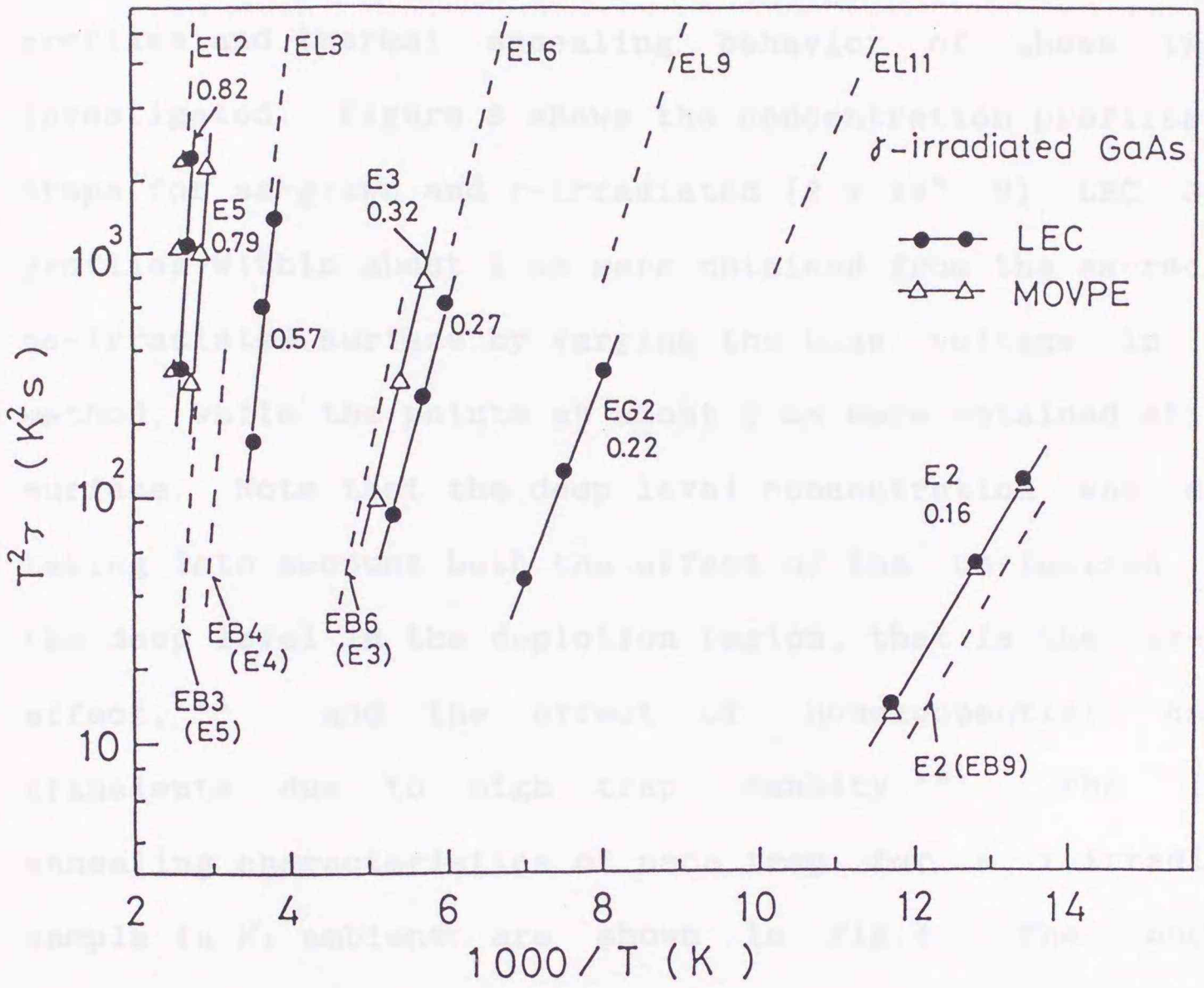

Figure 2. Arrhenius plots of the levels in γ-irradiated LEC and control samples. Numbers indicate the activation energy of each level in eV. Comparative data are taken from ref.2 (Pons and Bourgoin) and ref.11 (Martin et al).

To clarify the relationship between the creation of newtraps and the variation of the grown-in EL-levels,the concentration profiles and thermal annealing behavior of these traps were investigated. Figure 3 shows the concentration profiles of the traps for as-grown and γ-irradiated (2×10^8 R) LEC GaAs. The profiles within about 1 μm were obtained from the as-received or as-irradiated surface by varying the bias voltage in the DLTS method, while the points at about 2 μm were obtained at an etched surface. Note that the deep level concentration was calculated taking into account both the effect of the un-ionized width of the deep level in the depletion region, that is the so-called λ effect,[11] and the effect of nonexponential capacitance transients due to high trap density.[12] The isochronal annealing characteristics of each trap for a γ-irradiated LEC sample in N_2 ambient are shown in Fig.4. The concentration plotted in Fig.4 was in the region about 0.4 μm from the surface.

The E2 level had a constant profile similar to that for control samples. This indicates the uniformity of defect distribution as expected by the transmitting ability and the displacement cross section of the γ ray. Furthermore, the thermal behavior of E2 corresponds to that of the E traps introduced by electron-irradiation[13], i.e., it annealed at low temperature of about 300 C. These E traps are thought to be simple vacancy- or interstitial-type defects from the following characteristics:

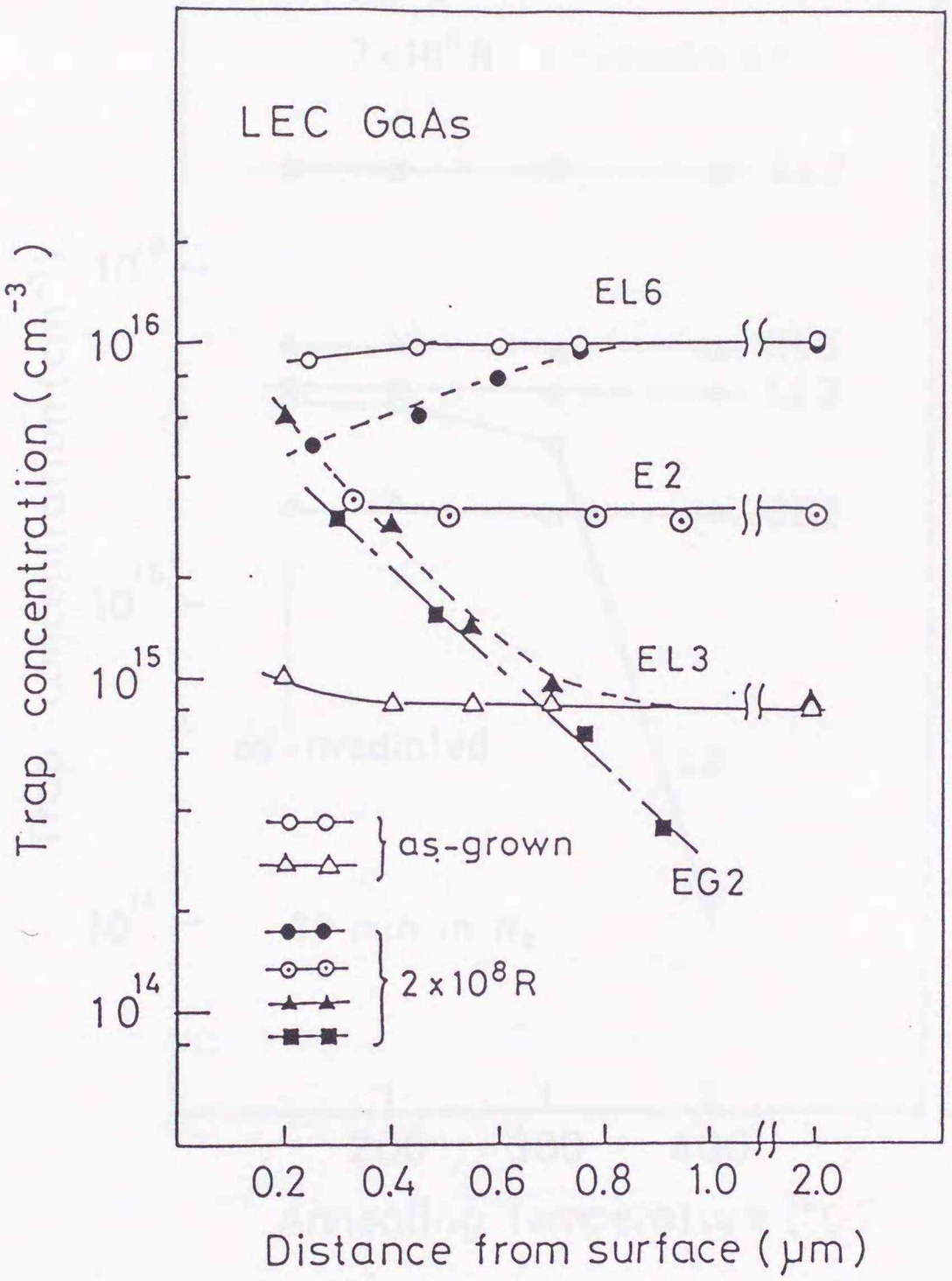

Figure 3. Concentration profiles of the traps for as-grown and γ-irradiated LEC GaAs. The points at about 2 μm were obtained at an etched surface. The others were determined at an irradiated surface by varying the DLTS bias voltage.

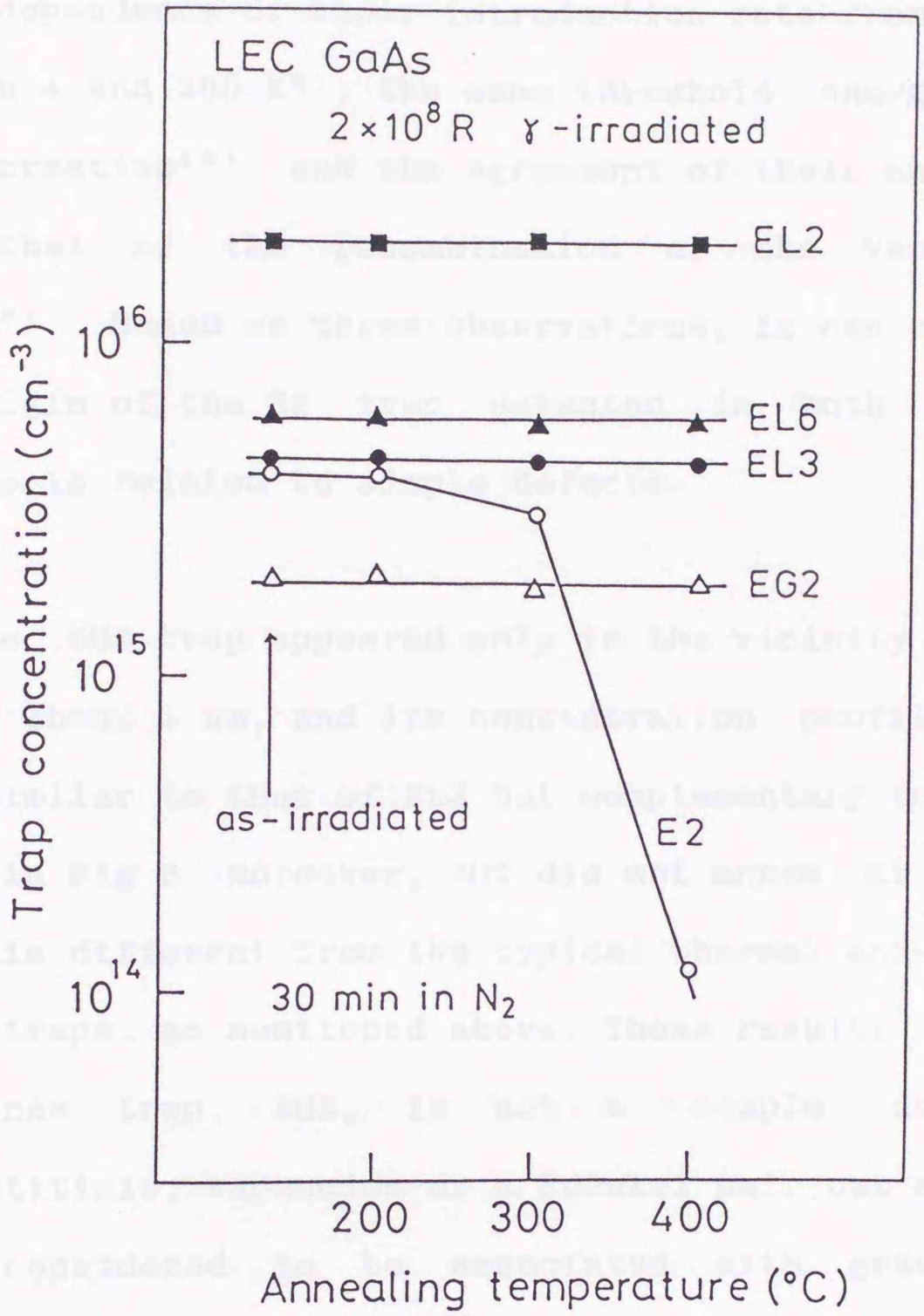

Figure 4. Isochronal annealing characteristics of the traps for γ-irradiated LEC GaAs. The concentration obtained was in the region about 0.4 μm from the irradiated surface.

the independence of their introduction rate from the temperature between 4 and 300 K[2], the same threshold energy (~ 10 eV) of their creation[14] and the agreement of their annealing kinetics with that of the recombination of the vacancy-interstitial pair.[13] Based on these observations, it can be concluded that the origin of the E2 trap detected in both LEC and control samples is related to simple defects.

The EG2 trap appeared only in the vicinity of the surface, within about 1 μm, and its concentration profile was not only very similar to that of EL3 but complementary to that of EL6, as shown in Fig 3. Moreover, EG2 did not anneal at low temperature, which is different from the typical thermal annealing behavior of the E traps, as mentioned above. These results strongly indicate that new trap, EG2, is not a simple defect such as interstitials, vacancies or a Frenkel pair but a complex defect, being considered to be associated with grown-in defects or impurities in LEC GaAs because EG2 was not created in control samples by γ-irradiation.

Stievanard and Bourgoin[15] reported that new defects other than E traps were created in VPE and LEC GaAs by electron-irradiation at 300 ℃. They suggested that these traps were complex defects created by mobile As interstitial (As_I) at high-enough temperature. Further evidence on the creation of new defects has been found in SI LEC material by γ-irradiation[16]

and in n-type VPE material by electron irradiation.[17] Based on analysis of the temperature-dependent Hall measurement, Look and Sizelove[17] pointed out that the acceptor level lying below E_C-0.3 eV, which cannot be detected by DLTS, is produced in n-type VPE GaAs with a higher introduction rate than that of the E traps by electron irradiation. They also claimed that this acceptor level is mainly connected with Ga-sublattice damage. Furthermore, positron lifetime measurements showed that Ga vacancies induced by electron irradiation exist at temperature up to about 300 K.[18] Similarly, there may be a possibility that the simple irradiation-induced defects, E traps or undetected levels that escaped from recombination, are mobile during γ-irradiation. This situation could create new defects such as EG2 state.

Apparently, the grown-in defects exist over more orders of magnitude in LEC materials than in epitaxial layers. Since the LEC material used in the present study was an n-type grown under As-rich conditions, Ga vacancy (V_{Ga}) seems to be one of the most likely simple defects.[19] These grown-in defects may assist some of the primary simple defects induced by γ-irradiation at the surface to move toward the bulk region, which may result in the interaction between them near the surface in LEC GaAs.

It is interesting that the EG2 profile is very similar to that of the EL3 level in γ-irradiated LEC material, as shown in Fig.3. EL3 is very often detected in bulk n-type GaAs crystals and has a

tendency for the concentration of the level to decrease with the increase of carrier concentration, as shown in Fig.5 together with the data of other workers.[20-26] Since the materials in Fig.5 are doped with Si or grown from SiO_2 crucible, the decrease of EL3 concentration is considered to be related to the interaction of Si atoms with the grown-in defects. Vanasupa et al[27] suggested an activation mechanism in which the implanted Si atoms locally redistribute to vacant sites rather than exchanging positions with lattice atoms. Thus, the similar concentration profiles of EG2 and EL3 indicate that the origin of the EG2 level seems to be related to V_{Ga} or As vacancy (V_{As}).

The remaining grown-in level, EL6, was decreased by irradiation only near surface region. This seemed to be caused by the interaction of the component of EL6 with the irradiation-induced defects as mentioned above. This drastic change of EL6 is consistent with that caused by ion-implantation,[28] neutron irradiation,[29] plastic deformation[25,30,31] and annealing at 500-800 ℃,[32] indicating that the origin of EL6 is related to defects which may be easily created or decomposed by various surrounding conditions. This tendency could be responsible for the significant effect of EL6 on the compensation mechanism in LEC GaAs, as well as EL2, especially in annealing processes.[33]

6.3.2. Metastable Behavior of EL2

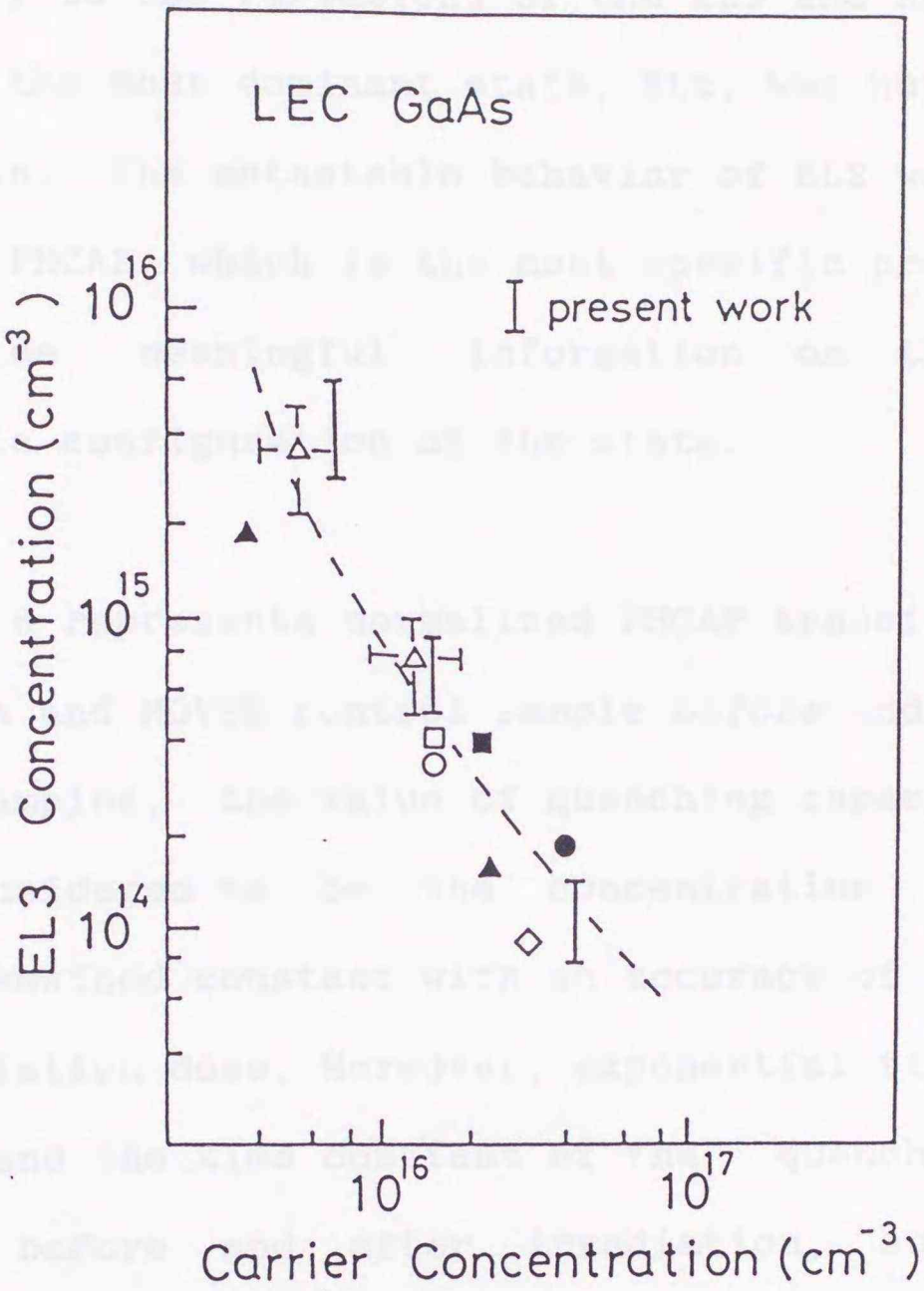

Figure 5. EL3 concentration as a function of carrier concentration in LEC GaAs doped with Si or grown from SiO_2 crucible. Data shown in open triangles are taken from ref.20, the open square from ref.21, the open circle from ref.22, the closed circle from ref.23, the closed square from ref.24, the closed triangles from ref.25 and the open rhombus from ref.26.

Contrary to the variations of the EL3 and EL6 states, the DLTS signal of the most dominant state, EL2, was not influenced by γ-irradiation. The metastable behavior of EL2 was investigated by measuring PHCAP, which is the most specific property of EL2 and can provide meaningful information on the physical and microscopic configuration of the state.

Figure 6 represents normalized PHCAP transients at 60 K for LEC sample and MOVPE control sample before and after irradiation. In both samples, the value of quenching capacitance (C_Q), which may be considered to be the concentration of quenchable EL2 center, remained constant with an accuracy of 5%, independent of the irradiation dose. Moreover, exponential time dependence was observed and the time constant of the quenching transient was the same before and after irradiation, suggesting that the electron transfer mechanism from the ground state to the metastable state of the EL2 level dose not seem to be affected by γ-irradiation. In fact, it has been reported that the photoquenching effect should take place by a successive transition of electrons with the interaction between the excited state and the metastable state.[34,35]

In addition, the recovery process of EL2 from the metastable state to the ground state, which was examined according to an earlier procedure,[36] did not change with irradiation, as shown

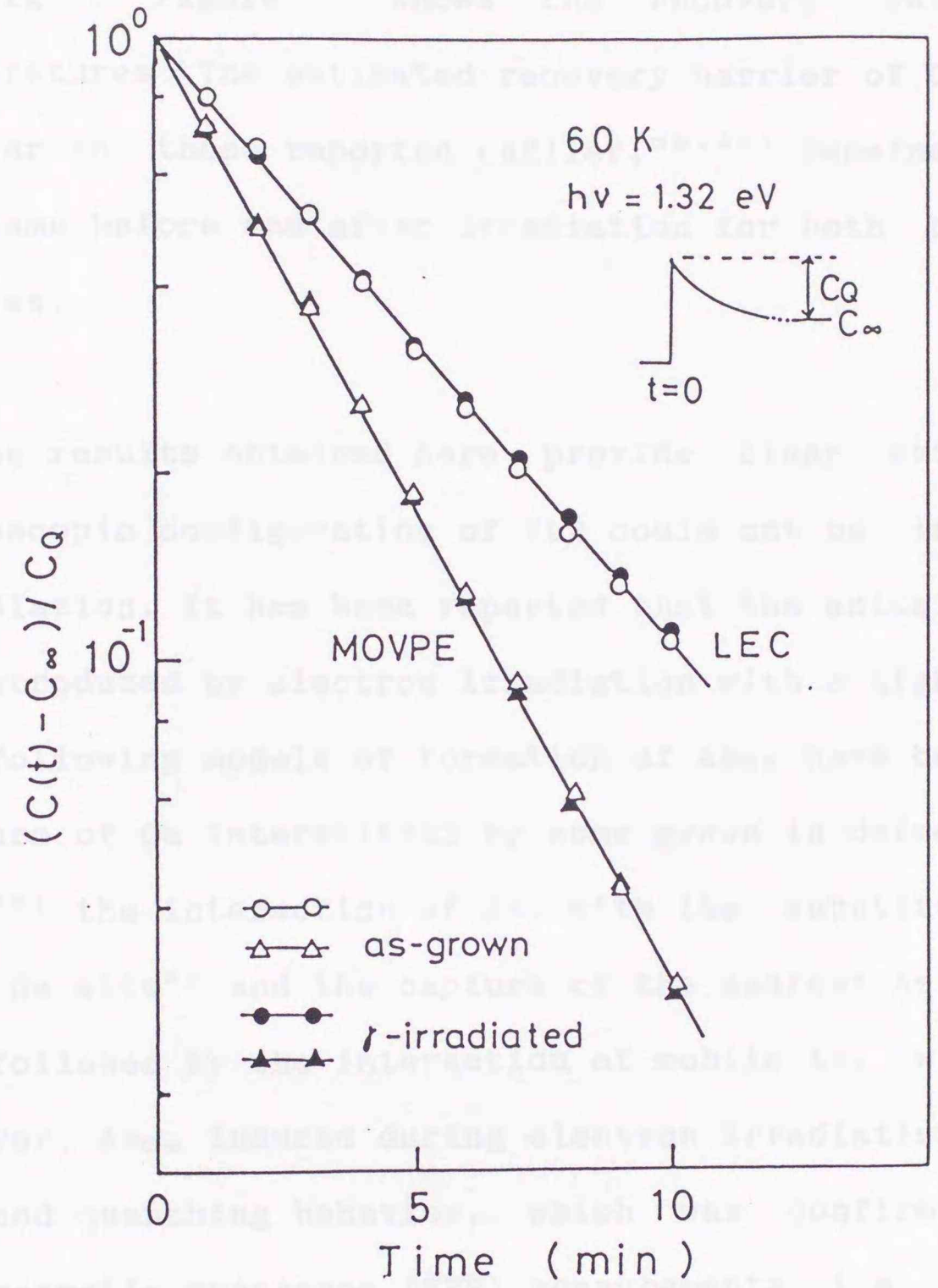

Figure 6. Photocapacitance transient normalized by the quenching capacitance in LEC and control samples before and after irradiation.

in Fig.7. Figure 7 shows the recovery rate at various temperatures. The estimated recovery barrier of 0.35 eV, which is similar to those reported earlier,[36,37] remained more or less the same before and after irradiation for both LEC and control samples.

The results obtained here provide clear evidence that the microscopic configuration of EL2 could not be influenced by γ-irradiation. It has been reported that the antisite defect, As_{Ga}, is introduced by electron irradiation with a high dose,[38,39] and the following models of formation of As_{Ga} have been proposed: the capture of Ga interstitial by some grown-in defects such as As_{Ga}-V_{Ga},[38] the interaction of As_I with the substitutional impurity on a Ga site[2] and the capture of the nearest As atom by unstable V_{Ga} followed by the interaction of mobile As_I with As_{Ga}-V_{As}.[39] However, As_{Ga} induced during electron irradiation shows no photo-induced quenching behavior, which was confirmed by electron paramagnetic resonance (EPR) measurements, i.e., the As_{Ga} defect induced by electron irradiation is not EL2 but an isolated one.[39] Similarly, although isolated As_{Ga} can be induced, the As_{Ga} complex and/or aggregate that constitutes the EL2 state seems not to be created and not to be decomposed during γ-irradiation.

As shown by the results obtained here as well as in other reports, the basic properties of EL2 cannot be easily modified by

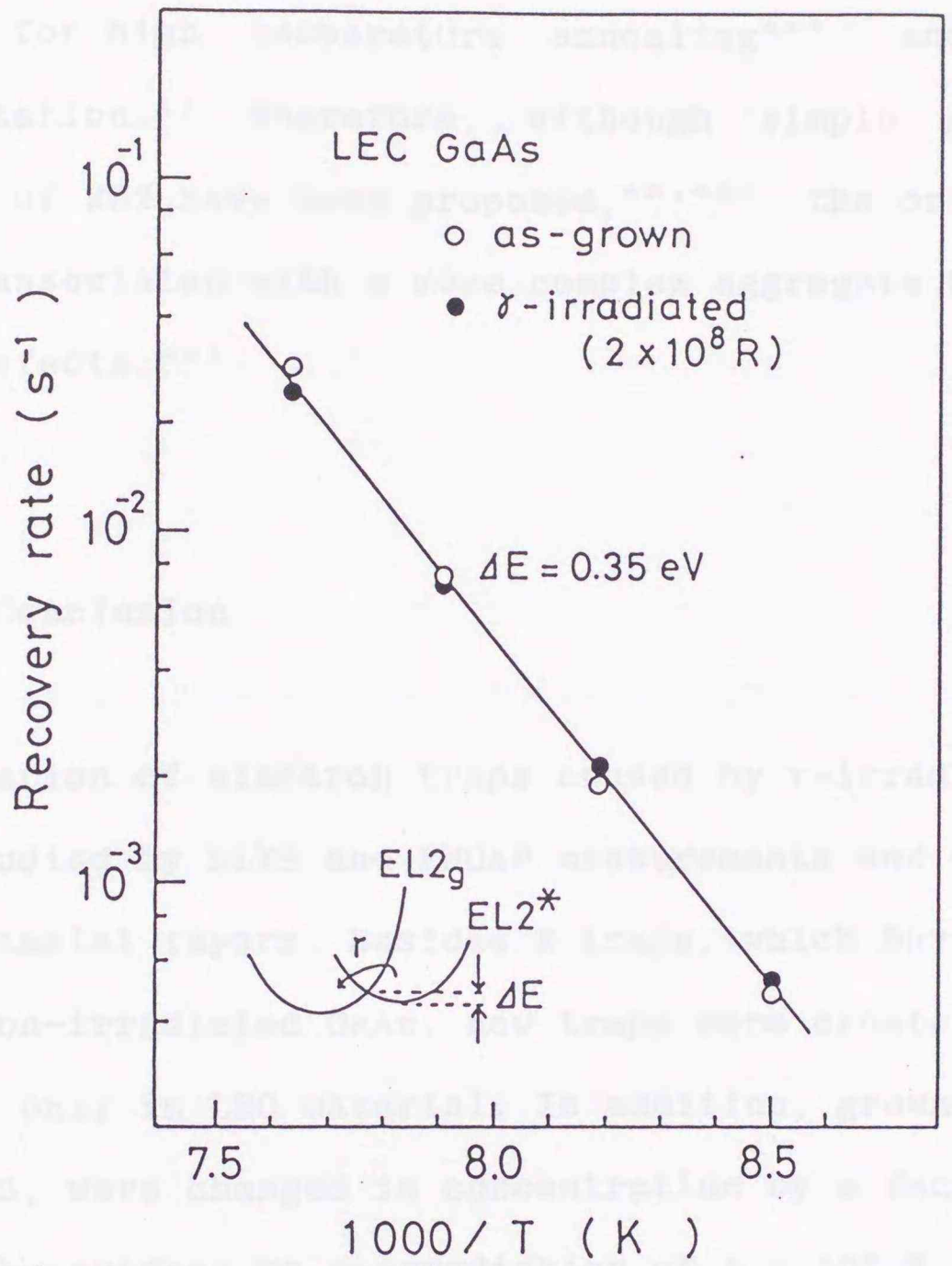

Figure 7. Thermal recovery rate of EL2 from the metastable state to the ground state as a function of reciprocal temperature.

the alloying effect[40] and plastic deformation,[25,30,31] except for high temperature annealing[41] and heavy particle implantation.[1] Therefore, although simple As_{Ga}-related pair models of EL2 have been proposed,[42,43] the origin of EL2 seems to be associated with a more complex aggregate rather than simple pair defects.[44]

6.4. Conclusion

Variation of electron traps caused by γ-irradiation in LEC GaAs was studied by DLTS and PHCAP measurements and compared with that in epitaxial layers. Besides E traps, which have been found in electron-irradiated GaAs, new traps were created near the surface region only in LEC material. In addition, grown-in defects, EL6 and EL3, were changed in concentration by a factor of 3 to 10 near the surface by γ-irradiation of 2×10^8 R. New traps did not anneal at around 300 C and their concentration profiles obtained from DLTS correlated with the profiles of the grown-in EL defects. These results strongly indicate that new traps in LEC GaAs are not simple defects but complex ones, possibly created by the interaction between the grown-in defects and the irradiation-induced defects. In the contrast, neither the DLTS spectrum nor the metastable behavior of EL2 changed after irradiation, i.e., the microscopic configuration of EL2 was not directly affected by irradiation.

References

1) G.Guillot,Rev.Phys.Appl.23,833(1988)

2) D.Pons and J.C.Bourgoin,J.Phys.C 18,3839(1985)

3) Y.Kitagawara,N.Noto,T.Takahashi and T.Takenaka,*Semi-Insulating III-V Materials* (Ohmusha,Tokyo,1986),p293

4) S.Reichlmaier,K.Loehnert and M.Baumgartner,Jpn.J.Appl.Phys. 27,2329(1988)

5) R.Zuleeg and K.Lehovec,IEEE Trans.Nucl.Sci.NS-25,1444(1978)

6) W.T.Anderson,M.Simons,A.Christou and J.Beall,IEEE Trans Nucl. Sci.NS-32,4040(1985)

7) A.B.Campbell,A.R.Knudsen,W.J.Staper,G.Summers,M.A.Xapsos, M.Jessee,T.Palmer,R.Zuleeg and C.J.Dale,IEEE Trans.Nucl.Sci. NS-33,1435(1986)

8) B.K.Janousek,W.E.Yamada,R.J.Krantz and W.L.Bloss,J.Appl.Phys. 63,1678(1988)

9) G.M.Martin,A.Mitonneau,and A.Mircea,Electron.Lett.13,191 (1977)

10) D.V.Lang, and L.C.Kimmerling,Inst.Phys.Conf.Ser.23,581(1975)

11) Y.Zohta and M.O.Watanabe,J.Appl.Phys.53,1809(1982)

12) A.C.Wang and C.T.Sah,J.Appl.Phys.55,565(1984)

13) D.Pons,A.Mircea and J.C.Bourgoin,J.Appl.Phys.51,4150(1980)

14) D.Pons,P.M.Mooney and J.C.Bourgoin,J.Appl.Phys.51,2038(1980)

15) D.Stievenard and J.C.Bougoin,J.Appl.Phys.59,743(1986)

16) M.Tomozane,Y.Nannichi,H.Kamada,and K.Ando,Jpn.J.Appl.Phys.26, L1076(1987)

17) D.C.Look,and J.R.Sizelove,J.Appl.Phys.62,3660(1987)

18) P.Hautojarvi,P.Moser,M.Stucky,C.Corbel and F.Plazaola,Appl. Phys.Lett.48,809(1986)

19) G.A.Baraff,and M.Schluter,Phys.Rev.Lett.55,1327(1985)

20) M.Taniguchi,and T.Ikoma,J.Appl.Phys.54,6448(1983)

21) M.Kitayama,A.Usami,T.Wada,and Y.Tokuda,J.Appl.Phys.62,528 (1987)

22) Y.Kitagawara,N.Noto,T.Takahashi,and T.Takenaka,Appl.Phys. Lett.48,1664(1986)

23) F.D.Auret,A.W.R.Leitch,and J.S.Vermaak,J.Appl.Phys.59,158 (1986)

24) S.Chichibu,N.Ohkubo,and S.Matsumoto,J.Appl.Phys.64,3987 (1988)

25) E.Gombia,C.Ghezzi,and R.Mosca,J.Appl.Phys.58,1285(1985)

26) T.Wosinski and T.Figielski,Solid State Commun.63,885(1987)

27) L.S.Vanasupa,M.D.Deal and J.D.Plummer,Appl.Phys.Lett.55 274(1989)

28) G.M.Martin,E.Esteve,P.Langlade and S.Makram-Ebeid,J.Appl. Phys.56,2655(1984)

29) J.Samitier,J.R.Morante,L.Giraudet and S.Gourrier,Appl.Phys. Lett.48,1138(1986)

30) P.Omling,E.R.Weber and L.Samuelson,Phys.Rev.B 33,5880(1986)

31) T.Haga,M.Suezawa and K.Sumino,Jpn.J.Appl.Phys.27,1929(1988)

32) Y.Kitagawara,N.Noto,T.Takahashi and T.Takenaka,Appl.Phys. Lett.52,221(1988)

33) D.C.Look,*Semi-Insulating III-V Materials* (IOP Publishing,UK,

1988),p1

34) M.Kaminska,M.Skowronski,and W.Kuszko,Phys.Rev.Lett.55,2204 (1985)

35) Y.Mochizuki,and T.Ikoma,*Semi-Insulating III-V Materials* (OHMUSHA,Tokyo,1986),p.323

36) A.Mitonneau,and A.Mircea,Solid State Commun.30,157(1979)

37) G.Vincent,D.Vois,and A.Chantre:J.Appl.Phys.53,3643(1982)

38) R.B.Beall,R.C.Newman,J.E.Whitehouse and J.Woodhead:J.Phys.C 17,2653(1984)

391) H.J.von Bardeleben,D.Stievenard,J.C.Bourgoin,and A.Huber: Appl.Phys.Lett.47,970(1985)

40) L.Samuelson,Physica 117B,104(1984)

41) J.Lagowski,H.C.Gatos,C.H.Kang,M.Skowronski,K.Y.Ko and D.G. Lin,Appl.Phys.Lett.49,892(1986)

42) J.Lagowski,M.Kaminska,J.M.Parsey,H.C.Gatos and W.Walukiewicz, Inst.Phys.Conf.Ser.65 (Institute of Physics,Bristol, U.K.,1983),p41

43) H.J.von Bardeleben,D.Stievenard,D.Deresmes,A.Huber and J.C. Bourgoin,Phys.Rev.B 34,7192(1986)

44) M.O.Monasreh and D.W.Fischer,Phys.Rev.B 39,3239(1989)

CHAPTER 7

VARIATION OF NEAR-SURFACE DEEP LEVELS IN CAPPED GaAs CAUSED BY ANNEALING

7.1 Introduction

Much effort has been devoted to investigate the various insulating films as an annealing encapsulant for ion-implanted GaAs, because of their practical importance for field effect transistor fabrication. However, none of the films is entirely satisfactory. For example, the case of SiO_2 suffers from Ga outdiffusion into SiO_2 film, and the annealing using SiN has a serious problem of the stress between SiN film and GaAs.[1,2] Recently, an attention has been paid to the application of rapid thermal annealing (RTA)[3] to the post-implantation annealing. In this method, it is expected that the required encapsulant thickness may be reduced compared to that of conventional furnace annealing (FA) because of its short annealing time, thereby reducing the stress at the surface of GaAs substrate. However, problems concerning the newly induced defects[4,5] or As evaporation even in encapsulated GaAs[6] are still remained.

In this chapter, taking these situations into account, Al_2O_3 capped annealing is investigated. The Al_2O_3 film as an improved encapsulant for GaAs is prepared by the dynamic mixing method. This method allows film formation at room temperature. The low-temperature deposition methods should be desirable as to suppressing the degradation of GaAs substrate due to the As evaporation during deposition. A particular attention is paid on the change of the interface configuration and the variation of near-surface deep levels of GaAs substrate which is one of the most important terms for the degradation of the substrate.

7.2 Experimental

The substrates used in the present work were Si-doped n-type LEC (100) GaAs with the carrier concentration of 4×10^{16} cm^{-3}. Al_2O_3 films of 1100 A thickness were prepared at room temperature by the dynamic mixing method[7] using ion beam and simultaneous vapor deposition. Schematic diagram of the growth system is shown in Fig.1. Ion beam energy is 5keV. Typical growth rate is 1 A/sec and ion current density is 100 μAcm^{-2}. Annealing of Al_2O_3/GaAs was carried out by FA and RTA in flowing H_2 or Ar gas. FA was performed at 700-800 ℃ for 15 min with heating rate of 2℃/sec, whereas RTA at 800 ℃ for 10 sec with 30-50 ℃/sec.

Al_2O_3/GaAs systems were analyzed by Auger electron

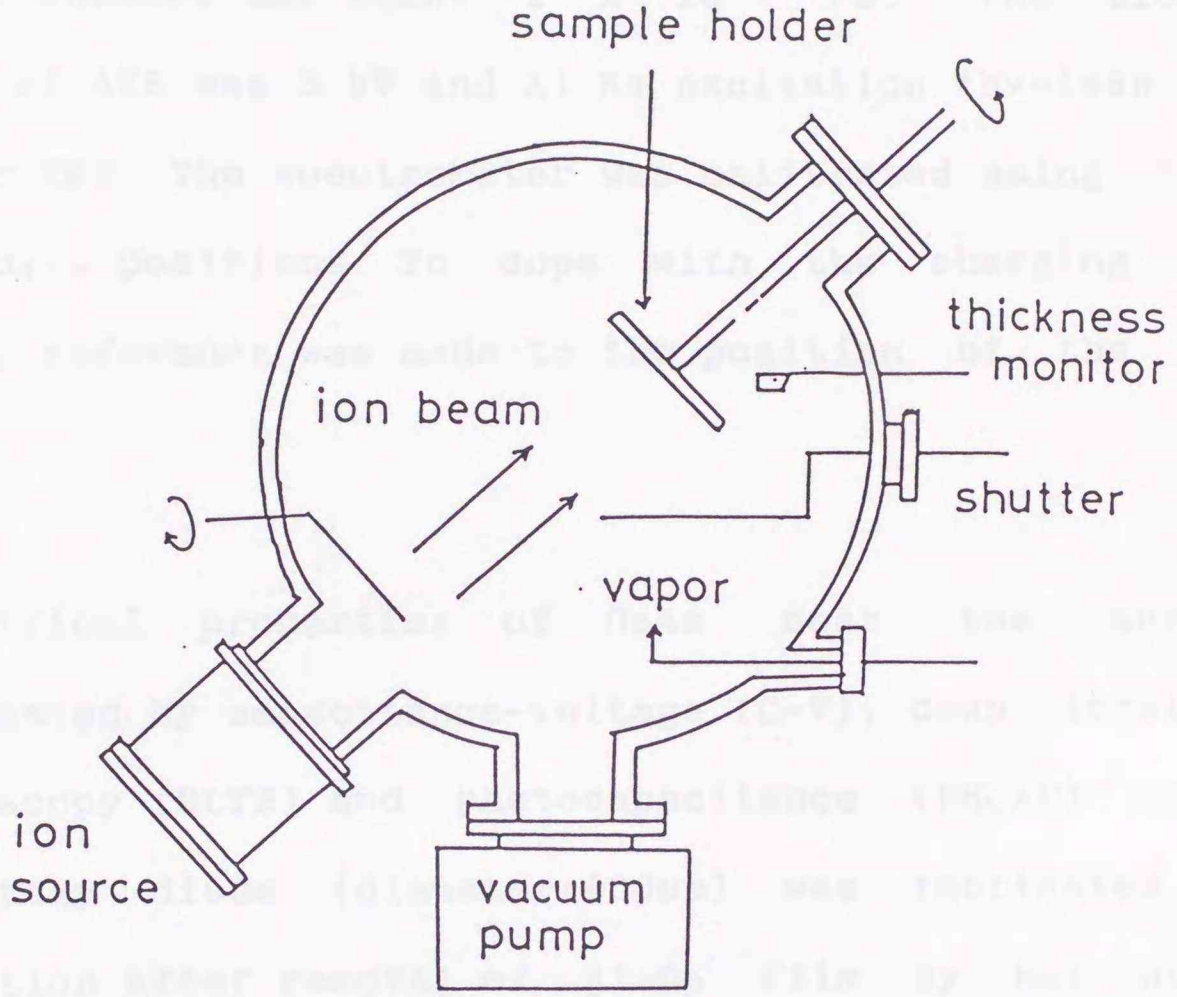

Figure 1. Schematic diagram of the growth system used in the present work.

spectroscopy (AES) and X-ray photoelectron spectroscopy (XPS) with ULVAC-PHI 255. The electron energy analyser was a cylindrical mirror analyser and the background pressure of the analysis chamber was about 2 x 10^{-8} Pa. The electron beam voltage of AES was 3 kV and Al Kα excitation (hν=1486.6 eV) was used for XPS. The spectrometer was calibrated using the Au4$f_{7/2}$ and Cu2$p_{3/2}$ positions. To cope with the charging up to the samples, reference was made to the position of the hydrocarbon C1s.

Electrical properties of GaAs near the surface were investigated by capacitance-voltage (C-V), deep level transient spectroscopy (DLTS) and photocapacitance (PHCAP) measurements. Al Schottky diode (diameter:800μm) was fabricated by vacuum evaporation after removal of Al_2O_3 film by hot hydrophosphic acid.

7.3 Results

7.3.1. Analysis of Al_2O_3 Film and Al_2O_3/GaAs Interface

Figure 2 shows AES line shape for as-deposited Al_2O_3/GaAs system. The thickness and refractive index of Al_2O_3 film estimated from ellipsometry were 1100 A and 1.8, respectively. There was no peak other than Al, O and C at Al_2O_3 surface. XPS

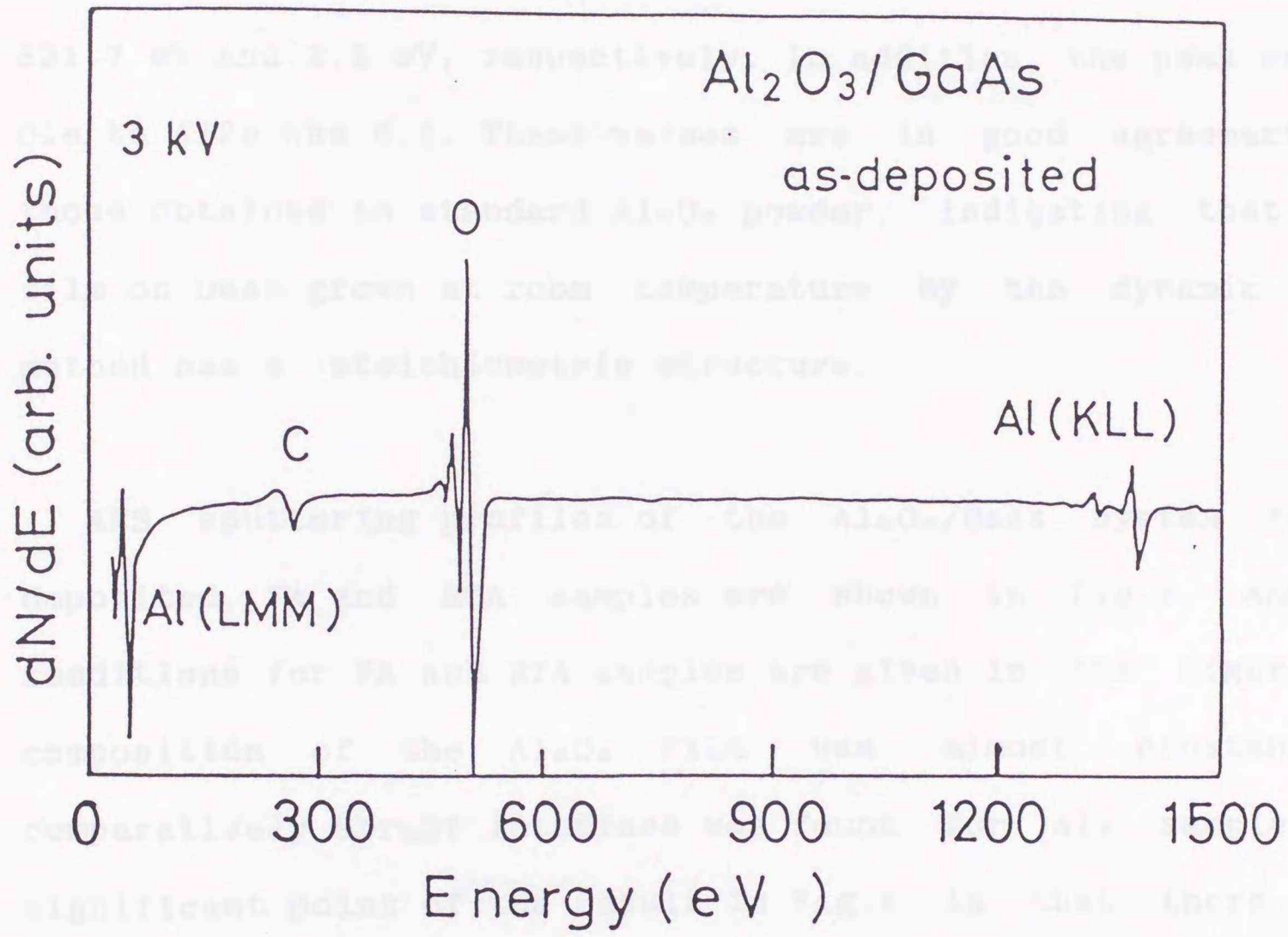

Figure 2. AES line shape for as-deposited Al_2O_3 surface. The film thickness is 1100 A and the electron beam voltage used for AES analysis is 3 kV.

spectra of as-deposited Al_2O_3 surface are shown in Fig.2. Al2*p* and O1*s* lines can be fitted to single Gaussian distribution function. Al2*p* spectrum has the peak binding energy of 74.9 eV and the full width at half maximum (FWHM) of 2.0 eV, and O1*s* has 531.7 eV and 2.2 eV, respectively. In addition, the peak ratio of O1*s* to Al2*p* was 6.6. These values are in good agreement with those obtained in standard Al_2O_3 powder, indicating that Al_2O_3 film on GaAs grown at room temperature by the dynamic mixing method has a stoichiometric structure.

AES sputtering profiles of the Al_2O_3/GaAs system for as-deposited, FA and RTA samples are shown in Fig.4. Annealing conditions for FA and RTA samples are given in the figure. The composition of the Al_2O_3 film was almost constant and comparatively abrupt interface was found for all samples. The significant point of the result in Fig.4 is that there is no identification of As or Ga outdiffusion into Al_2O_3 film during annealing process, which is also confirmed by XPS measurement. The outdiffusion of Ga atom is serious problem of SiO_2 passivation film on GaAs. Near the Al_2O_3/GaAs interface, different profiles with different samples were obtained. For as-deposited sample, the oxygen signal slightly extended into GaAs substrate compared to Al one. After FA processing, As signal exceeded Ga one, whereas Ga composition at the interface exceeded stoichometric value after RTA. This indicates that the Al_2O_3/GaAs interface structure was changed by the annealing

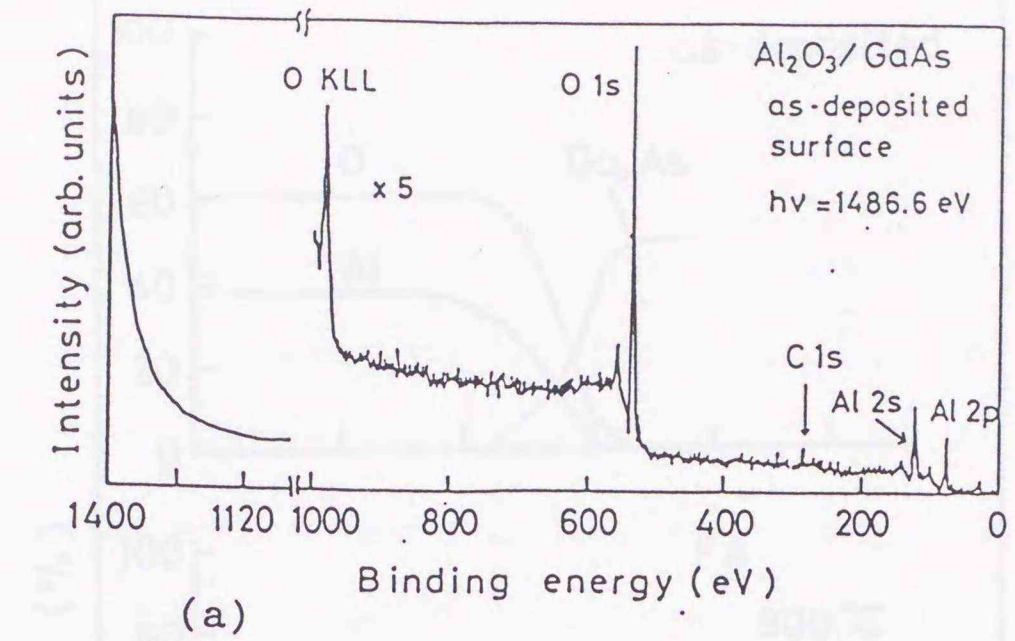

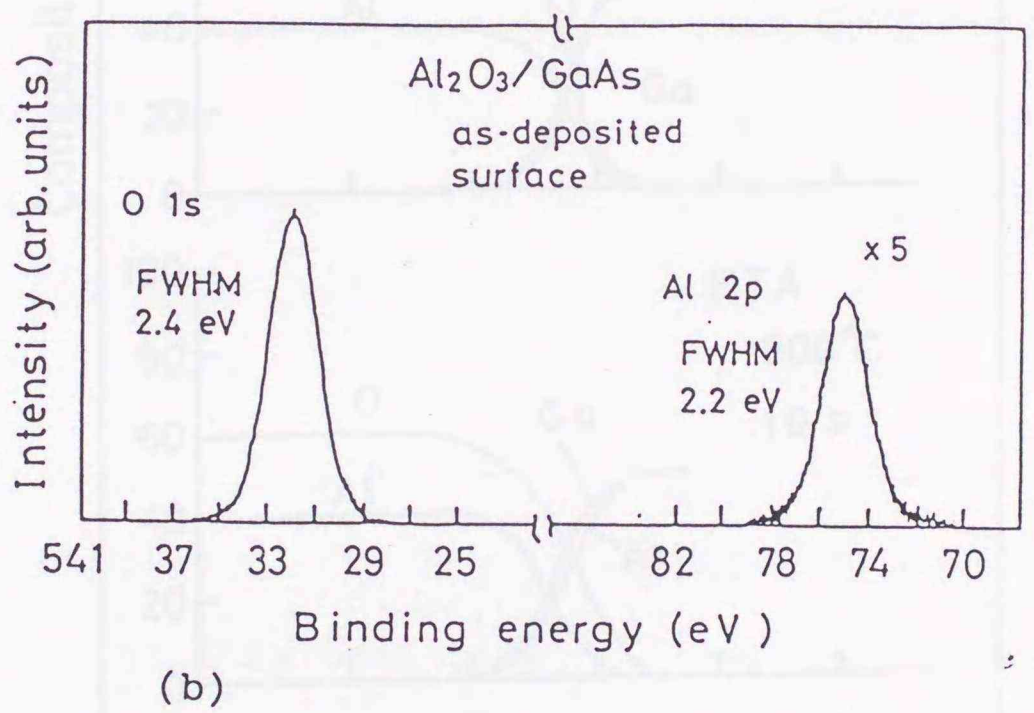

Figure 3. (a) XPS spectrum of as-deposited Al_2O_3 surface. (b) XPS spectra of Al2*p* and O1*s*. The peak binding energy, FWHM and peak ratio of both lines were comparable with those for standard powder sample.

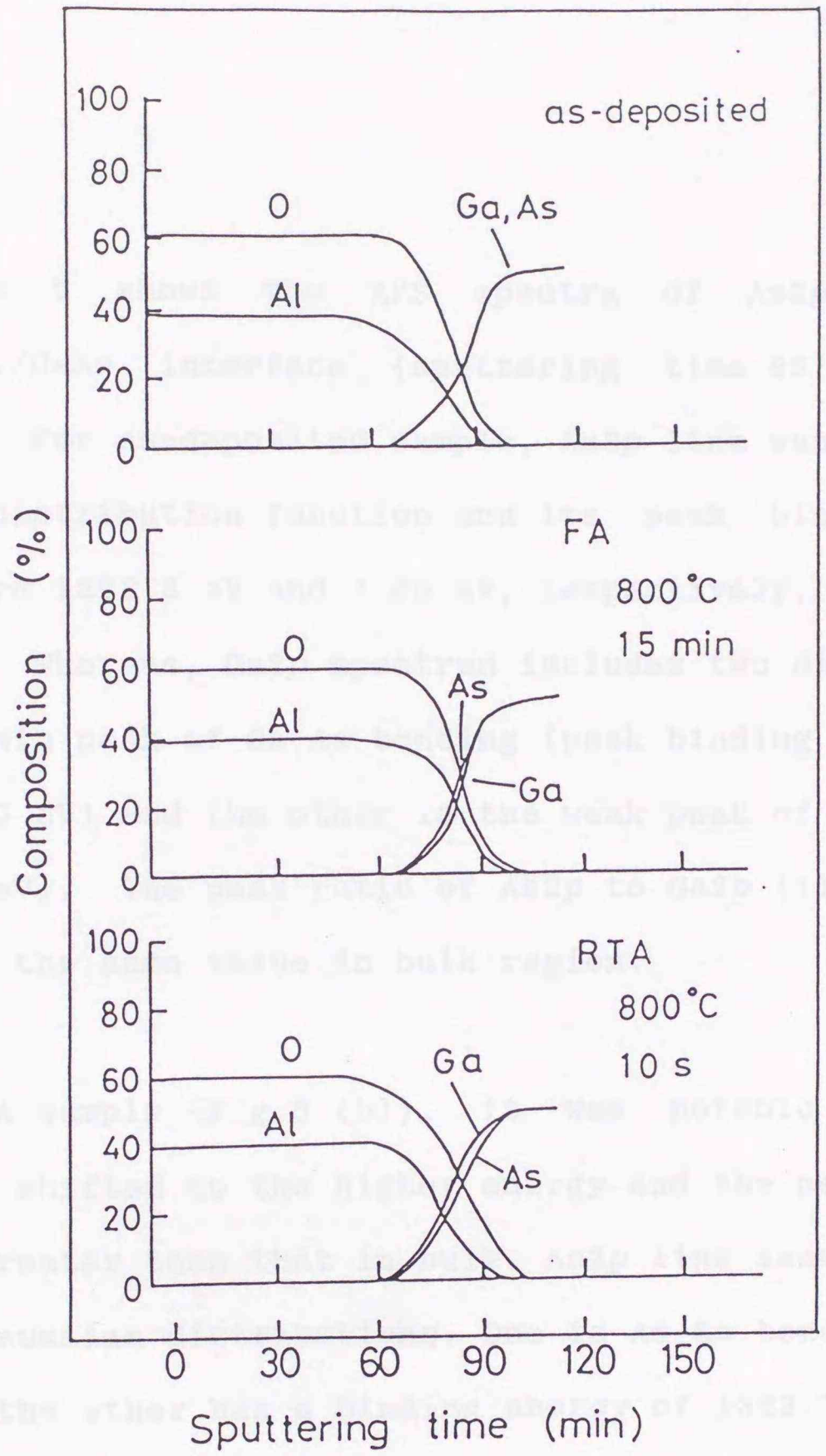

Figure 4. AES sputtering profiles of Al_2O_3/GaAs system for as-deposited, FA and RTA samples.

process.

Figure 5 shows the XPS spectra of As2*p* and Ga2*p* near the Al_2O_3/GaAs interface (sputtering time:85 min) of three samples. For as-deposited sample, As2*p* line was fitted by one Gassian distribution function and its peak binding energy and FWHM were 1322.3 eV and 1.80 eV, respectively, indicating As-Ga bonding. Whereas, Ga2*p* spectrum includes two distributions: one is the main peak of Ga-As bonding (peak binding energy:1117.2 eV, FWHM:1.70 eV) and the other is the weak peak of Ga oxide (1118.5 eV, 2.5 eV). The peak ratio of As2*p* to Ga2*p* (1117.2 eV) was 1.3 which is the same value in bulk region.

For FA sample (Fig.5 (b)), it was notable that As2*p* line slightly shifted to the higher energy and the peak ratio of As to Ga was greater than that in bulk. As2*p* line seems to be composed of two Gaussian distributions. One is As-Ga bonding peak (1322.3 eV) and the other has a binding energy of 1323.3 eV and FWHM of 2.20 eV. Since it has been examined that As oxide had the higher binding energy (1326.0 eV) at chemically etched GaAs surface,[8,9] the latter peak seems to correspond to elemental As. On the contrary, Ga2*p* line is almost the same as that of as-deposited sample. Therefore, it may be considered that elemental As accumulates near the interface during FA processing. XPS spectra of As2*p* and Ga2*p* at the interface after RTA were shown in Fig.5 (c). Distinctively, Ga2*p* spectrum after RTA included a lot of Ga

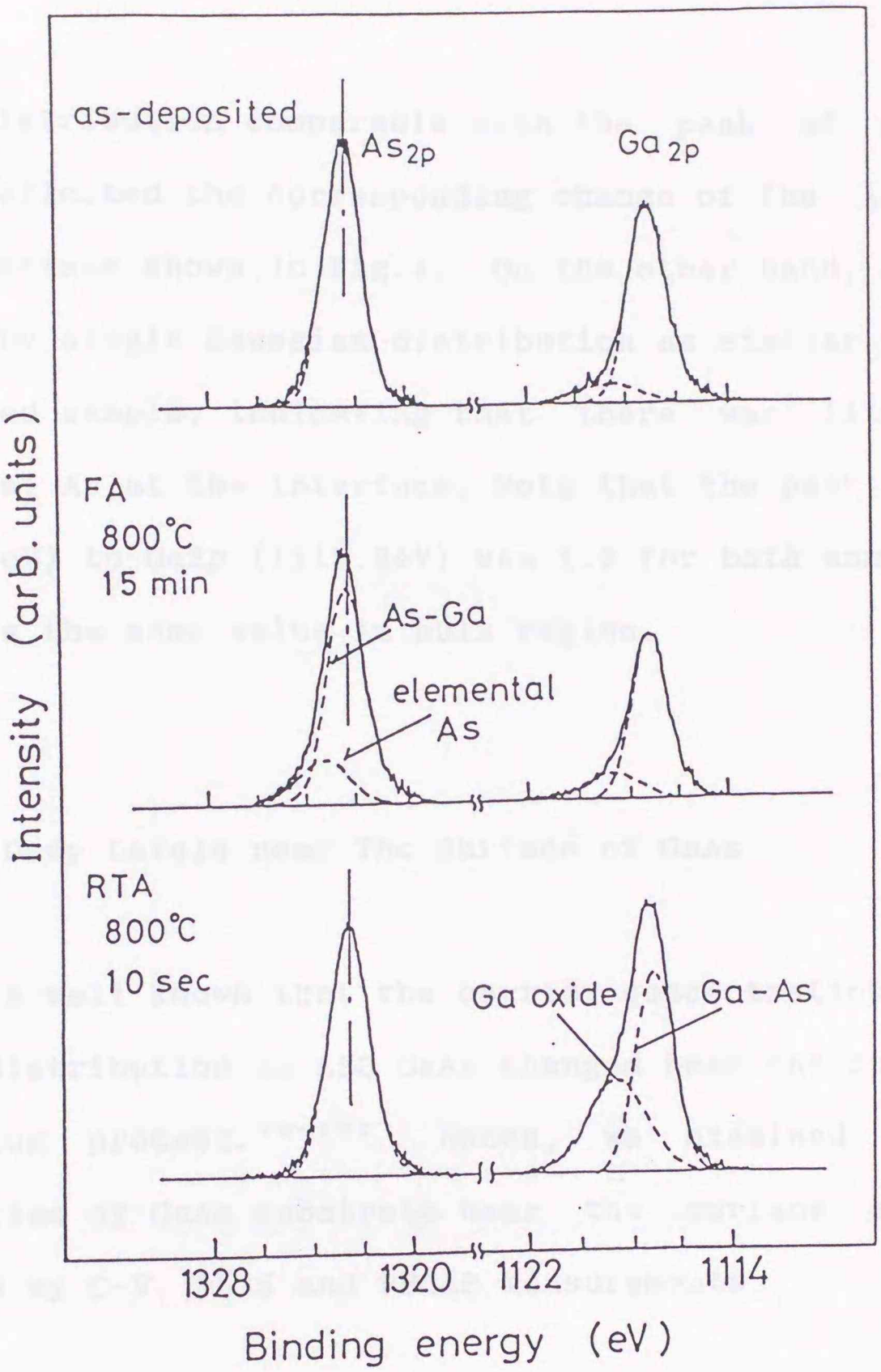

Figure 5. XPS spectra of As2*p* and Ga2*p* near Al_2O_3/GaAs interface for three samples. The sputtering time was 80 min which is corresponding to AES profiles. Both spectra were fitted using values obtained in bulk GaAs.

oxide distribution comparable with the peak of Ga-As bonding, which reflected the corresponding change of the AES profile at the interface shown in Fig.4. On the other hand, As2*p* line was fitted by single Gaussian distribution as similar to that of as-deposited sample, indicating that there was little amount of elemental As at the interface. Note that the peak ratio of As2*p* (1322.3eV) to Ga2*p* (1117.2eV) was 1.3 for both annealed samples, which is the same value in bulk region.

7.3.2. Deep Levels near The Surface of GaAs

It is well known that the carrier concentration and the deep level distribution in LEC GaAs changed near the surface after cap annealing process.[10-13] Hence, we examined the electrical properties of GaAs substrate near the surface after annealing process by C-V, DLTS and PHCAP measurements.

Figure 6 shows carrier concentration profiles obtained by C-V curves of the annealed samples. The carrier concentration of the as-grown GaAs is indicated by the arrow in Fig 6. The sample after FA processing represented little deviation from the ideal Schottky C-V behavior and the carrier concentration profile was almost constant. On the other hand, the profile showing the carrier accumulation near the surface can be seen after RTA processing. There are two possible terms to understand the change

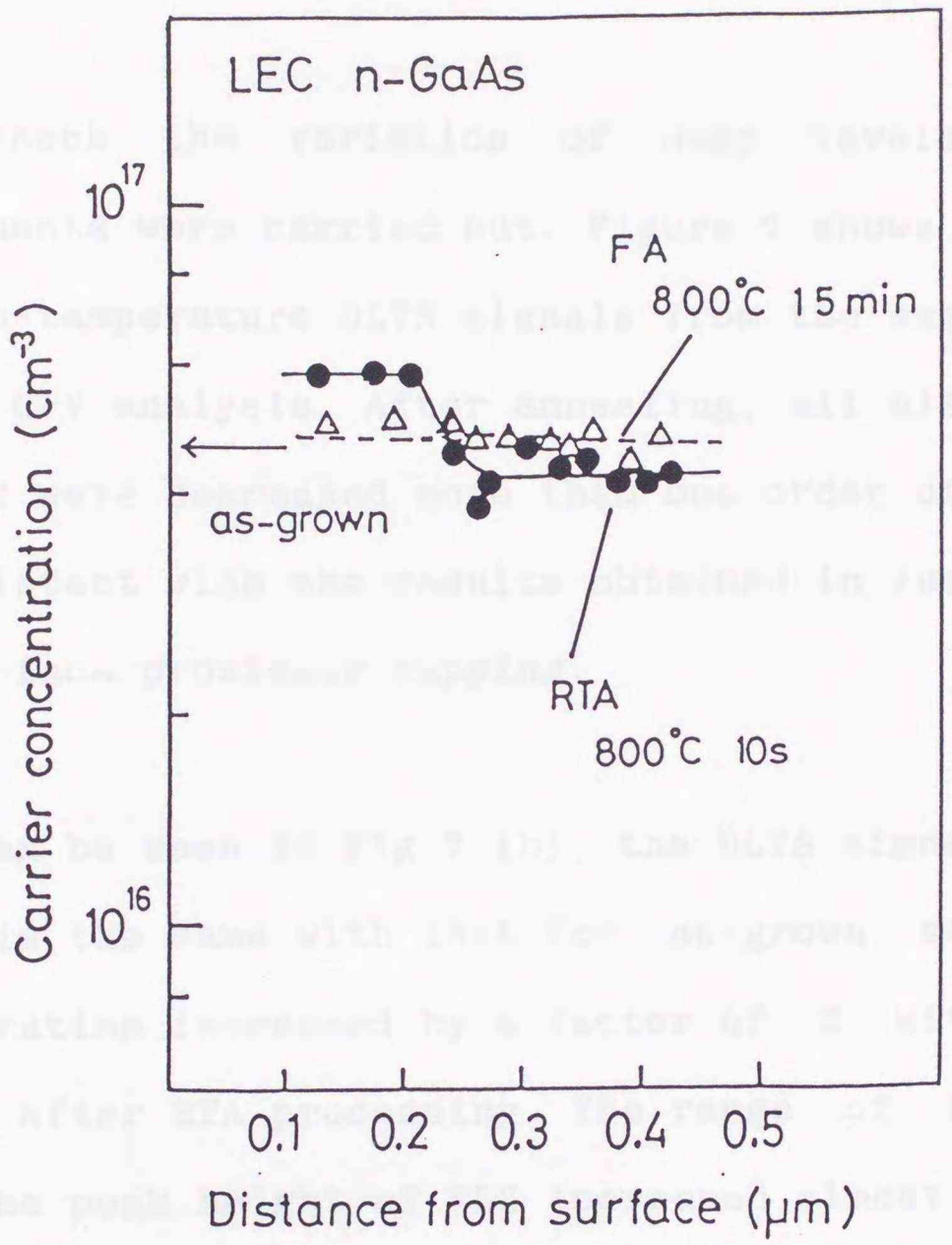

Figure 6. Carrier concentration profiles obtained by C-V curves of the annealed samples. The arrow indicates the carrier concentration of as-grown GaAs.

of profile: one is impurity incorporation and/or redistribution, and the other is the variation of deep levels in LEC material.

To check the variation of deep levels, DLTS and PHCAP measurements were carried out. Figure 7 shows the low-temperature and high-temperature DLTS signals from the same Schottky diodes used in C-V analysis. After annealing, all electron traps other than EL2 were decreased more than one order of magnitude, which is consistent with the results obtained in furnace annealing with face-to-face proximity capping.

As can be seen in Fig.7 (b), the DLTS signal of EL2 for FA sample is the same with that for as-grown sample, whereas EL2 concentration increased by a factor of 2 with decreasing bias voltage after RTA processing. The range of DLTS probing depth where the peak height of EL2 increased almost coincides with the region where the change of carrier profile was observed. Additionally, change of the photoquenching behavior appeared after RTA. Figure 8 shows PHCAP response of the Schottky diodes after FA and RTA processing. By RTA, non-exponential quenching spectrum was apparently observed. This means that electron transfer mechanism from the ground state to the metastable state through the excited state[14,15] might be modified by RTA or other members of EL2 induced by RTA might disturb the photoquenching behavior of grown-in EL2.

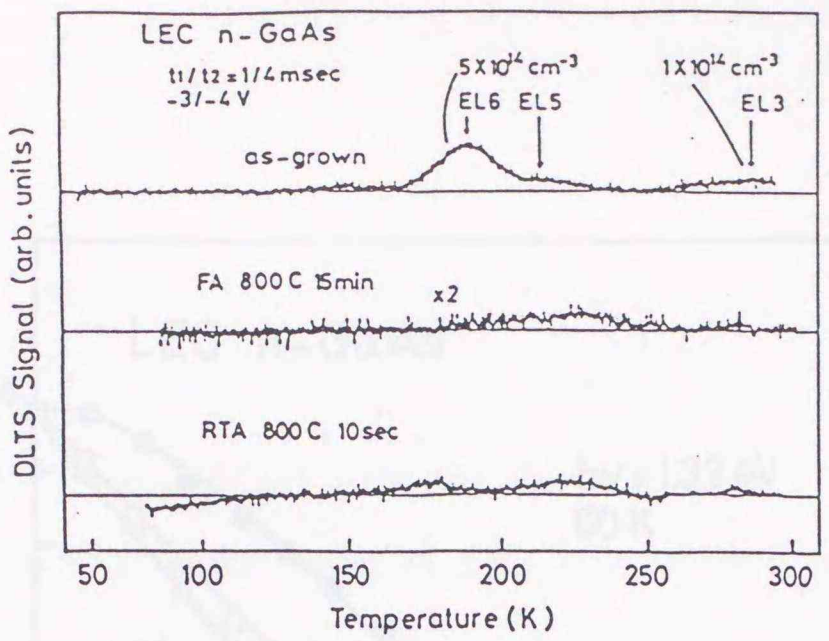

(a)

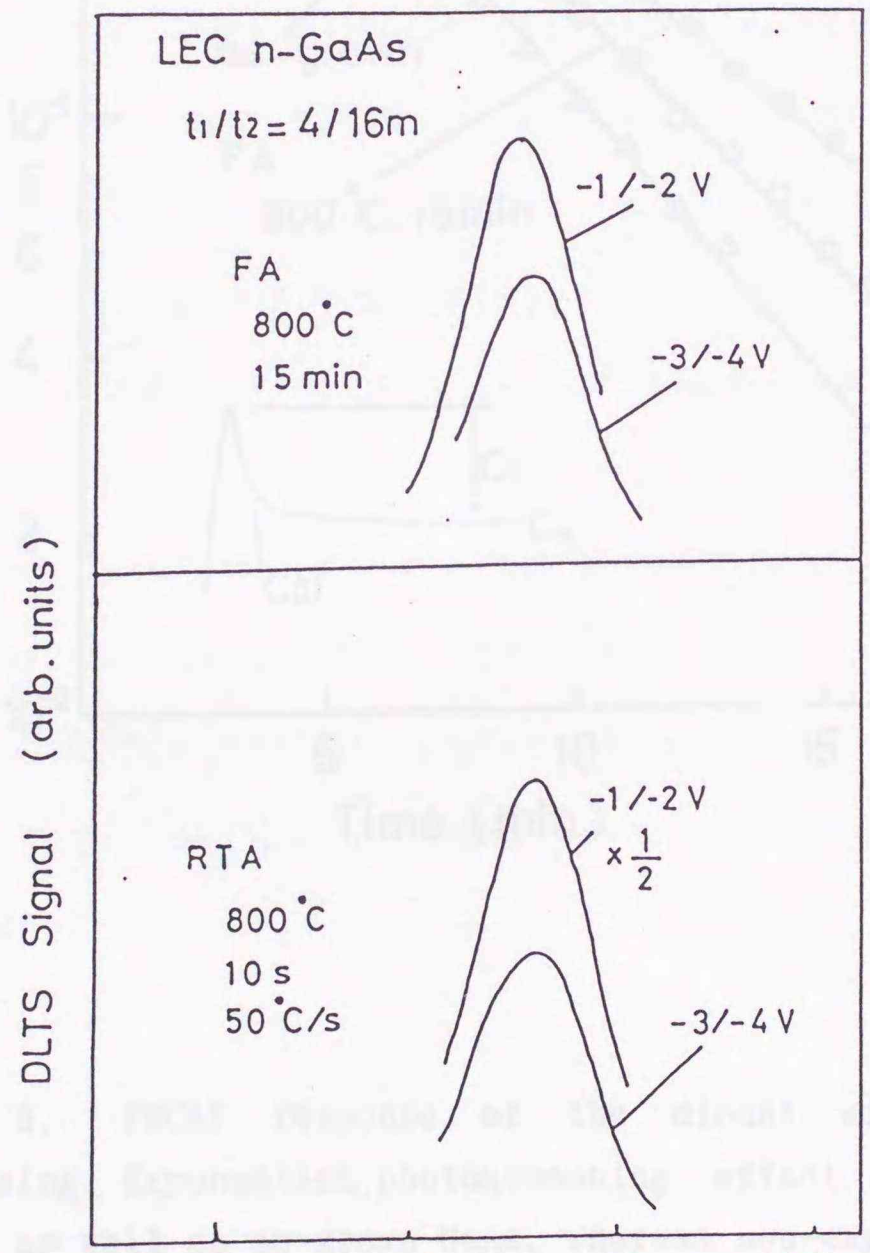

(b)

Figure 7. DLTS signals from the same diodes used in C-V analysis in (a) low temperature and (b) high temperature region.

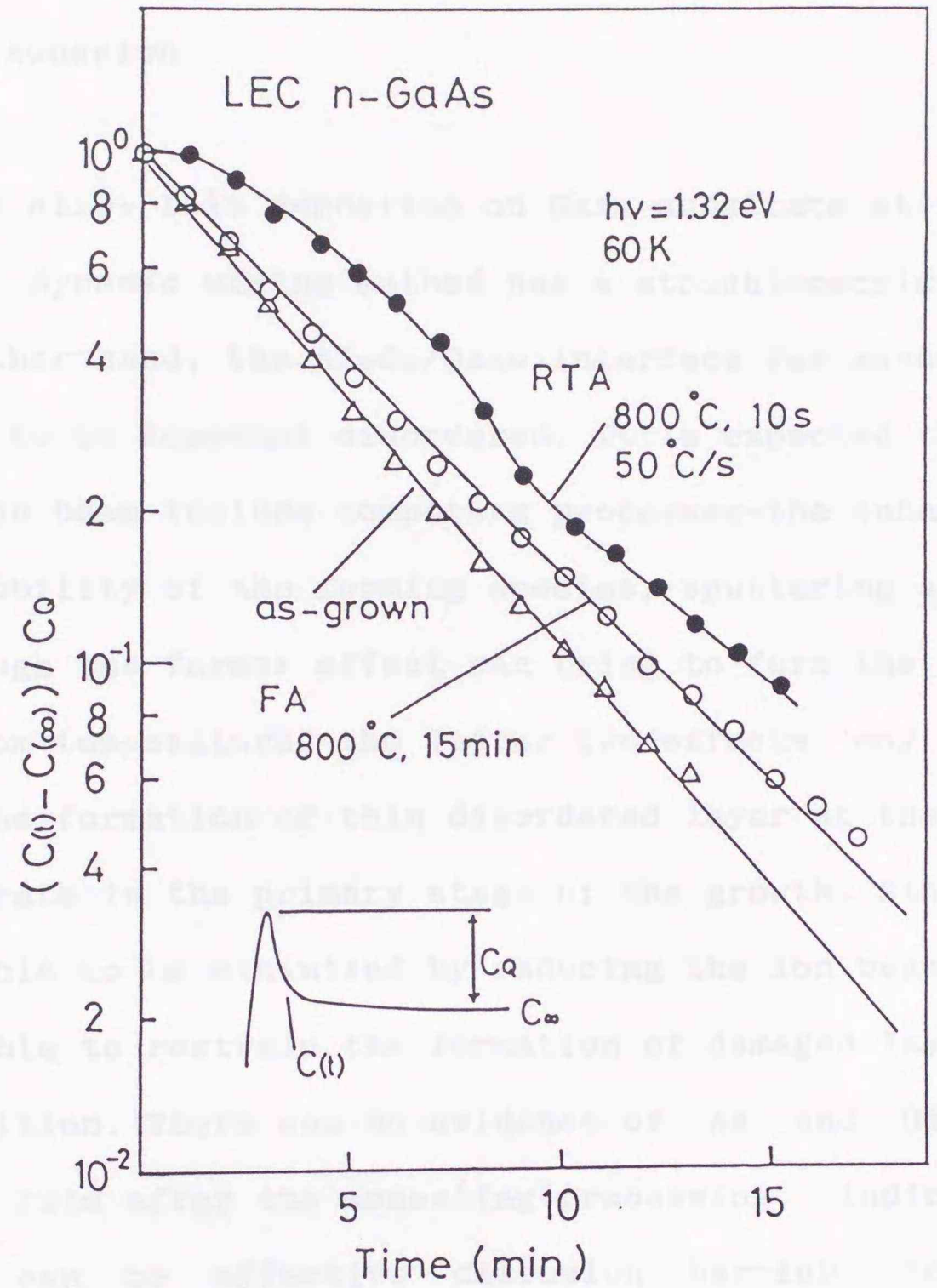

Figure 8. PHCAP response of the diodes after FA and RTA processing. Exponential photoquenching effect appeared for FA sample as well as as-grown GaAs, whereas non-exponential behavior was apparently observed after RTA.

7.4 Discussion

The Al_2O_3 film deposited on GaAs substrate at room temperature by the dynamic mixing method has a stoichiometric structure. On the other hand, the Al_2O_3/GaAs interface for as-deposited sample seems to be somewhat disordered. It is expected that effects of the ion beam include competing processes-the enhanced reactivity and mobility of the forming species, sputtering and implantation. Although the former effect can bring to form the insulator film at room temperature, the latter two effects may be responsible for the formation of thin disordered layer at the surface of GaAs substrate in the primary stage of the growth. Since these effects are able to be minimized by reducing the ion beam energy, it is possible to restrain the formation of damaged layer during film deposition. There was no evidence of As and Ga signals into Al_2O_3 film after the annealing processing, indicating that the film can be effective diffusion barrier to As and Ga outdiffusion.

It is apparent that there is a difference between FA sample and RTA sample in the structural change of the Al_2O_3/GaAs interface. As given in XPS spectra (Fig.5), elemental As was mainly created for FA sample, while a lot of Ga oxide was generated for RTA sample at the interface. In addition, the properties of EL2 state varied only after RTA processing (Figs.7 and 8). Both changes of the interface structure after FA and RTA

seem to be attributed to the same source, i.e., the disordered layer at the interface probably formed during the primary stage of the deposition as mentioned above. The stress due to the difference of the thermal expansion coefficient between Al_2O_3 and GaAs can produce the same effect on FA and RTA processing at the same temperature. Therefore, it seems difficult to explain what we have observed by only the stress caused by the difference of the thermal expansion.

The most significant term giving rise to the different annealing behavior at the interface is considered to be the heating rate.[16] In the initial heating state for RTA, GaAs substrate mainly absorbed the infrared power. The enhanced heating rate can extremely produce the large temperature difference between GaAs and the insulator, thereby resulting in the large stress at the interface for RTA processing. It is thought that this large momentary stress causes to cut the Ga-As bonding near the surface, and then the reaction of Ga with excess oxygen occurred.

Furthermore, the large temperature gradient also likely accounts for the change of the properties of EL2 after RTA processing. The facts that the EL2 concentration increased near the surface and the non-exponential photoquenching behavior appeared after RTA are similar to those reported in the plastically deformed GaAs.[17-19] Newly appeared defects in

deformed GaAs have been considered to be the EL2-related level[19] or dislocation-related[18] one. It is possible that the stress due to the large temperature difference at the interface for RTA may produce the same effects as plastic deformation on the surface of GaAs substrate. The reason why no change of EL2 properties appeared after FA processing seems to be that the stress at the interface is comparatively small with that for SiO_2/GaAs or SiN/GaAs systems, since the thermal expansion coefficient of Al_2O_3 film is rather close to that of GaAs.

7.5 Conclusion

The effect of annealing process on the Al_2O_3/GaAs system prepared at room temperature by the dynamic mixing method using ion beam and simultaneous vapor evaporation have been investigated. XPS and AES studies showed that there was no evidence of As or Ga outdiffusion into Al_2O_3 film during conventional furnace annealing (FA) and rapid thermal annealing (RTA). This means that it is possible to use the Al_2O_3 film as a passivation film for the post-implantation annealing of GaAs.

The different structural change of the interface properties appeared with the different annealing processes, i.e., FA and RTA. For FA, elemental As accumulated at the interface and no change of EL2 properties, which are examined by DLTS and PHCAP

measurements, occurred near the surface of GaAs substrate. On the other hand, a lot of Ga oxide was created at the interface and the increase of the EL2 concentration and the non-exponential photoquenching behavior were observed only for RTA sample. The different phenomena may be governed by the different heating rate which seems to produce a large temperature gradient at the interface for RTA.

References

1) U.Konig,and E.Sasse,J.Electrochem.Soc.,130,950(1983)

2) C.P.Lee,R.Zucca,and B.M.Welch,Appl.Phys.Lett.,37,311(1980)

3) R.Singh,J.Appl.Phys.,63,R59(1988)

4) M Katayama,A.Usami,T.Wada,and Y.Tokuda,J.Appl.Phys.,62, 528(1987)

5) D.Wong,H.K.Kim,Z.Q.Fang,T.E.Schlesinger,and A.G.Milnes,J.Appl. Phys.,66,2002(1989)

6) T.E.Haynes,W.K.Chu,and S.T.Picraux,Appl.Phys.Lett,50, 1071(1987)

7) M.Satoh and F.Fujimoto,Jpn.J.Appl.Phys.,22,L171(1983)

8) J.Massies, and J.P.Contour,J.Appl.Phys.,58,806(1985)

9) H.Hasegawa,H.Ishii,T.Sawada,T.Saitoh,S.Konishi,Y.Liu,and H.Ohno,J.Vac.Sci.Technol.B6,1184(1988)

10) B.Hughes and C.Li,Inst.Phys.Conf.Ser.,65,57(1983)

11) F Hasegawa,N.Yamamoto,and Y.Nannichi,Appl.Phys Lett,45,461 (1984)

12) F.Hasegawa,T.Takahashi,K.Kubo,S.Ohnari,Y.Nannichi,and T.Arai, Jpn.J.Appl.Phys.,26,L1448(1987)

13) M.Katayama,A.Usami,T.Wada,and Y.Tokuda,J.Appl.Phys.,62,528 (1987)

14) M.Kaminska,M.Skowronski,and W Kuszko,Phys.Rev.Lett.,55,2204 (1985)

15) Y Mochizuki and T Ikoma, *Semi-Insulating* III -V *materials*

(OHMUSHA,Tokyo,1986),p.323

16) M.Katayama,Y.Tokuda,N.Ando,Y.Inoue,A.Usami,and T.Wada,Appl. Phys.Lett.,54,2561(1989)

17) T.Wosinski,and T.Figielski,Solid State Commun.,63,885(1987)

18) T Wosinski,J.Appl.Phys.65,1566(1989)

19) T.Haga,M.Suezawa,and K.Sumino,Jpn.J.Appl.Phys.,27,1929(1988)

CHAPTER 8

CONCLUSION

Deep levels in epitaxial GaAs and AlGaAs as well as bulk GaAs are investigated. Epitaxial layers are grown by MBE and MOVPE, and bulk GaAs is grown by the LEC method. The properties of irradiation induced defects and the effect of an annealing processing on the deep levels are studied in detail.

Summary and conclusion of the present work are the following:

CHAPTER 3

Properties of deep electron traps and their roles in the compensation mechanism in undoped GaAs grown by the LEC method have been clarified. The obtained results are following:

(1) Six electron traps with activation energies ranging from 0.14 to 0.82eV were detected by DLTS in as-grown GaAs. The dominant levels were EL6 and EL2 of which concentration was in

the range of 10^{15}-10^{16} cm^{-3}.

(2) Electron traps shallower than EL2, namely EL6, can cause a decrease in the resistivity of undoped material which has a low concentration of acceptor impurities.

(3) The concentration of EL6 was decreased by more than one order of magnitude by an 800℃ treatment. Whereas, the EL2 level in bulk region remained stable at around 800℃ .

CHAPTER 4

Deep levels in epitaxial GaAs grown by MOVPE and MBE have been investigated by DLTS. The effect of the purity of source materials on deep level in MOVPE GaAs and the effect of coincident Pb flux on deep levels in MBE GaAs have been clarified. The summary and conclusion are the following:

(1) The dominant electron traps in MOVPE GaAs was the EL2 with the concentration of $1x10^{14}$-$4x10^{15}$ cm^{-3}. Other traps observed were closely related to impurities introduced with source materials.

(2) Six electron traps with activation energies ranging from 0.08 to 0.55eV were detected in undoped MBE GaAs. The

concentration of four traps was reduced by a factor of 3-5 by increasing the growth temperature from 560 to 580℃ .

(3) With a Pb flux of $1x10^{15}cm^{-2}s^{-1}$, which corresponds to 0.05 monolayer coverage at 560℃ , the concentration of all the observed levels in undoped layers was reduced in the range of $10^{13}cm^{-3}$. The RHEED pattern was changed from (2x4) to diffuse (2x3) with application of the Pb flux. The reduction of deep level concentration is closely associated with the surface process modification such as the change in surface stoichiometry.

CHAPTER 5

Properties of midgap levels in undoped $Al_xGa_{1-x}As$ grown by MOVPE have been investigated with AlAs composition x as parameter. The optical properties of the levels were clarified in detail by a new PHCAP measurement procedure by which the effect of the photoionization of the DX center is separated from the photoquenching of the midgap levels. The important results are following:

(1) Two levels, i.e., the ML and MH levels, were found to exist in $Al_xGa_{1-x}As$ with x=0 to 0.47. Their energy positions stay constant with respect to the hybrid orbital energy level E_{HO} when the alloy composition is varied. The higher lying MH level lies

at about 0.58eV from E_{HO}, and the lower lying ML level lies at about 0.24ev from E_{HO} which corresponds to that of EL2 in GaAs and $GaAs_xP_{1-x}$.

(2) The concentration of the ML level was almost independent of x, whereas that of the MH level was zero in GaAs and increased with x.

(3) The ML level exhibits an remarkable photoquenching for $x<0.3$, which disappears above $x=0.3$. The optical cross sections of the ML level are almost the same with those of the EL2 in GaAs. These observations as well as the constant energy position have led to the conclusion that the ML level is closely related to the EL2 in GaAs and originates from a certain complex defect related to As. On the other hand, the MH level did not show photoqenching for all x.

CHAPTER 6

The effect of γ-irradiation on deep levels in LEC GaAs has been investigated by DLTS and PHCAP, and compared with that in epitaxial layers. The obtained results are followings:

(1) Besides E traps, which have been found in electron-irradiated GaAs, new traps were created near the surface region

(about 2 μm) by γ-irradiation of $2x10^8$ R only in LEC GaAs. In addition, grown-in EL6 and EL3 levels were changed in concentration by a factor of 3 to 10 near the surface.

(2) The concentration profiles of new traps correlated with those of the grown-in levels and new traps were not annealed at around 300℃ at which the recovery of simple defects induced by electron irradiation is observed. These results provide clear evidence that new traps in LEC GaAs are complex defects created by the interaction between the grown-in defects and the irradiation-induced defects.

(3) The electrical and optical properties of the EL2 level were not changed by γ-irradiation.

CHAPTER 7

The effect of annealing process on Al_2O_3/GaAs system and on deep levels near the interface have been investigated. Al_2O_3/GaAs system was analyzed by AES and XPS. Annealing of Al_2O_3/GaAs was carried out by furnace annealing (FA) and rapid thermal annealing (RTA) techniques. Results are summarized as the following:

(1) There was no evidence of As or Ga outdiffusion into Al_2O_3 film after FA and RTA.

(2) After FA, a slight amount of elemental As accumulated at the interface and no change of EL2 properties occurred near the interface. Whereas, a lot of Ga oxide was created at the interface and the increase of EL2 concentration was observed near the interface after RTA. Large temperature gradient during RTA can cause to produce the large stress at the Al_2O_3/GaAs interface, thereby changing the EL2 properties.

APPENDIX

When the concentration of the deep level (N_T) approaches or exceeds that of the shallow impurities (N_D), nonexponential capacitance transient may occur and fitting of the transient curve to an exponential gives erroneous emission rates. Thus, the DLTS signal has a tendency to lower the peak height and to shift the peak temperature. In the appendix, the capacitance transient and DLTS spectrum are calculated for various values of N_T/N_D, and the validity of usual method to estimate the characteristic values of the deep level is discussed.

The junction capacitance, C(t), can be generally expressed as

$$C(t)=\frac{\varepsilon\{N_D+N_T^+(t)\}}{\lambda N_T^+(t)+\sqrt{\{\lambda N_T^+(t)\}^2-\{N_D+N_T^+(t)\}\{N_T X_A^2+N_T^+(t)(\lambda^2-X_A^2)-\frac{2\varepsilon(V_D+V_B)}{q}\}}} \qquad (A1)$$

where $N_T^+(t)$ is the charge density due to thermal ionization of the deep level, λ the distance from the depletion layer edge to

the crossover position of Fermi level and the deep level, V_D the diffusion potential, V_B the bias voltage and x_A the crossover position of Fermi level and the deep level when $V=V_A$, respectively, as shown in Fig.A1. λ and $N_T^+(t)$ are given by next equations

$$\lambda = \sqrt{2\varepsilon(E_F-E_T)/(qN_D)} \qquad (A2)$$

and

$$N_T^+(t)= N_T-f_TN_T = N_T\{ 1-\exp(-t/\tau)\}. \qquad (A3)$$

where τ is the transient time constant. From the principle of detailed balance, τ can be given as

$$\tau = \frac{1}{e_n^t} = \frac{1}{\sigma v_{tho} N_{co} T^2} \exp\left(\frac{E_C-E_T}{kT}\right) \qquad (A4)$$

where e_n^t is the thermal emission rate for electrons, σ the thermal capture cross section, v_{tho} the coefficient of thermal velocity of the electron equal to $\sqrt{3k/m^*}$, N_{co} the coefficient of effective density of state in conduction band equal to $2(2\pi m^*k/h^2)^{3/2}$ and E_C the energy at the bottom of the conduction band.

Figure A2 shows calculated capacitance transient for three values of N_T/N_D, assuming the existence of the EL2 level with the concentration of N_T. In the case of low relative

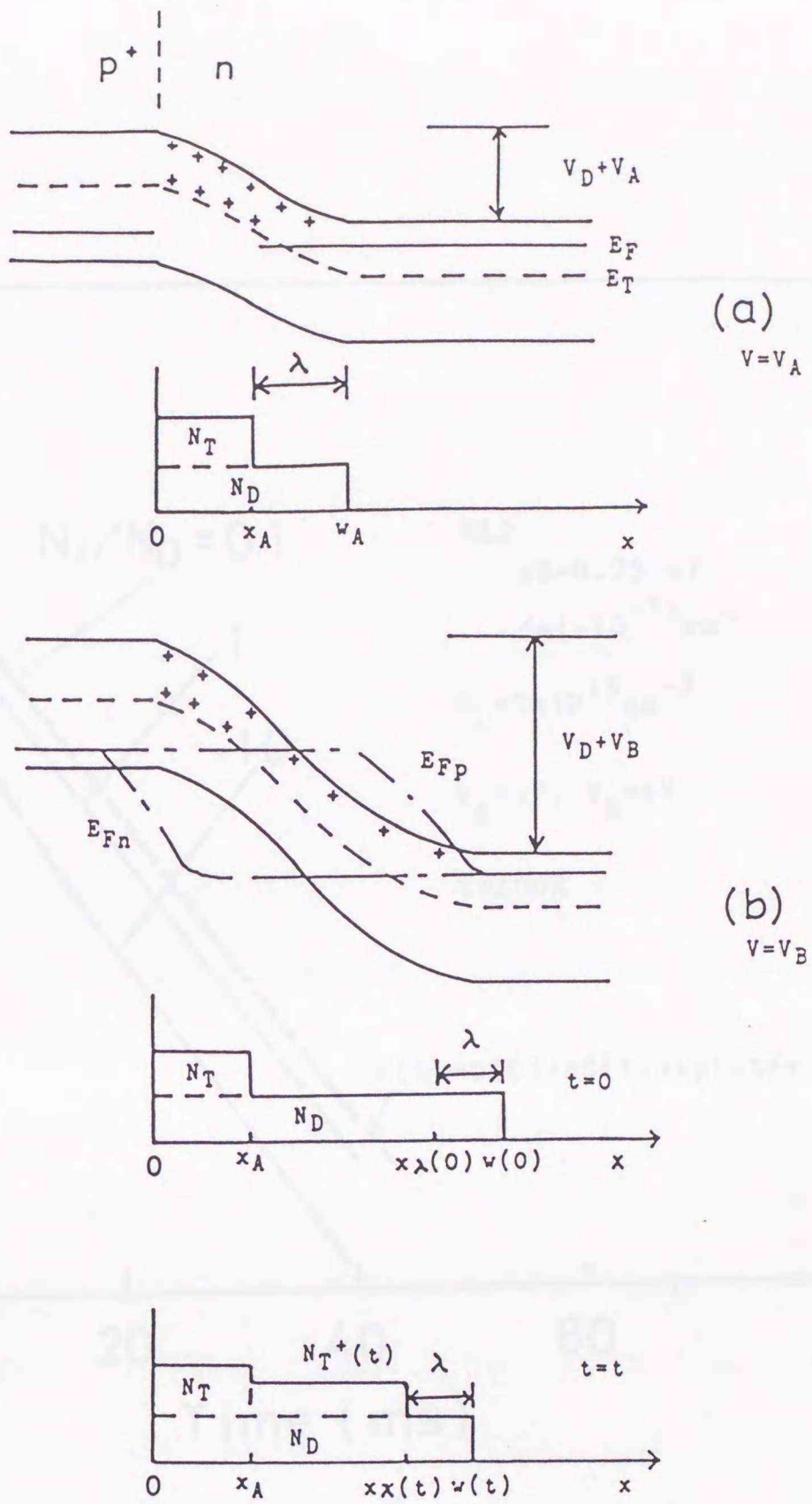

Figure A1. The change of band bending and space charge distribution during voltage switching.

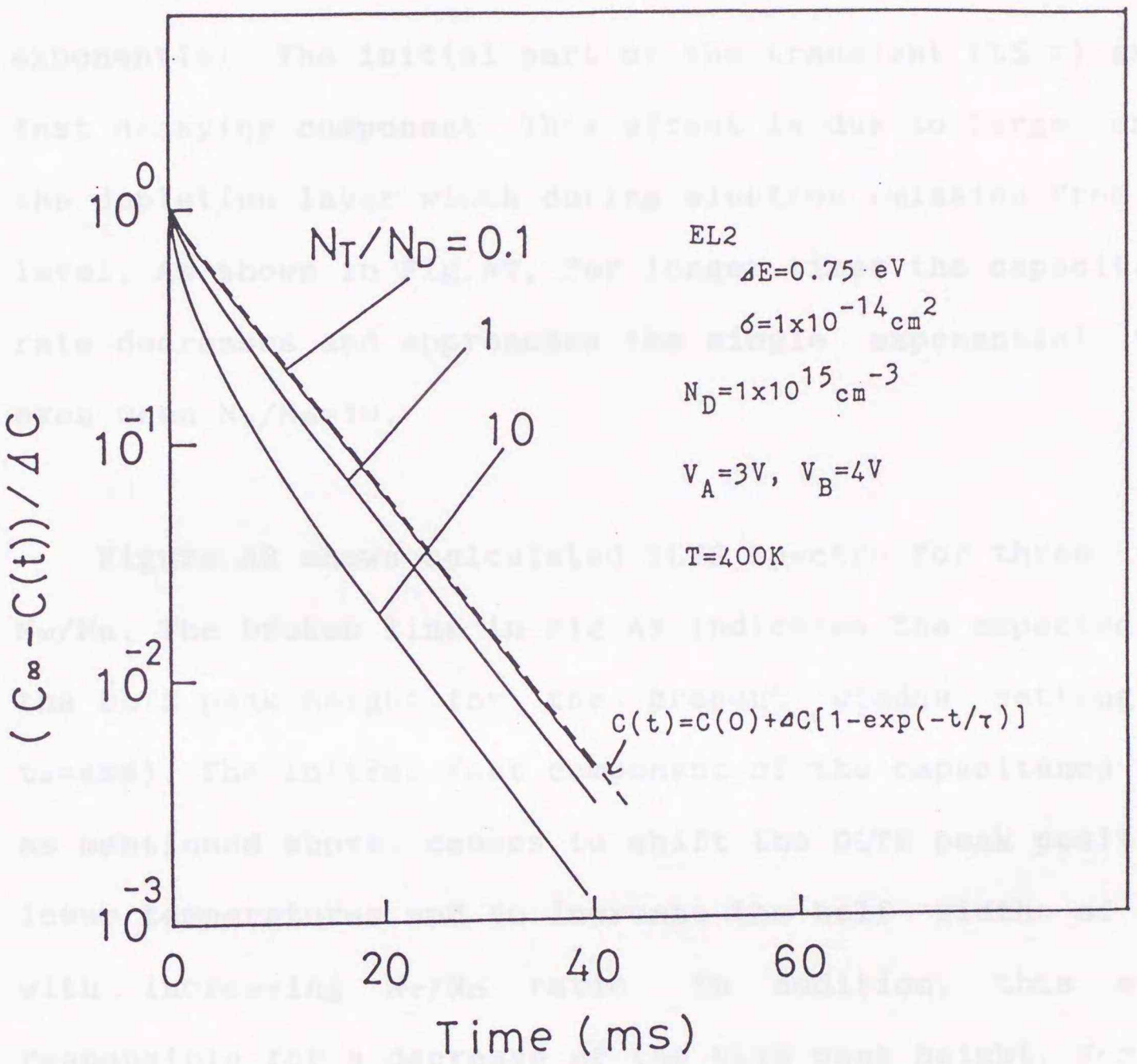

Figure A2. Calculated capacitance transient for three values of N_T/N_D.

concentration of the EL2 (N_T/N_D=0.1), the time dependence of the capacitance transient becomes s simple exponential form. However, when $N_T/N_D \geqq 1$, the capacitance transient is no longer exponential. The initial part of the transient ($t \leqq \tau$) exhibits a fast decaying component. This effect is due to large changes in the depletion layer width during electron emission from the deep level. As shown in Fig.A2, for longer times the capacitance decay rate decreases and approaches the single exponential transient, even when N_T/N_D=10.

Figure A3 shows calculated DLTS spectra for three values of N_T/N_D. The broken line in Fig.A3 indicates the expected value of the DLTS peak height for the present window setting (t_1=1ms, t_2=4ms). The initial fast component of the capacitance transient, as mentioned above, causes to shift the DLTS peak position toward lower temperatures and to increase the half width of the peak with increasing N_T/N_D ratio. In addition, this effect is responsible for a decrease of the DLTS peak height. For example, in the case N_T=10N_D, the concentration of EL2 obtained from the DLTS peak height is underestimated to be about 30%.

The activation energy and capture cross section of the deep levels can be obtained by DLTS measurement using next equations.

$$\ln(T_{max}^2 \tau_{max}) = \frac{E_C - E_T}{kT_{max}} + \ln \frac{1}{\sigma v_{tho} N_{CO}} \qquad (A5)$$

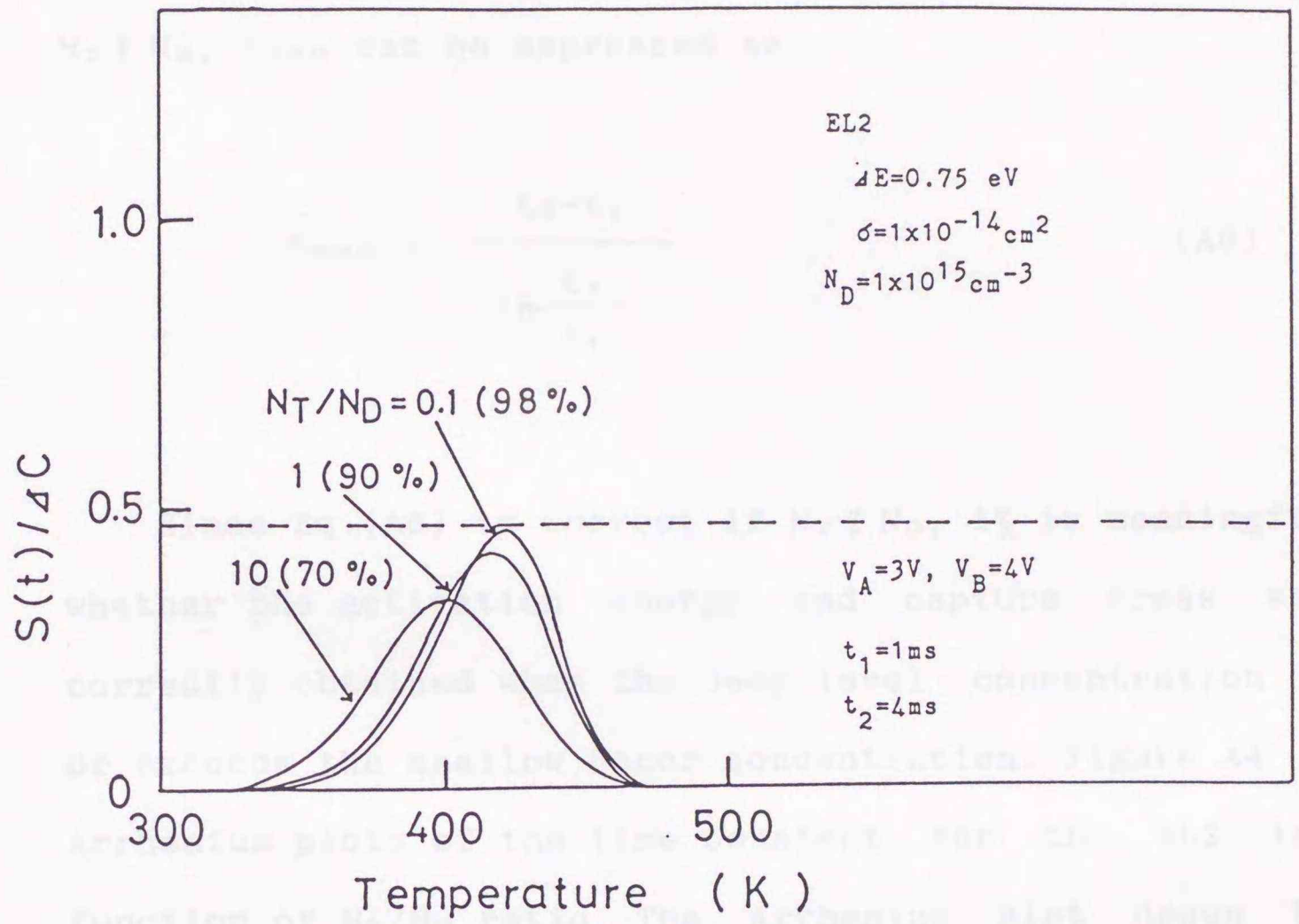

Figure A3. Calculated EL2 DLTS spectra for three values of N_T/N_D. The broken line indicates the expected peak height for the present window setting.

where T_{max} is the peak temperature of the DLTS spectrum and τ_{max} the value of τ at the maximum of the DLTS spectrum. Assuming $N_T \ll N_D$, τ_{max} can be expressed as

$$\tau_{max} = \frac{t_2 - t_1}{\ln \frac{t_2}{t_1}} \qquad \text{(A6)}$$

Since Eq.(A6) is correct if $N_T \ll N_D$, it is meaningful to check whether the activation energy and capture cross section are correctly obtained when the deep level concentration approaches or exceeds the shallow donor concentration. Figure A4 shows the Arrhenius plots of the time constant for the EL2 level as a function of N_T/N_D ratio. The Arrhenius plot drown by Eq.(A5) using the same parameters is also given in Fig.A4 as a broken line. The calculated lines are parallel to the broken line and move toward lower side of that line with increasing N_T/N_D ratio. Figure A4 demonstrates very well that the activation energy is correctly obtained by usual calculated method due to the same slope with a wide range of N_T/N_D ratio and the capture cross section is overestimated when $N_T \geqq N_D$.

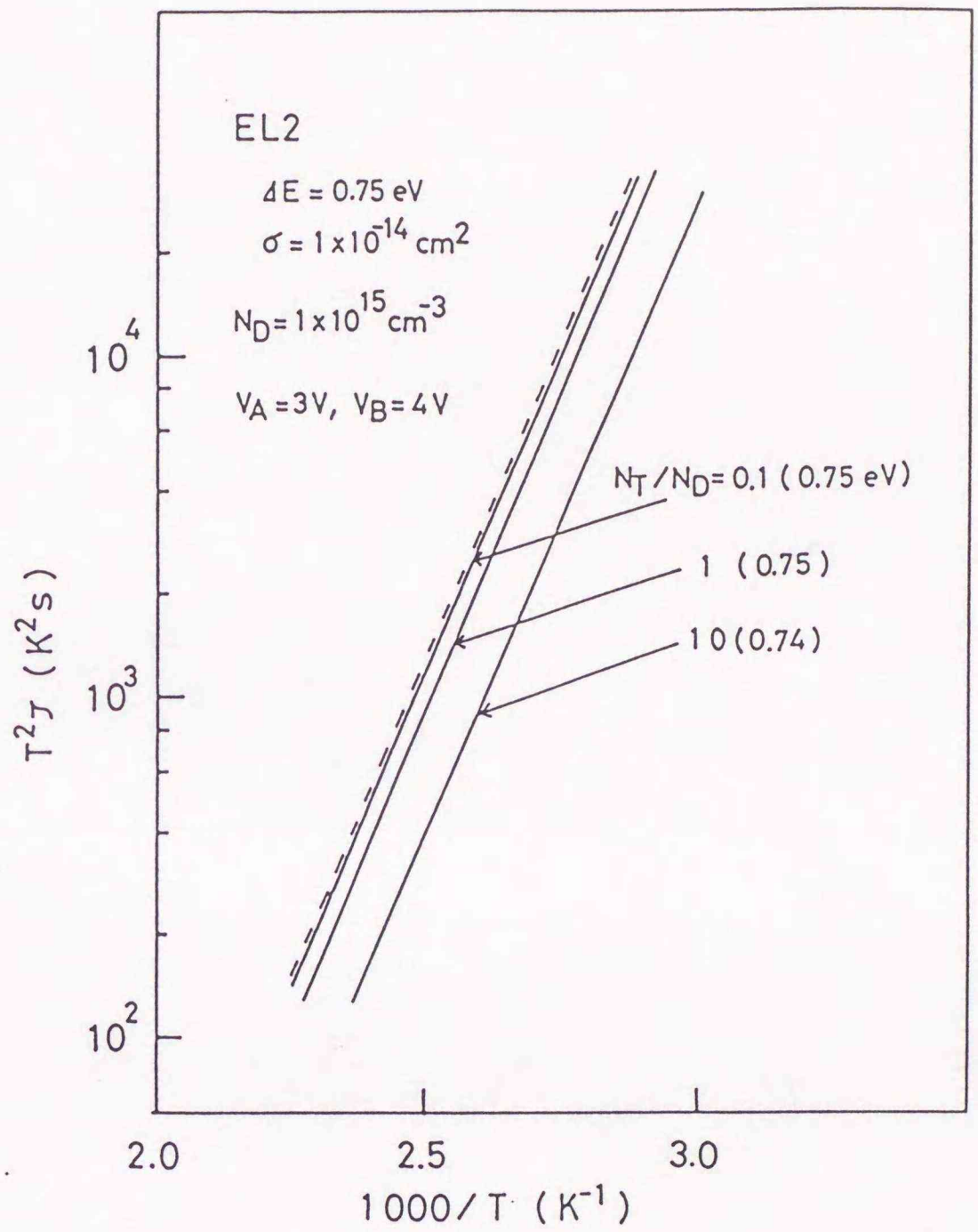

Figure A4. Calculated Arrhenius plots of the time constant for the EL2 level obtained by the calculated DLTS spectra as a function of N_T/N_D ratio. The broken line is obtaimed by Eq.(A5).

inches 1 2 3 4 5 6 7 8

cm 1 2 3 4 5 6 7 8 9 10 11 12 13 14 15 16 17 18 19

Kodak Color Control Patches

Blue Cyan Green Yellow Red Magenta White 3/Color Black

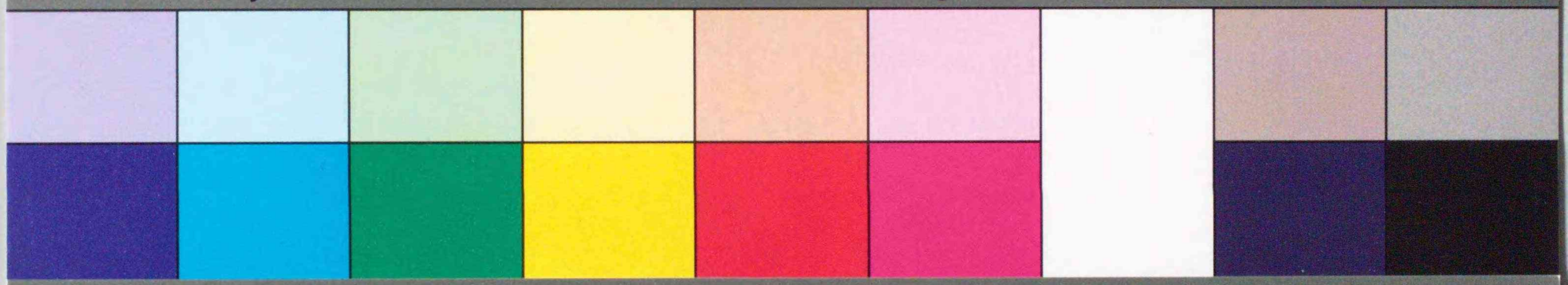

Kodak Gray Scale

C Y M

A 1 2 3 4 5 6 M 8 9 10 11 12 13 14 15 B 17 18 19